

THE UNIVERSITY OF CALGARY

Study of Chloride Migration in Cold Lake, Alberta, Canada

by

Egide Nzojibwami

A THESIS

SUBMITTED TO THE FACULTY OF GRADUATE STUDIES

IN PARTIAL FULFILMENT OF THE REQUIREMENTS FOR THE

DEGREE OF MASTER OF SCIENCE

DEPARTMENT OF CIVIL ENGINEERING

CALGARY, ALBERTA

APRIL, 1999

© Egide Nzojibwami 1999



National Library
of Canada

Acquisitions and
Bibliographic Services

395 Wellington Street
Ottawa ON K1A 0N4
Canada

Bibliothèque nationale
du Canada

Acquisitions et
services bibliographiques

395, rue Wellington
Ottawa ON K1A 0N4
Canada

Your file *Votre référence*

Our file *Notre référence*

The author has granted a non-exclusive licence allowing the National Library of Canada to reproduce, loan, distribute or sell copies of this thesis in microform, paper or electronic formats.

The author retains ownership of the copyright in this thesis. Neither the thesis nor substantial extracts from it may be printed or otherwise reproduced without the author's permission.

L'auteur a accordé une licence non exclusive permettant à la Bibliothèque nationale du Canada de reproduire, prêter, distribuer ou vendre des copies de cette thèse sous la forme de microfiche/film, de reproduction sur papier ou sur format électronique.

L'auteur conserve la propriété du droit d'auteur qui protège cette thèse. Ni la thèse ni des extraits substantiels de celle-ci ne doivent être imprimés ou autrement reproduits sans son autorisation.

0-612-38637-6

ABSTRACT

In the Cold Lake area, the Colorado Shale forms the uppermost part of a thick sedimentary bedrock, containing considerable amounts of chloride. Chloride transfer from the shale to overlying fresh-water Quaternary aquifers was studied, using numerical models based on chemico-osmotic and transport equations, and laboratory experiments. The Colorado Shale diffusion coefficient was approximated between $1.7 \times 10^{-11} \text{ m}^2/\text{s}$ and $1.27 \times 10^{-10} \text{ m}^2/\text{s}$, from diffusion tests conducted on five core samples. Excess pore pressure and chloride concentration variations were studied as well. The chloride migration was simulated with MT3D transport model, for an 8,500m two-dimensional section calibrated with two wells, located south of Imperial Oil Cold Lake Operations. Model parameters included calculated diffusion coefficients and collected field data. The simulation showed that chloride concentration increases in Quaternary aquifers (i) from recharging to discharging areas, (ii) towards bedrock contact, (iii) with hydraulic velocity decrease, (iv) for higher chloride bedrock content and, (v) for higher diffusion coefficients.

ACKNOWLEDGMENTS

This research program was conducted under the kind supervision of Dr Ron C.K. Wong. His high professional guidance through every step of the study, his words of encouragement, his patience and availability were greatly appreciated. The Department of Civil Engineering provided me with the financial assistance and a supportive working environment that was necessary to complete this work.

The Research Department of Imperial Oil supported financially the laboratory experiments and allowed the access to all available data needed to conduct successfully this program. Dr. Bruce S. Carey, George R. Scott, Drew D. Irwin, Randy J. Ottenbreit, Russ W. Costello and Cal B. Sikstrom of Imperial Oil, and Jon W. Fennel of Komex International reviewed all or part of this thesis and improved considerably its substance by their constructive remarks.

TABLE OF CONTENTS

Approval Page.....	ii
Abstract.....	iii
Acknowledgments.....	iv
Table of Contents.....	v
List of Tables.....	x
List of Figures.....	xi
List of Symbols.....	xiv

CHAPTER ONE

INTRODUCTION.....	1
1.1 Scope of the Study.....	1
1.2 Thesis Organization.....	3
1.3 Geological Context	4
1.3.1 Stratigraphy.....	4
1.3.1.1 The Cambrian Basal Sandstone.....	5
1.3.1.2 Devonian Evaporitic Formations.....	5
1.3.1.3 The Lower Cretaceous Oil Bearing Mannville Group.....	10
1.3.1.4 Upper Cretaceous Colorado Group Shales and Lea Park Formation.....	10
1.3.1.5 The Quaternary Unconsolidated Sediments.....	12
1.3.2 Hydrogeology.....	14
1.3.2.1 Characteristics of the Main Bedrock Aquifers.....	14
1.3.2.2 The Colorado Aquitard System.....	18
1.3.2.3 Fracture Systems in the Upper Colorado Shale.....	20
1.3.2.4 Quaternary Aquifers.....	23
1.3.3 Importance of Geological Data for the Modeling Study.....	32

CHAPTER TWO

THEORETICAL AND EXPERIMENTAL STUDIES OF FLUID

	AND SOLUTE FLOW IN THE COLORADO SHALE.....	35
2.1	State of Water in a Shale Microstructure	35
2.2	Flow Mechanisms in a Shale.....	37
2.2.1	Fluid Flow.....	37
2.2.1.1	Fluid Flow under Hydraulic Gradient.....	37
2.2.1.2	Fluid Flow under Chemico-Osmotic Gradient.....	38
2.2.2	Solute flow	40
2.2.2.1	Solute Flow by Diffusion.....	40
2.2.2.2	The Dispersion Process.....	41
2.2.2.3	The Hydrodynamic Dispersion.....	44
2.2.2.4	Solute Flow by Advection.....	45
2.2.2.5	The Retardation Process.....	46
2.3	Laboratory Investigations.....	50
2.3.1	The Purpose of Experimental Investigations.....	50
2.3.2	Experimental Procedures.....	50
2.3.3	Analytical Results.....	56
2.4	Application of Theoretical Concepts and Experimental Data to the Flow in the Colorado Shale.....	58

CHAPTER THREE

NUMERICAL MODELING OF THE CHEMICO-OSMOTIC

	FLOW IN A SHALE FORMATION.....	60
3.1	Basic Assumptions.....	60
3.2	Definition of the Governing Equation for the Fluid Flow.....	61
3.2.1	Continuity of Fluid.....	61
3.2.2	Constitutive Law.....	62

3.2.3	Darcy's Law.....	63
3.2.4	Governing Equation for the Fluid Flow.....	63
3.3	Definition of the Governing Equation for the Solute Flow.....	64
3.3.1	Continuity for the Solute.....	64
3.3.2	Solute Flow Law.....	65
3.4	Numerical Solving.....	67
3.4.1	Explicit formulation.....	67
3.4.2	Dimensionless Governing Equations.....	68
3.4.3	Numerical Approximations.....	69
3.4.4	Initial and Boundary Conditions.....	71
3.4.5	Parameters Used for the Simulation.....	73
3.5	Simulation Results.....	74
3.5.1	Calculation of the Molecular Diffusion Coefficient.....	74
3.5.2	Chloride Concentration Distribution.....	79
3.5.3	Pore Pressure Distribution.....	79
3.5.4	Sensitivity Analysis.....	80
3.5.4.1	<i>The Chloride Outflow.....</i>	<i>80</i>
3.5.4.2	<i>The Pore Pressure.....</i>	<i>80</i>
3.5.5	<i>Effect of the Pore Pressure Variation on the Chloride Outflow.....</i>	<i>81</i>

CHAPTER FOUR

NUMERICAL SIMULATION OF CHLORIDE TRANSPORT

	IN THE COLD LAKE AREA.....	89
4.1	Introduction.....	89
4.2	Governing Equation.....	90
4.3	Advection term.....	91
4.3.1	Partial Differential Equations for Velocity Calculation.....	91
4.3.2	Numerical Calculation of Hydraulic Heads by MODFLOW.....	92

4.3.3	Velocity Numerical Interpolation.....	94
4.3.4	Numerical Solution for the Advection Term.....	95
4.3.4.1	<i>The Finite Difference Method.....</i>	95
4.3.4.2	<i>The Particle Tracking Methods.....</i>	96
4.4	Dispersion Term.....	105
4.5	Sinks and Sources.....	108
4.6	Chemical Reactions.....	109
4.7	Geological Data for the Model.....	109
4.8	Model Set Up.....	110
4.9	Initial and Boundary Conditions.....	113
4.9.1	The Initial Chloride Content.....	113
4.9.2	The Hydraulic Head Boundary.....	114
4.9.3	The Flow Boundary.....	114
4.10	Simulation of the Base Case.....	115
4.11	Effect of Groundwater Velocity in the Quaternary Aquifer.....	124
4.12	Effect of the Variation of the Hydraulic Conductivity in the Fractured Colorado Shale Layer.....	131
4.13	Effect of the Initial Chloride Concentration in the Bedrock	135
4.14	Effect of the Dispersion on the Solute Flow.....	137
4.15	Effect of the Porosity on the Solute Flow.....	139
4.16	Effect of Different Numerical Methods on the Simulation Results...	140

CHAPTER FIVE

CONCLUSIONS AND RECOMMENDATIONS.....	145
--------------------------------------	-----

BIBLIOGRAPHY.....	151
-------------------	-----

APPENDIX I - CHEMICAL ANALYSES.....	157
-------------------------------------	-----

APPENDIX II - LOG ANALYSES FOR WELLS LOCATED AT GEW97-3 AND GEW97-9.....	167
---	-----

APPENDIX III - ALGORITHM FOR A ONE DIMENSIONAL PORE PRESSURE AND CONCENTRATION CALCULATION FOR THE CHEMICO-OSMOTIC MODEL.....	172
APPENDIX IV - COMPUTER AIDED TOMOGRAPHY (CAT) SCAN FOR SAMPLES LP, MP AND HP.....	179

List of Tables

Table 1.1	Stratigraphy of the Cold Lake area
Table 1.2	Quaternary stratigraphy in the Cold Lake Area
Table 1.3	Main bedrock aquifers in the Cold Lake area: chemical and physical characteristics
Table 1.4	Main bedrock aquifers in the Cold Lake area: hydraulic characteristics
Table 1.5	Hydrogeological data from recent monitoring wells in the fractured upper zone of the Colorado Shale around the Imperial Oil Cold Lake Operations
Table 1.6	Chemical composition of water samples from the Colorado aquitard
Table 1.7	Hydraulic and chemical properties of Quaternary aquifers around the Imperial Oil Cold Lake Operations
Table 2.1	Size and weight of the samples used for the laboratory tests
Table 2.2	Chloride content of water after laboratory tests
Table 2.3	Water content in major ions after diffusion test
Table 3.1	Excess pore pressures in swelling samples 3a and 3b for different confining pressures, for a maximum swelling pressure of 1200 kPa
Table 4.1	Properties used for the simulation of the base case
Table 4.2	Comparison between simulated and analytical chloride concentrations for the base case
Table 4.3	Impact of the velocity in the Quaternary aquifer on the amount of chloride remaining in the system
Table 4.4	Influence of the velocity in the fractured Colorado Shale on the chloride concentration in the Quaternary aquifer
Table 4.5	Effect of the initial bedrock concentration on the chloride concentration in the Quaternary aquifer
Table 4.6	Effect of diffusion coefficient variation in the Colorado Shale on the chloride concentration in the Quaternary aquifer
Table 4.7	Effect of the porosity variation in the Colorado Shale on the chloride concentration in the Quaternary aquifer

List of Figures

- Figure 1.1 Location map of the Imperial Oil Cold Lake Production Project
- Figure 1.2 Stratigraphy of the Cold Lake area
- Figure 1.3 Topography of the top of the Colorado Shale around the Imperial Oil Cold Lake Development Projects in Cold Lake
- Figure 1.4 Quaternary formations in Cold Lake
- Figure 1.5 Fracture orientation sets used for the evaluation of D & E Pad fracture systems in Cold Lake
- Figure 1.6 Stereographic plot of the fracture sets
- Figure 1.7 Fracture density log in one of the wells in Cold Lake
- Figure 1.8 Piezometric contours and flow directions in the Empress Formation Unit 1 aquifer
- Figure 1.9 Piezometric contours and flow directions in the Empress Formation Unit 3 aquifer
- Figure 1.10 Piezometric contours and flow directions in the Muriel Lake Formation aquifer
- Figure 1.11 Piezometric contours and flow directions in the Beaver River Interval aquifer
- Figure 2.1 Shale fabric structure
- Figure 2.2 Double layers near clay particles
- Figure 2.3 Factors causing pore-scale longitudinal dispersion
- Figure 2.4 Flow path that causes lateral hydrodynamic dispersion
- Figure 2.5 Equipment used for the diffusion test
- Figure 2.6 Experimental apparatus for swelling tests
- Figure 2.7 Confining pressures for swelling test on samples 3a and 3b
- Figure 2.8 Evolution of chloride concentration with time in the water in contact with Colorado Shale samples LP, MP, and HP
- Figure 2.9 Evolution of chloride concentration with time in the water in contact with Colorado Shale samples 3a and 3b
- Figure 3.1 Grid and computational molecule for the explicit formulation
- Figure 3.2 Sample LP - solute flow rate
- Figure 3.3 Sample MP - solute flow rate
- Figure 3.4 Sample HP - solute flow rate
- Figure 3.5 Sample 3a - solute flow rate
- Figure 3.6 Sample 3b - solute flow rate
- Figure 3.7 Sample 3a - variation of the diffusion coefficient in comparison with the swelling of the sample
- Figure 3.8 Sample 3b - variation of the diffusion coefficient in comparison with the swelling of the sample
- Figure 3.9 Sample LP - concentration isochrones at different times
- Figure 3.10 Sample MP - concentration isochrones at different times
- Figure 3.11 Sample HP - concentration isochrones at different times

Figure 3.12	Sample 3a - concentration isochrones at different times during swelling test
Figure 3.13	Sample 3b - concentration isochrones at different times during swelling test
Figure 3.14	Sample LP - Pore pressure isochrones at different times
Figure 3.15	Sample MP - Pore pressure isochrones at different times
Figure 3.16	Sample HP - Pore pressure isochrones at different times
Figure 3.17	Sample 3a - Pore pressure isochrones at different times during swelling test for one loading interval
Figure 3.18	Sample 3b - Pore pressure isochrones at different times during swelling test for one loading interval
Figure 3.19	Chloride flow rate variation with the diffusion coefficient
Figure 3.20	Sample 3a - pore pressure isochrones for an osmotic efficiency $\phi=0.1$
Figure 3.21	Sample 3a - pore pressure isochrones for an osmotic efficiency $\phi=0.4$
Figure 3.22	Sample 3a - Porosity change during swelling test
Figure 3.23	Sample 3b - Porosity change during swelling test
Figure 4.1	Numerical interpolations used to solve the advection term in MT3D
Figure 4.2	Illustration of moving particles used in the method of characteristics
Figure 4.3	Illustration of the modified method of characteristics
Figure 4.4	Chloride levels for Empress Formation Unit 3
Figure 4.5	Grid setup for the transport model
Figure 4.6a	Simulated chloride contours, hydraulic heads and flow directions for the base case
Figure 4.6b	Simulated chloride evolution with time for the base case
Figure 4.7a	Simulated chloride contours, hydraulic heads and flow directions for a groundwater velocity of 0m/year in the Quaternary aquifer
Figure 4.7b	Simulated chloride evolution with time for a groundwater velocity of 0m/year in the Quaternary aquifer
Figure 4.8a	Simulated chloride contours, hydraulic heads and flow directions for a groundwater velocity of 0.17m/year in the Quaternary aquifer
Figure 4.8b	Simulated chloride evolution with time for a groundwater velocity of 0.17m/year in the Quaternary aquifer
Figure 4.9a	Simulated chloride contours, hydraulic heads and flow directions for a groundwater velocity of 8.7m/year in the Quaternary aquifer
Figure 4.9b	Simulated chloride evolution with time for a groundwater velocity of 8.7m/year in the Quaternary aquifer
Figure 4.10a	Simulated chloride contours, hydraulic heads and flow directions for a groundwater velocity of 87m/year in the Quaternary aquifer
Figure 4.10b	Simulated chloride evolution with time for a groundwater velocity of 87m/year in the Quaternary aquifer
Figure 4.11a	Simulated chloride contours, hydraulic heads and flow directions for a hydraulic conductivity of 10^{-8} m/s in the fractured Colorado Shale
Figure 4.11b	Simulated chloride evolution with time for a hydraulic conductivity of 10^{-8} m/s in the fractured Colorado Shale

- Figure 4.12a Simulated chloride contours, hydraulic heads and flow directions for a hydraulic conductivity of $5 \times 10^{-7} \text{ m/s}$ in the fractured Colorado Shale
- Figure 4.12b Simulated chloride evolution with time for a hydraulic conductivity of $5 \times 10^{-7} \text{ m/s}$ in the fractured Colorado Shale
- Figure 4.13a Simulated chloride contours, hydraulic heads and flow directions for a bedrock initial chloride concentration of 10,000mg/L
- Figure 4.13b Simulated chloride evolution with time for a bedrock initial chloride concentration of 10,000mg/L
- Figure 4.14a Simulated chloride contours, hydraulic heads and flow directions for a bedrock initial chloride concentration of 20,000mg/L
- Figure 4.14b Simulated chloride evolution with time for a bedrock initial chloride concentration of 20,000mg/L
- Figure 4.15a Simulated chloride contours, hydraulic heads and flow directions for diffusion coefficients of $5.0 \times 10^{-10} \text{ m}^2/\text{s}$ in fractured Colorado Shale and $10^{-10} \text{ m}^2/\text{s}$ in non fractured shale
- Figure 4.15b Simulated chloride evolution with time for diffusion coefficients of $5.0 \times 10^{-10} \text{ m}^2/\text{s}$ in fractured Colorado Shale and $10^{-10} \text{ m}^2/\text{s}$ in non fractured shale
- Figure 4.16a Simulated chloride contours, hydraulic heads and flow directions for a porosity of 0.1 in the Colorado Shale
- Figure 4.16b Simulated chloride evolution with time for a porosity of 0.1 in the Colorado Shale
- Figure 4.17 Simulated chloride evolution with time for the base case using the method of characteristics
- Figure 4.18 Simulated chloride evolution with time for the base case using the modified method of characteristics
- Figure 4.19 Simulated chloride evolution with time for the base case using the hybrid method of characteristics

List of Symbols

a	Freundlich empirical exponent
C	solute concentration (M/L^3)
\bar{C}	sorbed concentration (M/L^3)
Ca	calcium
Cl	chloride
C_{max}	maximum concentration (M/L^3)
C_s	concentration of sources and sinks M/L^3
C_v	consolidation coefficient (L^2/T)
D	diffusion coefficient (L^2/T)
D^*	effective diffusion coefficient (L^2/T)
D_L	longitudinal dispersion coefficient (L)
D_{ij}	hydrodynamic dispersion tensor
D_{Tv}	transversal dispersion coefficient (L)
h	hydraulic head (L)
H	drainage path length (L)
HCO_3	bi-carbonate
k_c	osmotic conductivity (L/T)
K_d	distribution coefficient (L^3/M)
K_f	Freundlich empirical constant (L^3/M) ^a
k_h	hydraulic conductivity (L/T)
K_{ii}	principal component of the hydraulic conductivity tensor (L/T)
K_l	Langmuir constant (L^3/M)
L	flow length (L)
Mg	magnesium
M_c	coefficient of compressibility related to change in osmotic pressure (Pa^{-1})
M_v	coefficient of compressibility related to the change in pore pressure (Pa^{-1})
n	total porosity (dimensionless)
n_e	effective porosity (dimensionless)
Na	sodium
$NaCl$	sodium chloride
NO_2	nitrite
NO_3	nitrate
N	nitrogen
NP	number of particles
P_e	Peclet number (dimensionless)
q_s	solute flow rate (L^3/T)
q_w	water flow rate (L^3/T)
q_{ws}	water flow rate per unit volume of aquifer representing sources and sinks (T^{-1})
R	universal gas constant ($=8.31450m^3Pa/K$)
RHS	right hand side term
R_t	retardation factor (dimensionless)
\bar{S}	total concentration of available sorption sites (M/M)

SO ₄	sulfate
S _s	specific storage (L ⁻¹)
t	time (T)
T	dimensionless time
t _{1/2}	half-time of degradable materials
T _e	absolute temperature (°K)
TDS	total dissolved solids
u	pore pressure (Pa)
U	dimensionless pore pressure at old time level
UV	dimensionless pore pressure at new time level
u _{max}	maximum pore pressure (Pa)
V	volume
v _x	x-component of average linear velocity (L/T)
\bar{v}_i	retarded velocity $\left(= \frac{v_i}{R_i} \right)$ for the i-component of the velocity
w	empirical coefficient used to determine the effective diffusion coefficient
x	distance (L)
X	dimensionless concentration at old time level
XV	dimensionless concentration at new time level
z	distance (L)
Z	dimensionless distance
α _L	dynamic longitudinal dispersivity coefficient (L)
α _{TH}	dynamic trasversal horizontal dispersivity coefficient (L)
α _{TV}	dynamic transversal vertical dispersivity coefficient (L)
α _x	linear interpolation factor for the x-component
α _y	linear interpolation factor for the y-component
Δ	increment
ε	axial strain (L/L)
γ _w	unit weight of water (M/L ³)
φ	osmotic efficiency (dimensionless)
λ	degradation rate constant
λ ₁	degradation rate constant for dissolved phase
λ ₂	degradation rate constant for adsorbed phase
π	osmotic pressure (kPa)
θ	volumetric moisture content of the soil (dimensionless) (also total porosity in saturated conditions)
ρ _b	dry bulk mass density of the porous medium (M/L ³)
σ	total stress (Pa)
ω	weighting factor for concentration

CHAPTER ONE

INTRODUCTION

1.1 Scope of the Study

Understanding solute transport processes in clay and shale formations requires a comprehensive knowledge of the complex world of clay minerals and their behavior under different hydrogeological and geotechnical conditions.

One major characteristic of clay minerals is their affinity to absorb water into their structure. As a consequence, a number of clays and shales may swell to accommodate the change in pore pressure. The ionic composition of the original water in the clay or shale may also change triggering the diffusion process of chemical species transfer from the formation to the water.

Swelling and chemical transport in groundwater have attracted the interest of many researchers due to their impact on the soil stability and the groundwater quality. A review of the literature in this domain shows that the bottom line is a problem of fluid and solute flow in clays and shales. Mathematically, two types of equations have been used to describe the fluid and solute flow in shales: (i) The *chemico-osmotic equations* (e.g. Mitchell et al., 1973) are commonly used by engineers interested in clay swelling

problems. These equations describe the fluid and solute flow in terms of a coupling process between the volume or pore pressure change and the ionic transfer by diffusion. Greenberg (1971) explained with these equations that diffusional flow of salt and water could be at the origin of important groundwater movements that do not obey the Darcy's law. (ii) The *transport equations* (e.g. Bear, 1979; Javandel et al., 1984) were designed to describe the fluid and solute flow transfer by diffusion, dispersion and advection. When applied to clays and shales, the transport equations do not take into consideration any volume change of the rock due to the change in its ionic content. They are mostly popular in water supply and water quality problems.

It is not the intent of this thesis to discuss further about these two types of equations. Each of them has proved to be enough accurate to account for fluid and solute flow in porous media when used carefully with required assumptions. Both equations were useful for the achievement of the objectives of this thesis for the interpretation of laboratory and field data.

This thesis was inspired by elevated chloride concentrations found in Quaternary aquifers around the Cold Lake Production Projects (CLPP) of Imperial Oil, Alberta, Canada. A careful study of available hydrogeological data conducted us to postulate that diffusion and dispersion of the chloride ions from the underlying marine Colorado Shale could be at the origin of above background level to elevated chlorides in upper fresh water Quaternary aquifers. This hypothesis was later corroborated by a number of chemical analyses and chloride monitoring tests in samples of originally distilled water that was left in contact with Colorado Shale samples for a few months.

The primary objective of this work is to study the importance and the extent of diffusion and dispersion processes in the chloride transport from the Colorado Shale to the upper Quaternary aquifers around the Cold Lake Production Projects of Imperial Oil. This was achieved in successive steps by:

- (i) running laboratory tests to monitor chloride transfer from a Colorado Shale sample to the fresh water;
- (ii) performing chemical analysis to determine the amount of chloride ions transferred to water and to analyze the quality of the originally distilled water in general;
- (iii) history matching laboratory data with a numerical model based on chemico-osmotic equations;
- (iv) interpreting the analytical data and analyzing the impact of hydraulic and mechanical parameters (porosity, conductivity, diffusion coefficient, compressibility) on the results of the model;
- (v) determining by numerical simulation, a range for the diffusion coefficient of the Colorado shale sample;
- (vi) applying the obtained range for the diffusion coefficient in a transport model used to simulate the chloride transfer in a field case;
- (vii) history matching the field case data with the transport model;
- (viii) performing a sensitivity analysis of the model to determine the influence of different parameters on the chloride transfer.

1.2 Thesis Organization

This thesis is divided into five chapters: In this first chapter, the purpose and the geological context of the study are presented. This introduction contains data necessary to understand the regional geological framework of the study and the field characteristics of the two formations involved in this work, the Colorado Shale and the Quaternary units.

The second chapter presents the theoretical and experimental approaches considered for the study of the fluid and the solute flow in the shale. General flow laws to be used in the models are discussed. The laboratory experiments are also presented.

In the third chapter, a theoretical chemico-osmotic model, used to simulate chloride monitoring laboratory data, is presented and solved by numerical approximations. A diffusion coefficient range resulting from the numerical simulation is interpreted in the light of laboratory data. Concentration and pore pressure variations are studied as well.

In the fourth chapter, a transport model used to simulate field conditions is presented. Available field data are history-matched with the use of the diffusion coefficient range obtained from the laboratory experiments. Sensitivity studies are done in the range of possible field variations of hydrogeological parameters (e.g. diffusion, dispersion, hydraulic conductivity, and porosity). The importance and the vertical extent of salt dispersion are presented.

The fifth chapter presents the conclusions and recommendations from the study.

1.3 Geological and Hydrogeological Context

1.3.1 Stratigraphy

The study area encompasses the zone operated by Imperial Oil Cold Lake Development Projects and the surroundings as indicated on the location map (Figure 1.1). The bitumen deposits at Imperial Oil Resources' Cold Lake Operation are mainly contained in the Lower Cretaceous sandstone of the Clearwater Formation at a depth of approximately 450 to 500m below ground level. The Clearwater Formation is covered by thick argillaceous formations including mainly the Colorado Shale. This low-permeability formation is believed to form a hydrogeological barrier between the bitumen deposits and the Quaternary fresh water aquifers. The regional geological context of these formations as

part of a large sedimentary deposit ranging from the Cambrian Sandstone to the Quaternary glacial till layers (Table 1.1, Figure 1.2), is summarized in this section.

1.3.1.1 The Cambrian Basal Sandstone

The basal Cambrian Sandstone is made up of a sequence of quartz sandstones and minor siltstones derived from the Precambrian shield. The work of Hitchon et al. (1989) indicates an uneven thickness on a regional scale, from a zero edge to the north to more than 150m to the southeast. In the study area, the basal sandstone is about 30 to 40m thick. It is used for disposal of produced water generated by the Imperial Oil Cold Lake Operations.

1.3.1.2 Devonian Evaporitic Formations

Overlying the basal Cambrian sandstone are the salt dominated deposits (evaporites) of the Lower to Middle Devonian Elk Point Group. This group comprises successively from top to bottom:

- Watt Mountain Formation (20m of shale);
- Prairie Formation (120 to 160m of massive anhydrite);
- Winnipegosis and Contact Rapids Formations (90m of dolomitic shales. argillaceous dolomite and dolomitic limestone);
- Cold Lake Formation (50m of salt);
- Ernestina Formation (less than 20m of argillaceous dolomite and dolomitic shales); and,
- Lotsberg Formation (240m of massive halite).

On top of the Elk Point Group, the Upper Devonian Beaverhill Lake Group is made up of limestone and interbedded shale of the Waterways formation with a thickness ranging from 300m to more than 500m in areas where the limestone was preserved by erosion.

However, in the Cold Lake area, the thickness of the formation appears as little as 100m because of the erosion at the pre-Cretaceous unconformity.

Table 1.1 Stratigraphy of the Cold Lake area (Imperial Oil, 1998)

Quaternary		Pleistocene Drift	Grand Centre Sand River Marie Creek Ethel Lake (Beaver River) Bonnyville Muriel Lake (Durlingville) Bronson Lake Empress (Empress)
Upper Cretaceous	Colorado Group	Second White Specs Formation	
		Belle Fourche Formation	
		Fish Scale Zone	
		Westgate Formation	
		Viking / Pelican Formation	
		Joli Fou Formation	
Lower Cretaceous	Mannville Group	Grand Rapids Formation	
		Clearwater Formation	
		Wabaskaw Member	
		McMurray Formation	
Upper Devonian	Beaverhill Lake Group	Waterways Formation	
Lower - Middle Devonian	Elk Point Group	Watt Mountain Formation	
		Prairie Formation	
		Winnipegosis Formation	
		Contact Rapids Formation	
		Cold Lake Formation	
		Ernestine Formation	
		Lotsberg Formation	
Cambrian		Sandstone	
PreCambrian			

Figure 1.1 **Location map of the Imperial Oil Cold Lake Production Project**

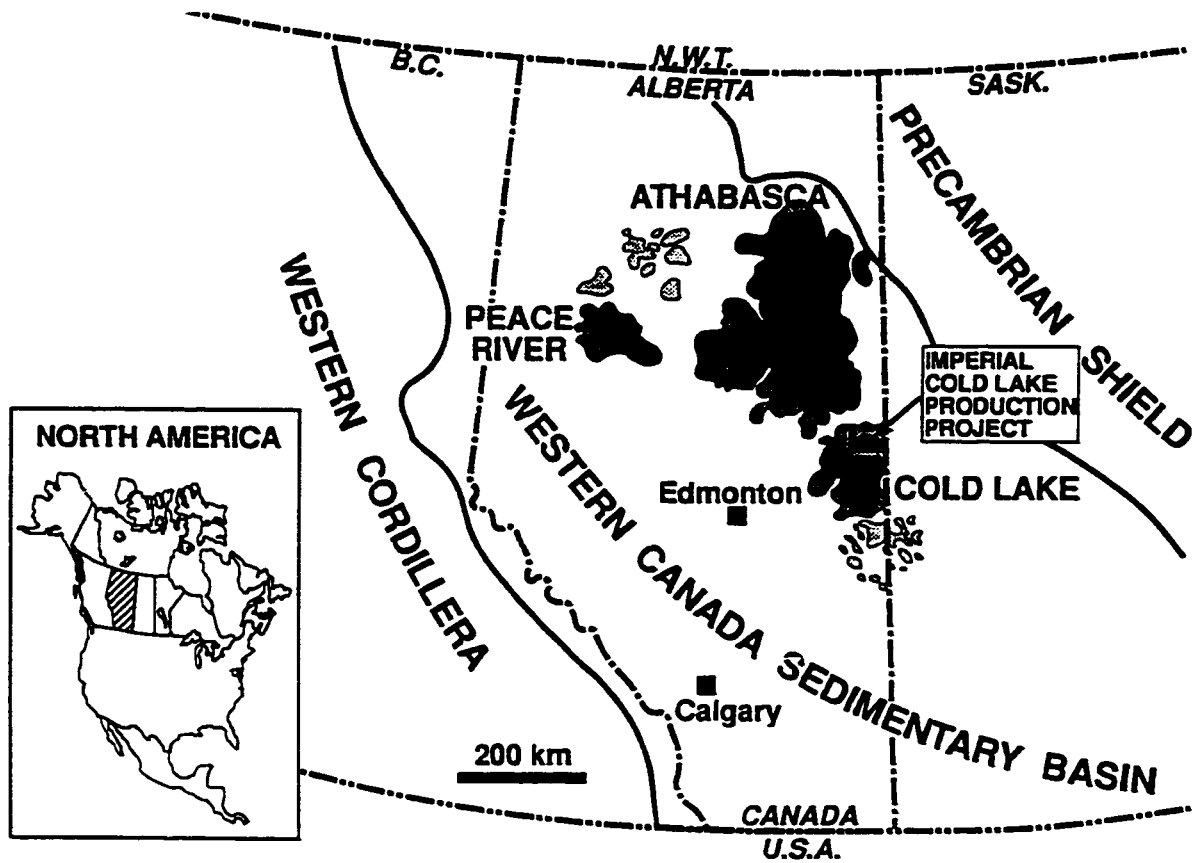


Figure 1.2 Stratigraphy of the Cold Lake area

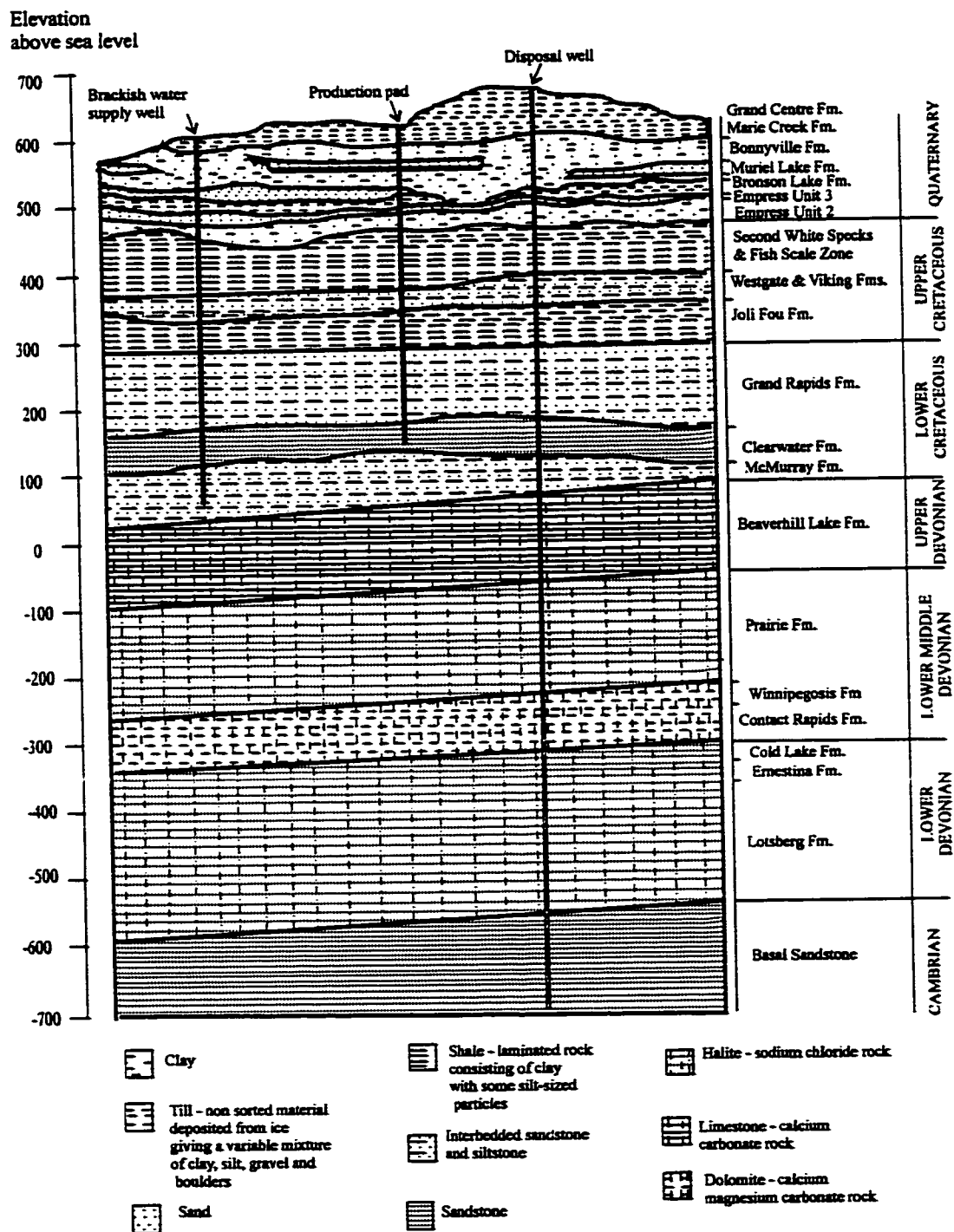
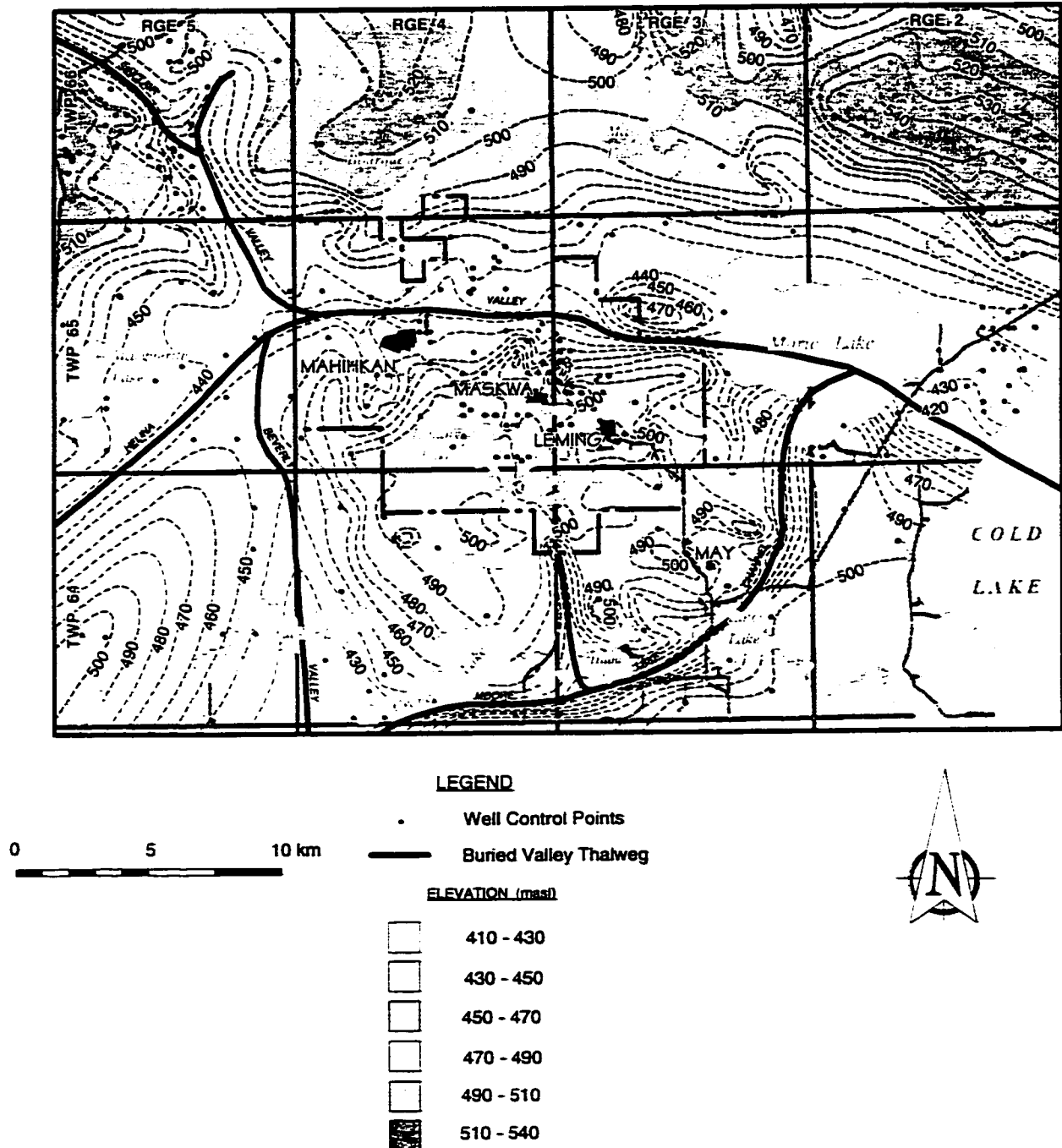


Figure 1.3 Topography of the top of the Colorado Shale around the Imperial Oil Cold Lake Production Project in Cold Lake (Imperial Oil, 1998)



1.3.1.3 The Lower Cretaceous Oil Bearing Mannville Group

The Lower Cretaceous formations of the Mannville Group are the first synorogenic consistently clastic sediments since the Cambrian. Differential erosion and incised drainage within the shallow-water basin led to the creation of a topographic relief formed by ridges and valleys which influenced sedimentation and the subsequent entrapment of heavy oil (Hitchon et al., 1989). In the study area, the Mannville Group is divided into three sub-units (Putnam, 1982; Jackson, 1984):

- the McMurray Formation composed of 90m of fluvial and estuarine valley-fill marine sandstone in the incised valleys of the pre-Cretaceous unconformity surface;
- the Clearwater Formation which consists of a 25 to 90m thick sandstone between thin shale layers;
- the Grand Rapids formation with 115 to 130m of thin sandstones interbedded with siltstones and shales.

Because of its homogeneity, the Clearwater Formation forms the major hydrocarbon resource in the area. The McMurray Formation which contains more silt and shale intercalations is not considered as a major hydrocarbon reservoir (Hitchon et al., 1989; Bachu et al., 1989). However, it does contain brackish water used for the cyclic steam stimulation process implemented by Imperial Oil.

1.3.1.4 Upper Cretaceous Colorado Group Shales and Lea Park Formation

Overlying the Mannville Group, the Upper Cretaceous shales of the Colorado Group consist of dark to pale gray, silty marine shales occasionally containing ironstone concretions and bentonite layers. Overall, the Colorado Group consists of about 300m of

marine shales with very minor amounts of sandstone (Hitchon et al., 1989). In the study area, the Colorado Shale Group comprises the following formations from top to bottom:

- The Second White Specks Formation;
- The Belle Fourche Formation;
- The Fish Scale Zones Formation;
- The Westgate Formation;
- The Viking Formation; and,
- The Joli Fou Formation.

The amount of relatively coarse-grained sediments between the Joli Fou and the Second White Specks Formations is small. In the study area, it is estimated at 25m thick of very fine-grained to silty sand associated with the Viking Formation. This dominantly argillaceous low-permeability Colorado Shale is believed to form a hydraulic barrier between the Clearwater hydrocarbon bearing layers and the upper Quaternary aquifer units (Imperial Oil, 1998). The Colorado Group Shales, together with the overlying Lea Park Formation shales, form the top of the Cretaceous bedrock in the Cold Lake area.

The Lea Park Formation and the Second White Specks are locally referred to as the Upper Colorado Shales. The lower layers of Quaternary sediments are thought to rest on top of the Lea Park Formation. However, the Second White Specks have also been found in direct contact with Quaternary formations in the Cold Lake area along the base of major buried channels (Imperial Oil, 1998).

Buried channels in the Colorado Shale were created by a pre-glacial river network existing on the surface of the bedrock before the deposition of Quaternary sediments. In the Cold Lake area, the major paleo-channels include Sinclair, Helina, Beverly and Moore Lake Valleys (Figure 1.3). The elevation difference between the highest and the lowest point of the top of the bedrock is approximately 90m (Imperial Oil, 1998). Minor

tributary channels feeding into adjacent major valleys were observed as well. The distribution of the lower Quaternary sediments is controlled by the main paleo-channels.

The pre-glacial erosion has also contributed to the formation of an extensive network of randomly oriented fractures in the upper 20 to 30m of the Colorado Shale as indicated by recent investigations. Below that depth, the density of fracturation decreases considerably. The high density fracturing in the upper portions of the bedrock beneath glacial sediments is a common occurrence in Western Canada (Imperial Oil, 1998).

1.3.1.5 The Quaternary Unconsolidated Sediments

Detailed geological and hydrogeological studies conducted in the Quaternary formations by Imperial Oil (1997, 1998) allowed the collection of a significant amount of information in Quaternary aquifers. Their description of the Quaternary stratigraphy in the Cold Lake area is indicated in Table 1.2 and Figure 1.4.

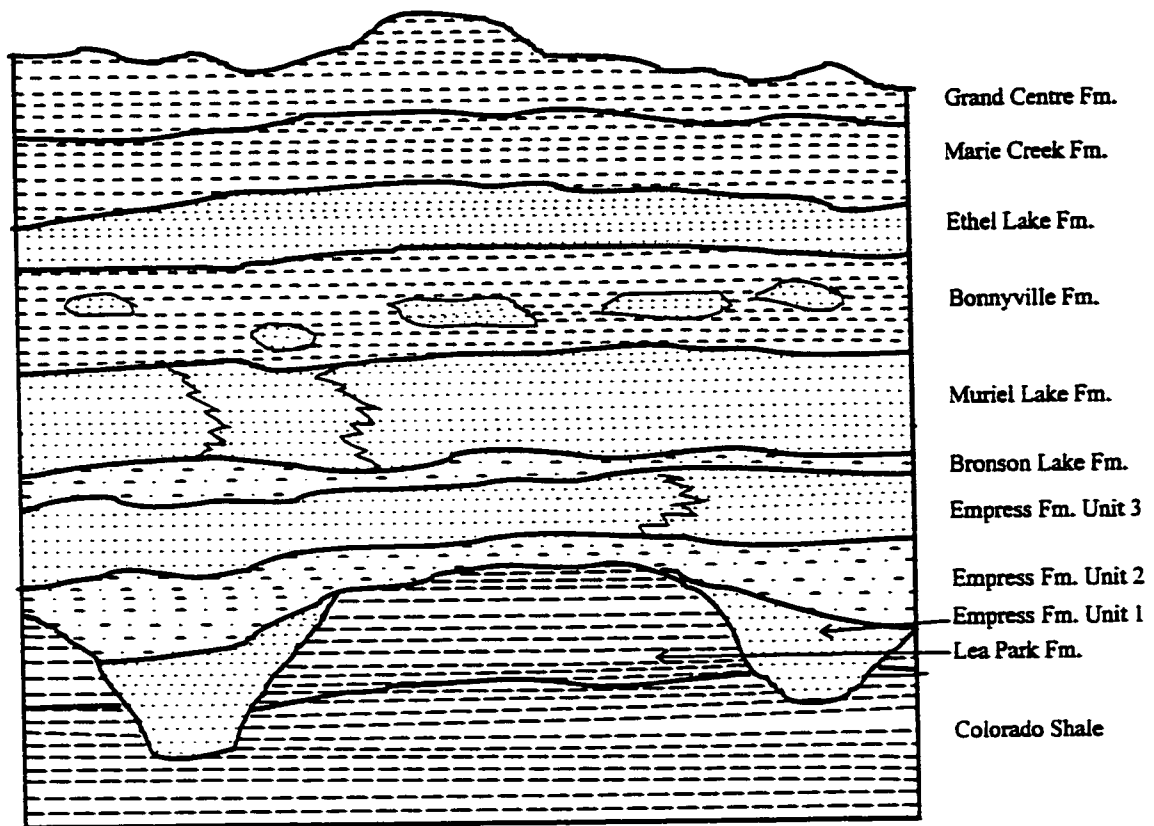
The Quaternary formations overlying the Colorado Shale are made up of sandy and gravel till layers alternating with silty till or lacustrine clay formations (Imperial Oil, 1998). The bottom layers were mainly deposited along the major thalweg channels created in the Colorado Shale during the post-Cretaceous erosional phase. The influence of the bedrock topography on the Quaternary sedimentation decreases progressively from the bottom and finally disappears in the upper layers. The thickness of the layers varies from a few meters to 30m with large lateral facies and thickness variations. The sandy and gravel layers generally form aquifers yielding fresh water for the local population and occasionally for industry purposes. They are confined within silty or argillaceous till layers acting as aquitards separating the aquifers.

Unlike the underlying marine bedrock, the Quaternary formations were deposited in a continental environment during the glaciation events.

Figure 1.4 Quaternary formations in Cold Lake

(The figure is not to scale)

Approximative total thickness of Quaternary formations = 100 to 150m



Legend





-  Till - non sorted material deposited from ice giving a variable mixture of clay, silt, gravel and boulders
-  Sand
-  Clay
-  Shale - laminated rock consisting of clay with some silt-sized particles

Table 1.2 Quaternary stratigraphy in the Cold Lake area (Imperial Oil, 1998)

Stratigraphic unit (registered name)	Dominant lithology	Aquifers (local names)	Origin of deposit
Grand Centre Formation	Silty clay till		Cold Lake Glaciation
Sand River Formation	Sand and silt	Sand River	
<i>Non-glacial period, weathering</i>			
Marie Creek Formation	Sandy silt, till		Ardmore Glaciation
Ethel Lake Formation	Sand, gravel, till	Beaver River	
<i>Non-glacial period, weathering</i>			
Bonnyville Formation - Unit 2	Sandy silt, till		Fort Kent Glaciation
Bonnyville Formation - Unit 1	Clay till, sand and gravel	Beaver River	
Muriel Lake Formation	Sand and gravel	Durlingville	
<i>Non-glacial period, weathering</i>			
Bronson Lake Formation	Till, lacustrine clay		Cherry Grove Glaciation
Empress Formation – Unit 3	Sand, gravel, clay	Empress 3	
Empress Formation – Unit 2	Lacustrine clay		
Empress Formation – Unit 1	Sand and gravel	Empress 1	
<i>Weathering period</i>			

1.3.2 Hydrogeology

1.3.2.1 Characteristics of the Main Bedrock Aquifers

The main regional characteristics of the aquifer systems in the bedrock as compiled by Bachu et al. (1989) and Hitchon et al. (1989) are presented in Tables 1.3 and 1.4. It appears from the data that the water density, as an expression of the salinity, increases

considerably with depth. The temperature increase with depth is correlated to the natural geothermal gradient of the area.

Table 1.3 Main bedrock aquifers in the Cold Lake area: chemical and physical characteristics (Bachu et al., 1989 and Hitchon et al., 1989)

Aquifer	Average thickness (m)	Average density of formation waters (kg/m ³)	Water temperature (°C)	Total Dissolved solids (mg/L)	Chloride Content (mg/L)
Mannville	188	1,007	15 - 40	10,000 - 60,000	5,000-40,000
Clearwater	35	1,005	18 - 31	10,000-6,0000	5,000-35,000
McMurray	60	1,006	15 - 36	10,000-60,000	5,000-35,000
Beaverhill Lake	303	1,033	25 - 45	20,000-200,000	10,000-150,000
Winnipegosis	112	1,093	19 - 33	55,000-295,000	30,000-175,000
Cambrian Sandstone	71	1,160	21 - 47	238,000-310,000	139,000-187,000

Table 1.4 Main bedrock aquifers in the Cold Lake area: hydraulic characteristics (Bachu et al., 1989 and Hitchon et al., 1989)

Aquifer	Vertical Flow Direction	Average Porosity	Regional hydraulic conductivity (m/s)	Anisotropy K_H/K_V	Specific storage (m^{-1})
Mannville	↓	0.24	4.0×10^{-7}	90.0	0.0050
Clearwater	↑	0.27	3.2×10^{-7}	200.0	0.0008
McMurray	↑	0.24	3.1×10^{-7}	120.0	0.0080
Beaverhill Lake	↓	0.10	3.5×10^{-8}	0.5	0.0004
Winnipegosis	↓	0.04	1.3×10^{-7}	0.8	0.0007
Cambrian Sandstone	↓	0.23	5.0×10^{-7}	80	0.0003

With the exception of the Winnipegosis and the Beaverhill Lake aquifers, the regional lateral flow is predominant as suggested by the ratios between the horizontal and the

vertical hydraulic conductivities (Table 1.4). The flow direction and the gradient vary from one aquifer to the other.

The vertical gradient is basically downward through the Paleozoic aquifer systems from the Beaverhill Lake, through the Winnipegosis, to the Cambrian aquifer. From the Paleozoic to the Lower Cretaceous, the flow is potentially upward from the Beaverhill Lake to the McMurray and Clearwater aquifers. Within the Cretaceous, the flow is downward between the Viking aquifer through the Mannville aquifer to the Clearwater and McMurray aquifers. In the Mannville aquifer, available data suggest a downward flow trend, with no major aquitard break caused by the oil sand layers.

The Cambrian Sandstone forms a continuous aquifer used for disposal of formation water produced by the Imperial Oil Cold Lake Operations. The aquifer is limited in places by the weak aquitard of the Middle and Upper Cambrian formed by thin intercalations of shale and sandstone. In spite of the presence of these thin beds of shale, the Cambrian rocks play a role of a single aquifer system. The salinity is very high, with a range of 238,000mg/L to 310,000mg/L in total dissolved solids (TDS). The dominant ions are Na (90,000mg/L to 117,000mg/L) and Cl (139,000 to 187,000mg/L) with high SO₄ content (1,570 to 6,500mg/L) and relatively low contents of Ca (1,250 to 3,400mg/L) and Mg (390 to 870mg/L). These features suggest an evaporitic origin of the solutes, mainly from halite. The lateral flow is generally from southwest to northeast with a downward vertical flow. Temperature values range from 21°C and 47°C at depths between 867m and 1,501m.

The massive Lotsberg and Cold Lake halite forms a thick (up to 375m) Lower Devonian aquiclude system which covers most of the Cold Lake area (Bachu et al., 1989), isolating completely the basal Cambrian aquifer. The salinity is comparable to the Cambrian.

The Winnipegosis aquifer encompasses the Contact Rapids and the Winnipegosis formations. The two units are in hydraulic continuity. The water TDS content decreases northeastward from 295,000mg/L to 55,000mg/L with corresponding decreases in Cl (175,000mg/L to 30,000mg/L), Ca (4,500 to 1,250mg/L) and Mg (1,150 to 290mg/L). Sulfate shows an opposite trend with values between 2,000mg/L and 5,000mg/L. The high salinity of the water is attributed to the dissolution of halite and anhydrite in the overlying Prairie Formation. The lateral regional flow varies from northwestward in the western part to northeastward in the eastern part. Temperatures vary between 19°C and 33°C for depths between 350m and 1045m.

The Prairie Formation halite and anhydrite overlying the Winnipegosis aquifer forms the major aquiclude in the study area. Brines recovered from the area show a chloride content between 98,000 and 213,000mg/L. Temperatures range from 24°C to 40°C at depths of 566 and 1,325m.

The Beaverhill Lake Group forms a thick carbonate aquifer system with a general eastward flow. The water TDS content decreases from about 200,000mg/L in the southwest to values around 20,000 to 50,000mg/L in the northeast with corresponding decreases in contents of Cl (150,000 to 10,000mg/L), Ca (20,000 to 1,000mg/L) and Mg (4,000 to 250mg/L). In some areas, the aquifer is connected with the overlying McMurray and Mannville aquifers. Isotherms at the top of the aquifer vary from 45 to 25°C from southwest to east.

The McMurray aquifer of the Lower Cretaceous succession is present in the northwestern part of the Cold Lake area. The flow is directed toward the overlapping area with the underlying Beaverhill aquifer. The TDS contents of formation waters decrease northward from 60,000mg/L to 10,000mg/L with corresponding decreases in Cl (35,000 to 5,000mg/L), Ca (1,000 to less than 250mg/L), Mg (700 to less than 100mg/L). Sulfate is

less than 100mg/L. The temperatures measured in the McMurray aquifer vary between 15 and 36°C at depths from 430 and 720m.

The thin arenaceous unit (35m) within the Clearwater formation is defined as the Clearwater aquifer. It is isolated between thin (up to 10m) aquitards formed by the shales of the Clearwater formation, separating the aquifer from the McMurray and the Mannville aquifers. The lateral flow and the composition of the formation waters are similar to those of the McMurray aquifer, suggesting that the lower Clearwater shale is a weak aquitard. The temperatures range from 18°C and 31°C between 400m and 715m.

The Mannville aquifer includes several oil sand layers generally acting as local weak aquitards. The water lateral flow is low with a westward trend in the study area. The hydraulic conductivity of the oil sand layers is estimated at 10^{-10} m/s (Hitchon et al., 1989). Salinity decreases from more than 60,000mg/L in the southwest to less than 10,000mg/L in the northeast of the Cold Lake area. Corresponding decreases are observed for Cl (40,000 to 5,000mg/L), Ca (2,000 to less than 250mg/L) and Mg (800 to less than 100mg/L) along with a corresponding increase for HCO_3 (200 to 900mg/L). The temperatures vary between 12°C at 275m and 40°C at 1,025m.

1.3.2.2 The Colorado Aquitard System

The Colorado Shale forms a thick aquitard system overlying the oil bearing Mannville aquifer. The thickness of the formation is estimated at about 300m in the study area, with a regional variation range from about 60m to 700m. The Colorado Shale is believed to form an effective hydrogeologic barrier between the exploited bitumen deposits within the Clearwater formation, and the overlying Quaternary aquifers.

The base of the Colorado Shale is formed by the Joli Fou aquitard. The Joli Fou aquitard has an average thickness of 26m and covers the whole study area. Its vertical hydraulic conductivity was estimated at 4.6×10^{-14} m/s (Hitchon et al., 1989).

The Joli Fou aquitard is overlain by the Viking aquifer. The Viking aquifer has an average thickness of 10m, comprising an aggregate of several thin sandstones. The flow directions vary locally without a general noticeable trend. The average horizontal hydraulic conductivity is estimated at 4.1×10^{-7} m/s. The TDS contents decrease gradually from 60,000mg/L in the south to 10,000mg/L in the northern area. Corresponding decreases for Cl (40,000 to 10,000mg/L), Ca (2,000 to less than 250mg/L) and Mg (800 to less than 100mg/L) are observed.

Table 1.5 Hydrogeological data from recent monitoring wells completed in the fractured upper zone of the Colorado Shale around the Imperial Oil Cold Lake Operations (Imperial Oil, 1998)

Stratigraphic Unit →	Colorado Shale		Second White Specks
Well No →	GEW 97-3	MAS 97-10	REG 96-2
Cl (mg/L)	5,100 – 5,150	3,460-3,800	9,830 -10,800
TDS (mg/L)	8,999	5,879	16,271
Hydraulic conductivity (m/s)	1.3×10^{-7}	7.9×10^{-7}	3.8×10^{-8}

Above the Viking sandstones are dominantly argillaceous strata with minor porous zones and low hydraulic conductivity. The vertical flow in the Colorado aquitard system is mostly downward, driven by the head difference between the Quaternary and the Mannville aquifer (Hitchon et al., 1989). However, from the recent investigations around the Imperial Oil Cold Lake operation, Imperial Oil (1998) has indicated that an upward

gradient exists in the upper fractured part of the Colorado Shale in the southern part of the study area.

Very few water analysis from the Colorado shale are available due to the difficulty of recovering formation water. From the data published by Hitchon et al. (1989), it appears that the salinity is always dominated by sodium chloride (Table 1.6). It is generally assumed that the chemical composition of the waters in the Colorado aquiclude ranges between those in the Viking formation and those in the Quaternary fresh water aquifers. Table 1.5 displays data from the recent investigations conducted by Imperial Oil (1998) which confirm the dominance of sodium chloride in the TDS content. The regional temperatures range from 15°C at 133m to 34°C at 770m.

Table 1.6 Chemical composition of water samples from the Colorado aquitard
(Hitchon et al., 1989)

Stratigraphic Unit →	Base of Fish Scales	Base of Fish Scales	Lea Park
Na (mg/L)	22,280	12,004	3,713
Ca (mg/L)	1,800	586	160
Mg (mg/L)	790	307	32
Cl (mg/L)	40,000	20,240	5,920
HCO ₃ (mg/L)	303	327	288
SO ₄ (mg/L)	2	25	23
TDS (mg/L)	67,605	35,180	10,440

1.3.2.3 Fracture Systems in the Upper Colorado Shale

As part of an investigation program implemented in the Cold Lake Area by Imperial Oil (1997 and 1998), a total of 20 wells were subjected to fracture mapping to define the presence and the orientation of fractures in the Colorado Shale. The formation micro-imaging (FMI) logging technology was used for the study. The FMI tool is a micro-

resistivity logging instrument with multiple sensors deployed about the circumference of the borehole.

Figure 1.5 Fracture orientation sets used for the evaluation of D & E Pad fracture systems in Cold Lake (Imperial Oil, 1998)

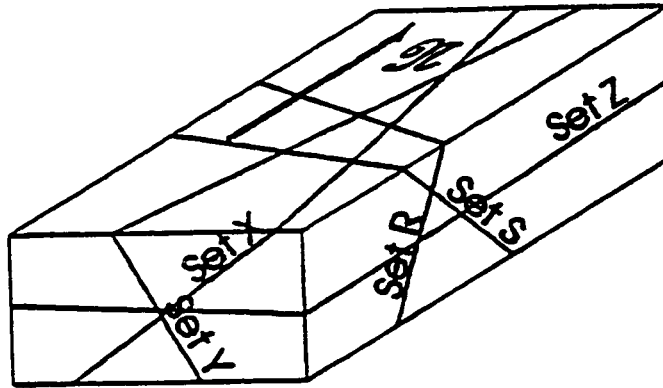


Figure 1.6 Stereographic plot of the fracture sets (Imperial Oil, 1998)

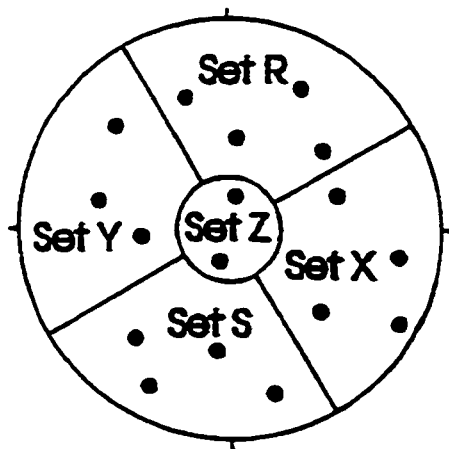
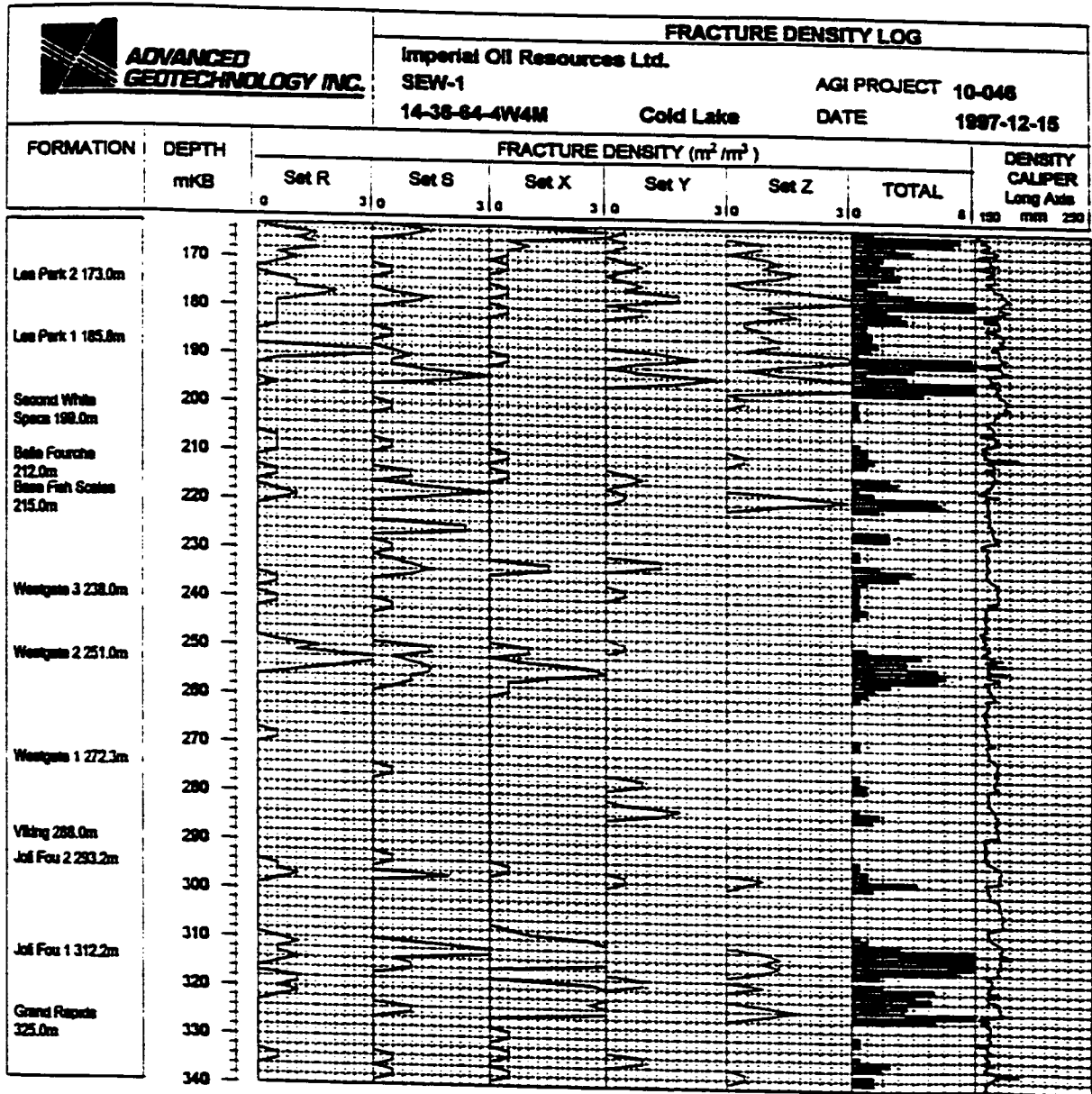


Figure 1.7 Fracture density log in one of the wells in Cold Lake (Imperial Oil, 1998)



The fractures were classified into sets of conjugated fractures as indicated in Figure 1.5. A stereographic plot of the fractures with their subdivisions is displayed in Figure 1.6. Data recorded from one of the wells, and interpreted in terms of fracture density, are given in Figure 1.7.

It was concluded from this study that fractures appear at different depths in the Colorado Group. The upper 20 to 30m of the Lea Park and Colorado Shale formations were consistently found to have the highest density of fractures. Horizontal fractures (set Z) are predominant in the upper stratigraphic portion of the Colorado Shale (Figure 1.7). Fractures inclined from 20 to 70 degrees are also significantly present in the formation. According to Imperial Oil (1998), these fractures were most likely induced by glacial loading and unloading cycles. Some of them might be related to tectonic events that shaped the structure of Western Canada. The fractures consistently observed in the upper part of the Colorado Shale are consistent with elevated hydraulic conductivities, in the order of 10^{-8} to 10^{-7} m/s, commonly encountered in the formation (Table 1.5). These permeability values are comparable to any bedrock aquifer.

1.3.2.4 Quaternary Aquifers

The Quaternary formations in the Cold Lake area form an alternating sequence of aquifers and aquitards that were previously presented in Table 1.2. Recent investigations (Imperial Oil 1997 and 1998; Tang 1998) around the Imperial Oil Operations allowed the gathering of a large amount of data on a number of hydraulic and chemical parameters. As the numerical models presented further in this study are calibrated against results obtained during these investigations, the main findings relevant to this study are given in this paragraph. Hydraulic and chemical parameters are summarized in Table 1.7. Corresponding well numbers indicated in Table 1.7 are found on the maps produced by Imperial Oil (1998) and referred to as Figures 1.8 through 1.11 in this study.

Five main Quaternary aquifer formations were recognized in the study area during the investigations conducted by Imperial Oil (1998): from top to bottom, the Sand River Formation, the Beaver River interval, the Muriel Lake Formation, the Empress Formation Unit 3 and the Empress Formation Unit 1. As indicated earlier in subsection 1.3.1, the sedimentation of the lower Quaternary formations was strongly influenced by topographic irregularities on the surface of the bedrock caused by the post-Cretaceous thalweg network erosion. As a consequence of the irregular bedrock surface, the three lower Quaternary aquifers, Muriel Lake, Empress Formation Unit 3 and Empress Formation Unit 1, were found in contact with the Colorado Shale bedrock.

The Empress Formation Unit 1 was the most influenced by the topography of the bedrock. According to the interpretation of Imperial Oil (1998) for the study area, its sedimentation was almost restricted to the main channels of the Helina, Beverly and Sinclair valleys created on top of the bedrock by the post-Cretaceous erosion (Figure 1.8). The lateral hydraulic flow is generally oriented eastward and is controlled by these channels.

The channel control of the bedrock is still present but less visible for the occurrence of Empress Formation - Unit 3 (Figure 1.9). The flow is dictated by a groundwater mound centered close to the Marie Highland, at the south of the Imperial Oil Leming plant. The flow enters the study area from the north and diverges on a semi-radial pattern to the south of the Maskwa Plant. This groundwater mound is interpreted in connection with a recharge from shallower units via some kind of hydraulic communication, either downcutting channels or other unidentified pathways (Imperial Oil, 1998).

The groundwater flow patterns in the Muriel Lake Formation, locally named the Durlingville aquifer, are similar to those observed in the Empress Formation - Unit 3, and are strongly controlled by the groundwater mound beneath the Marie Highland (Figure 1.10). The influence of the bedrock topography on the deposition is somewhat evident,

but less than for the Empress Formation Unit 3. The only locations where the Muriel Lake Formation is resting on top of the bedrock are the uppermost high points of the bedrock, in the southern half of the study area (Imperial Oil, 1998).

Table 1.7 Hydraulic and chemical properties of Quaternary aquifers around the Imperial Oil Cold Lake Operations (Imperial Oil, 1998)

Investigated Formation and Well No	Measured hydraulic conductivity (m/s)	Local lateral gradient (m/m)	Assumed effective porosity (%)	Calculated velocity (m/year)	Total Dissolved Solids (mg/L)	Chloride content (mg/L)
Sand River Formation						
MAH 92-2					450	<0.5-2.2
REG 96-5					357	<0.5-1.9
Beaver River Interval -Ethel Lake						
MAS 92-3					426	<0.5-2.4
MAH 92-4					454	<0.5-2.0
REG 96-1					993	4.7-7.3
REG 96-4	1.0×10^{-4}	0.002	25	25	424	<0.5-2.7
Beaver River Interval – Bonnyville Unit 1						
REG 96-3	6.2×10^{-5}	0.004	20	39	516	3.3-6.3
REG 96-4	3.9×10^{-5}	0.002	20	12	328	<0.5-1.4
GEW 97-6	8.3×10^{-5}	0.006	20	78	420	1.4-3.5
GEW 97-7	1.2×10^{-4}	0.010	25	151	817	20.8-49.4
GEW 97-8	7.0×10^{-8}	0.010	15	<1	852	12.0-15.7
Muriel Lake Formation – Durlingville						
MAS 92-5	4.4×10^{-5}	0.005	20	35	427	<0.5-2.2
MAH 92-6					746	8.8-12.0
REG 96-1	1.8×10^{-5}	0.008	20	23	539	20.9-29.5
REG 96-2	1.2×10^{-5}	0.010	20	19	1,159	76.0-85.2
REG 96-3	2.7×10^{-6}	0.003	15	2	506	5.8-9.3
GEW 97-2					1,185	59.3-80.8
GEW 97-3	5.8×10^{-6}	0.010	15	12	746	19.3-23.2

Table 1.7 (continued)

Investigated Formation and Well No	Measured hydraulic conductivity (m/s)	Local lateral gradient (m/m)	Assumed effective porosity (%)	Calculated velocity (m/year)	Total Dissolved Solids (mg/L)	Chloride content (mg/L)
Muriel Lake Formation - Durlingville (continued)						
GEW 97-4	3.3×10^{-4}	0.003	25	125	598	5.8-7.1
GEW 97-5	4.5×10^{-5}	0.010	20	71	811	48.5-53.6
GEW 97-6	6.5×10^{-5}	0.007	20	72	512	1.9-3.2
GEW 97-10					558	6.2-9.0
GEW 97-11	7.9×10^{-5}	0.009	20	112	828	32.4-36.4
GEW 97-12	1.5×10^{-5}	0.009	20	21	648	5.2-5.6
Empress Formation - Unit 3						
MAS 92-7	4.7×10^{-7}	0.002	15	<1	716	13.6-17.6
MAH 92-8					884	10.8-51.1
REG 96-1	5.5×10^{-5}	0.010	20	87	630	25.3-41.0
REG 96-3	3.9×10^{-5}	0.005	20	31		246-656
REG 96-4	2.2×10^{-6}	0.006	15	3	853	49.0-66.1
GEW 97-1					995	113-141
GEW 97-3	4.9×10^{-5}	0.007	20	54	1,653	664-777
GEW 97-4	2.8×10^{-7}	0.005	15	<1	1,413	669-1,320
GEW 97-8	1.7×10^{-7}	0.009	15	<1	931	9.5-13.2
GEW 97-9					869	1.5-8.3
GEW 97-11					881	265-314
GEW 97-12	1.9×10^{-4}	0.006	25	144	669	22.7-39.0
Empress Formation - Unit 1						
MAS 92-9	1.0×10^{-4}	0.002	25	25	488	<0.5-5.5
MAH 92-10					661	25.9-30.7
REG 96-1					1,093	28.0-592
REG 96-2						540-623
REG 96-4	2.7×10^{-7}	0.001	15	<1	837	42.8-596
P2 97-1	7.6×10^{-5}	0.004	20	48		

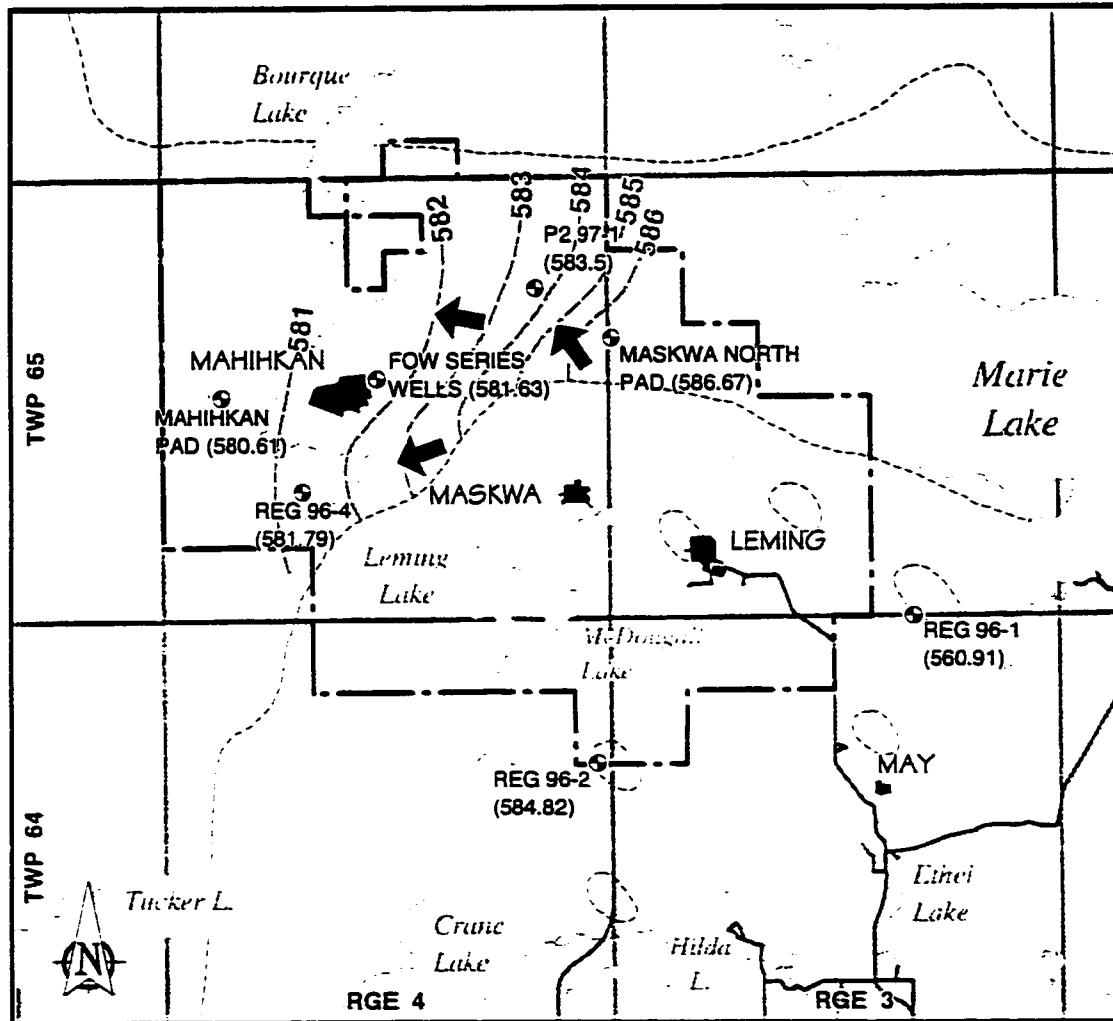
The Beaver River Interval is composed of two main formations including the Bonnyville Unit 1 and the Ethel Lake Formation. Because the sands within both these formations exhibit similar groundwater elevations and hydraulic characteristics, they are treated as a single hydrostratigraphic unit. The influence from the groundwater mound beneath the Marie Highland is still observable (Figure 1.11). Lateral flow is again outward from the mound and predominantly to the southwest, south and southeast.

The Sand River Formation is mainly restricted to the southern and the eastern portions of the study area. This formation was not targeted by the investigations, as it is generally not present beneath the Cold Lake Imperial Oil Operations.

Despite the unavailability of anisotropy data, flow in the aquifers is assumed to be mainly horizontal. The vertical flow is generally downward in the northern part of the study area, in accordance with the recharging character observed in that area. Conversely, the vertical flow is generally upward in the southern part, suggesting an overall discharging zone.

The hydraulic conductivities measured in Quaternary aquifers range from $7.0 \times 10^{-8} \text{ m/s}$ to $2.0 \times 10^{-4} \text{ m/s}$ with an average conductivity in the interval between 10^{-6} and 10^{-5} m/s (Table 1.7). These permeability values appear 2 to 3 orders higher than in the bedrock aquifers. Corresponding local velocities measured from well tests in Quaternary aquifers vary between 0 to 150m per year. The effective porosity is assumed to range from 15 to 25% with an average of 20%.

Figure 1.8 Piezometric contours and flow directions in the Empress Formation
Unit 1 aquifer (Imperial Oil, 1998)

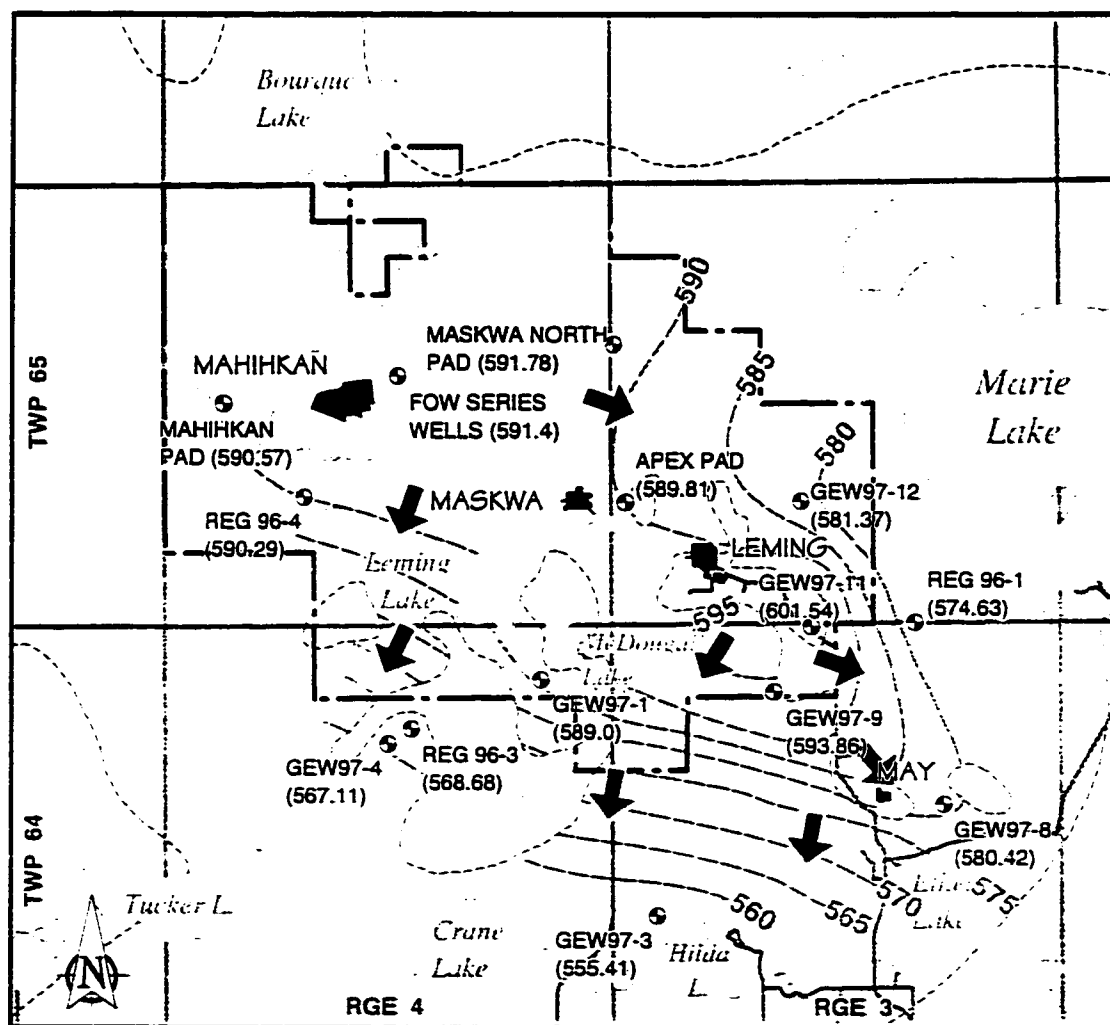


Legend

- | | | | |
|---|--|-------|---|
| ● | Monitoring well and groundwater elevation (masl) | ➔ | Inferred groundwater flow direction |
| □ | Disposition and extent of aquifer (interpreted) | —586— | Groundwater surface elevation contour line (masl) |

0 5 km

Figure 1.9 Piezometric contours and flow directions in the Empress Formation Unit 3 aquifer (Imperial Oil, 1998)



Legend

- Monitoring well and groundwater elevation (masl)
- Disposition and extent of aquifer (interpreted)



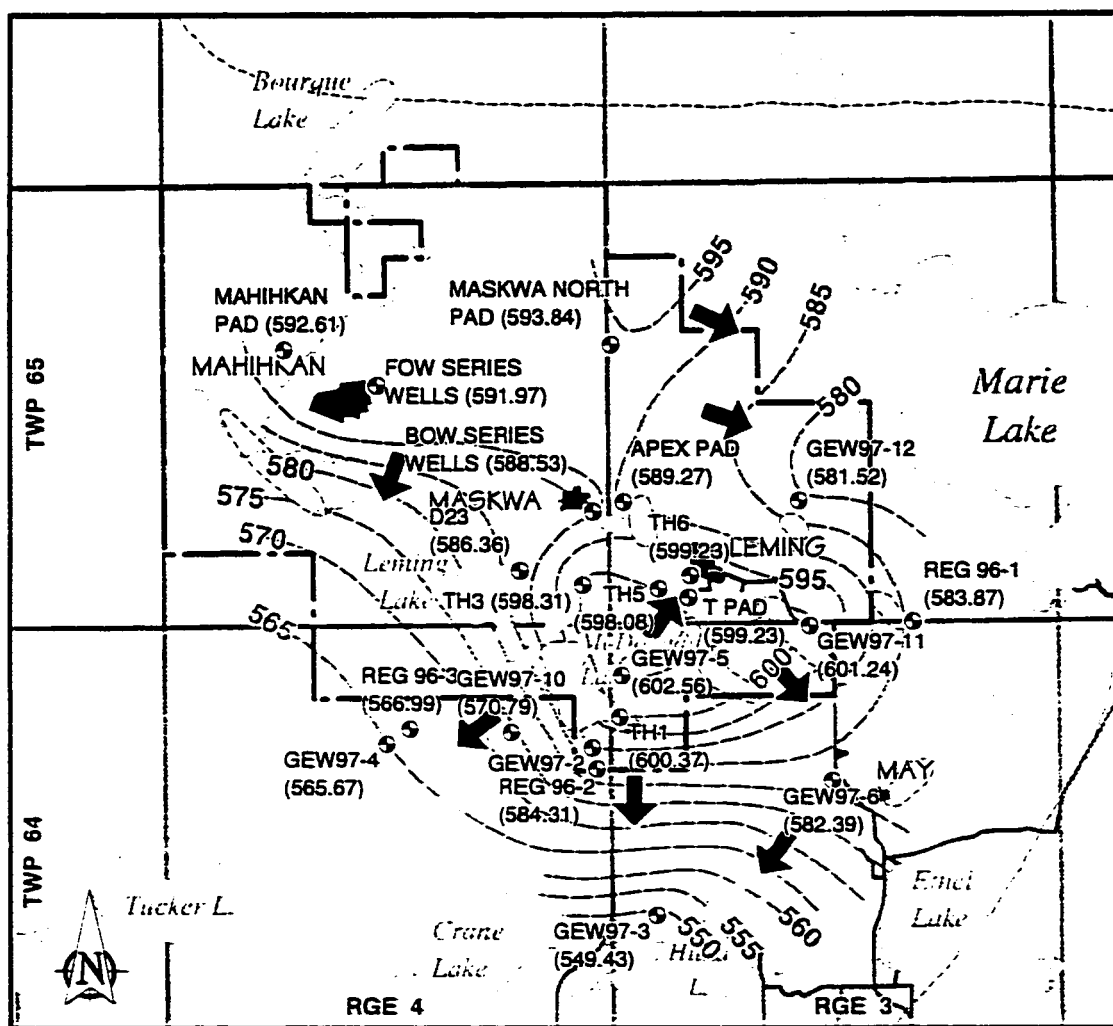
Inferred groundwater flow direction

—586—

Groundwater surface elevation contour line (masl)

0 5 km

Figure 1.10 Piezometric contours and flow directions in the Muriel Lake Formation aquifer (Imperial Oil, 1998)



Legend



Monitoring well and groundwater elevation (masl)



Disposition and extent of aquifer (interpreted)



Inferred groundwater flow direction

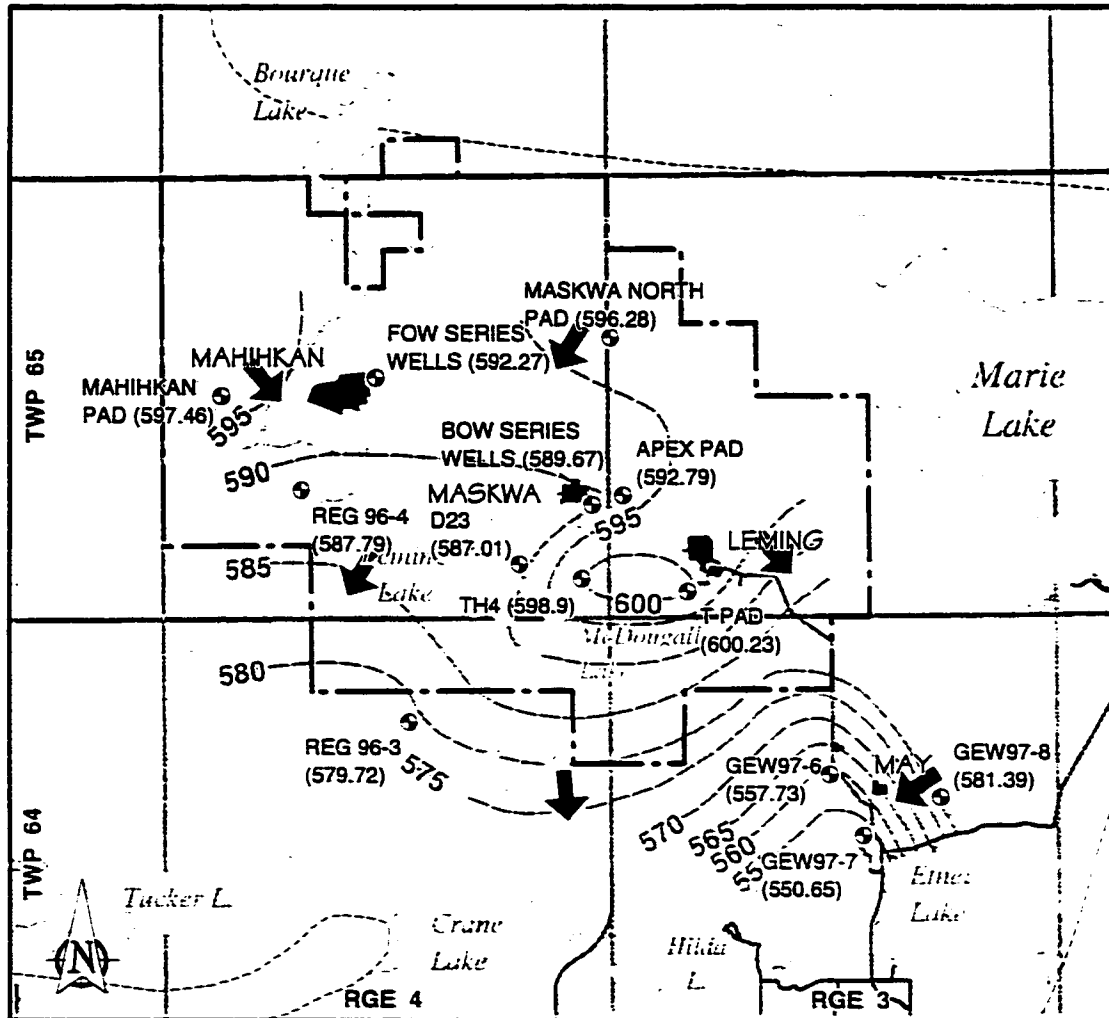


Groundwater surface elevation contour line (masl)

0

5 km

Figure 1.11 Piezometric contours and flow directions in the Beaver River Interval aquifer (Imperial Oil, 1998)



Legend

- | | | | |
|---|--|-------|---|
| ⊙ | Monitoring well and groundwater elevation (masl) | ➔ | Inferred groundwater flow direction |
| □ | Disposition and extent of aquifer (interpreted) | —586— | Groundwater surface elevation contour line (masl) |

0 5 km

As suggested by the data displayed in Table 1.7, the continental origin of the Quaternary formations is expressed by much lower TDS and chloride content than the underlying bedrock, making them suitable for groundwater supply. In many cases, the amount of chloride ions in the water is typically less than 10mg/L. Unlike the bedrock where the TDS content is dominated by sodium chloride, dissolved solids in Quaternary formations consist mainly of HCO_3^- ions. However, the chloride content increases gradually with depth. In the three lower aquifers, chloride contents above the expected levels were consistently recorded. Values attaining hundreds of mg/L were found in a number of areas near the bedrock. A maximum value of 1,320mg/L was obtained in the Empress Unit 3 Formation (Table 1.7). It appears at the same time that the TDS content becomes increasingly dominated by chloride ions, suggesting a bedrock influence. The bedrock signature in the bottom Quaternary aquifers was also suggested by a stable boron isotope study and review of selected ion ratios (Imperial Oil, 1998) that indicated a compositional transition from meteoric to bedrock water with an increasing bedrock fingerprint towards the bottom of the Quaternary.

1.3.3 Importance of Geological and Hydrogeological Data for the Modeling Study

The geological and hydrogeological information presented in this chapter includes available data on both the bedrock formations and the Quaternary strata. This information was designed to give a complete overview of geological features occurring in the area, which constitute the basic foundation for the models presented later in this work.

The data provided in the above sections pertain to three three main topics: (i) the geological constitution, (ii) the hydraulic parameters and, (iii) the water chemistry. The data were presented considering the three main geological subdivisions relevant to this study: the bedrock, the Colorado Shale and the Quaternary formations.

Above the basal Cambrian Sandstone, the bedrock is made up of large series of Devonian evaporitic formations underlying relatively thick layers of Cretaceous clastic sequences. The upper Cretaceous Colorado Shale and the Lea Park formations form the upper part of the bedrock. The evaporitic composition of the lower part of the bedrock appears to have an important influence on the water salinity of the whole bedrock sequence, with the upper clastic layers included. The total dissolved solids (TDS) content is consistently dominated by sodium chloride from the bottom to the top of the bedrock regardless of the lithology. The amount of chloride ions decreases progressively from more than 150,000mg/L in the Cambrian sandstone to about 5,000mg/L or less in the upper part of the Cretaceous Colorado Shale. It appears for modeling purposes that the bedrock has an endless source of chloride.

The Colorado Shale forms the most important clastic aquiclude in the bedrock. It forms a thick argillaceous sequence characterized by low permeabilities with very few fine-grained to silty sand layers. This interval is considered as an effective hydraulic barrier between the Clearwater bitumen formations and the Quaternary aquifers. The hydraulic conductivity increases significantly in the upper 20 to 30m of the formation where a high density of fractures was consistently observed. In the modeling process, fractured and non-fractured shale are considered as two separate layers with different hydraulic characteristics.

The salinity in the Colorado shale is dominated by sodium chloride, as with the rest of the bedrock formations. The water chloride content decreases from about 40,000mg/L in the bottom layers to about 5,000mg/L or less in the upper fractured part. This range of values will be considered for the determination of initial values to include in the models.

An important chemical contrast was observed between the continental Quaternary sediments with relatively fresh water and the evaporitic and marine formations of the bedrock with brackish water. The water-rock interaction process between the Colorado

Shale and the Quaternary aquifers forms the main purpose of this study. Available chemical and hydraulic data for the two stratigraphic series were detailed in the geological section to provide a substantial foundation for the models.

CHAPTER TWO

THEORETICAL AND EXPERIMENTAL STUDIES OF FLUID AND SOLUTE FLOW IN THE COLORADO SHALE

2.1 State of Water in a Shale Microstructure

A schematic description of the microstructure of a high-density clay or shale on the basis of clay mineralogy is shown in Figure 2.1 (Gens and Alonso, 1992; Hueckel, 1992). The data that are used in this paragraph were collected by Wong and Wang (1997), for the development of a three-dimensional swelling model for a clay shale. They highlighted three basic micro-fabric features: elementary particle clusters, particle assemblages and pore spaces.

The elementary particle clusters are made up of clay particles or minerals in parallel configuration. Silt or sand particles may be also present in various concentrations. Water absorbed within the clay parallel structure cannot flow in ambient conditions and is referred to as inter-lamellar water. The particle assemblages are formed by arrays of elementary particle clusters. The pore space is made up of intra-matrix pores existing between elementary particle clusters. Water present in the pore space can take two different forms: free water and inter-cluster water. Free water is able to move due to

hydraulic gradients. Inter-cluster water enveloping particle clusters is restricted from flowing under normal conditions.

Figure 2.1 Shale fabric structure (Wong and Wang, 1997)

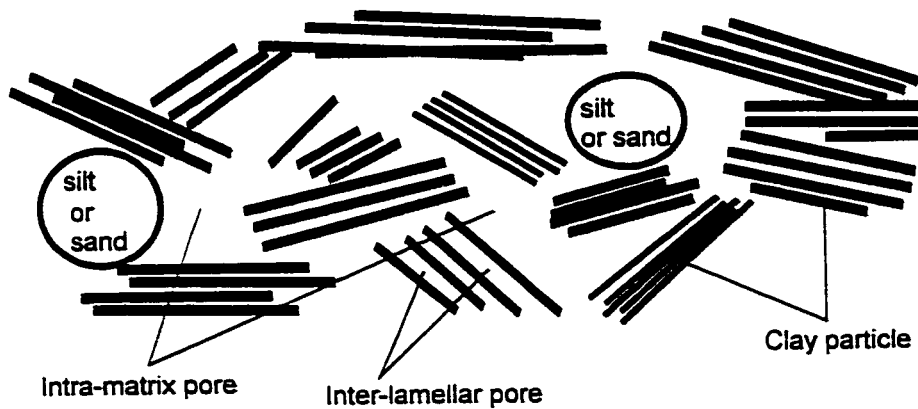
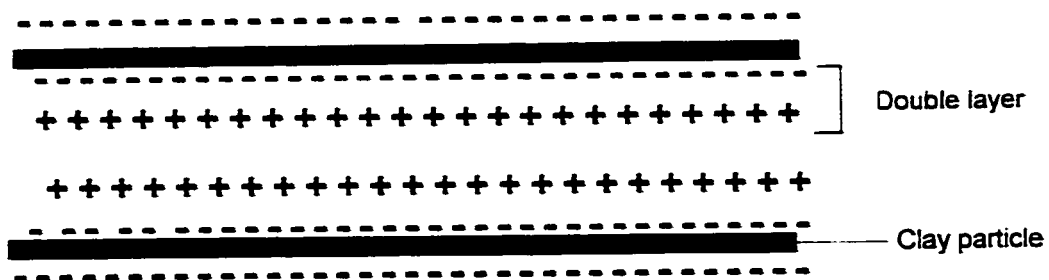


Figure 2.2 Double layers near clay particles



The surfaces of clay mineral particles carry residual negative charges, mainly as a result of the isomorphous substitution of aluminum or silicon atoms by atoms of lower valency. Negative charges in clay minerals can also be sometimes related to the dissociation of hydroxyl ions. As a consequence of the negative charge, cations present in the water are

being attracted to the particles, but at the same time, the cations tend to move away from each other because of their thermal energy. The net result is that the cations form a dispersed layer adjacent to the particle, with the cation concentration decreasing with increasing distance from the surface until the concentration becomes equal to that existing in normal water in the void space (Figure 2.2).

The negatively charged particle surface and the dispersed layer of cations form the “diffuse layer”. For a given particle, the thickness of the cation layer depends mainly on the valency and concentration of cations. A valency decrease (due to cation exchange) or a decrease in concentration will result in an increase in layer thickness.

2.2 Flow Mechanisms in a Shale

2.2.1 Fluid Flow

2.2.1.1 Fluid Flow under Hydraulic Gradient

In a shale, flow may occur under hydraulic gradient according to the Darcy’s law, meaning that the amount of flow in a porous media is proportional to the hydraulic conductivity of the water and the gradient of the total hydraulic head. This is expressed by the equation

$$q_w = k_h \nabla(-h) \quad (2.1)$$

where

q_w is the flow or flux of fluid in the porous media under a hydraulic gradient

k_h is the hydraulic conductivity (or permeability) coefficient of the water

h is the total hydraulic head

Despite the lack of reliable measurements, the hydraulic conductivity for non-fractured Colorado Shale is generally low. It is estimated between 10^{-9} m/s and 10^{-13} m/s (10^{-4} to 10^{-8} darcy) in similar materials (Driscoll, 1989). The horizontal conductivity is generally 1 or 2 orders higher than the vertical permeability, due to the strong anisotropy related to the lamellar structure of the shale (Bachu et al., 1989; Hitchon et al., 1989). The permeability can be substantially increased if the shale is fractured. Hydraulic conductivities were found in the range of 10^{-8} to 10^{-7} m/s (10^{-3} to 10^{-2} darcy) in the upper 20 to 30m of the Colorado Shale in Cold Lake due to the high density of fracturing in that portion of the formation (Imperial Oil, 1998).

2.2.1.2 Fluid Flow under Chemico-Osmotic Gradient

Data collected in chapter 1 indicate that the Colorado Shale contains high chloride concentrations. According to available chemical analysis, the chloride content varies from about 40,000mg/L in the bottom layers, to about 5,000mg/L or less in the upper fractured part of the shale. In contact with the fresh water of the Quaternary aquifers, an important chemical gradient occurs between the intra-matrix pore water of the shale and the fresh water. In response to the chemical gradient, a negative osmotic pressure develops in the shale causing the water to enter the clay structure. The introduction of water into the shale triggers the swelling process and the chemistry change in the intra-matrix water. In turn, the change in pore fluid chemistry causes the flow of the inter-lamellar water. Barbour and Fredlund (1989) suggested that the osmotic pressure concept relates the change in repulsive stress in clay particles to the change in the osmotic pressure difference between the inter-lamellar and the intra-matrix fluids. In a subsequent stage, water is released from the shale due to osmotic consolidation. The osmotic hydraulic flow is assumed to obey a law similar to Darcy's law, and is given by the equation,

$$q_{w2} = k_c \nabla(-\pi) \quad (2.2)$$

where

q_{w2} is the flux of fluid in the porous media under the osmotic pressure π

k_c is the osmotic permeability coefficient.

The osmotic permeability coefficient is often considered as a fraction of the hydraulic conductivity (Mitchell, 1993) so that the above relation can be expressed as

$$q_{w2} = \phi k_h \nabla(-\pi) \quad (2.3)$$

where

$\phi \left(= \frac{k_c}{k_h} \right)$ is the osmotic efficiency of the porous material.

The osmotic pressure is generally approximated by the Van't Hoff relation (Metten, 1966),

$$\pi = RT_e C \quad (2.4)$$

where,

R is the universal gas constant ($= 8.31450 \text{ m}^3 \text{ Pa/K}$)

T_e is the absolute temperature ($^{\circ}\text{K}$).

C is the concentration difference between the porous material and the datum: in this study, the concentration datum was fixed at 0.

If the clay behaves like a perfect semi-permeable membrane, only water will be transferred excluding the solute. In contrast, if the clay is leaky, the flowing water will carry some solute with it, depending on the osmotic efficiency. Barbour and Fredlund (1989) indicated that osmotic efficiency is strongly dependent on pore fluid chemistry, pore fluid concentration, void ratio, and inter-particle spacing. High osmotic efficiencies have been observed only at low pore fluid concentrations, or low void ratios. Olsen (1972) followed by Mitchell et al. (1973) suggested that a significant portion of the total

groundwater flow through deeply buried sediments should be attributable to chemico-osmotic gradients.

2.2.2 Solute flow

2.2.2.1 Solute Flow by Diffusion

Diffusion is the process by which both ionic and molecular species dissolved in the fluid move from areas of higher concentration to areas of lower concentration (Fetter, 1994). In one dimension and under steady state conditions, the flux of a solute is described by the Fick's law as follows:

$$q_s = -D \frac{\partial C}{\partial z} \quad (2.5)$$

where

q_s is the mass flux of solute per unit area per unit time

D is the diffusion coefficient

$\frac{\partial C}{\partial z}$ is the concentration gradient

When the concentrations are changing with time, the Fick's law is applied as follows in one dimension:

$$\frac{\partial C}{\partial t} = D \frac{\partial^2 C}{\partial z^2} \quad (2.6)$$

where

$\frac{\partial C}{\partial t}$ is the change in concentration with time.

In water, the values of D for the major ions range from 1.0×10^{-9} to $2.0 \times 10^{-9} \text{ m}^2/\text{s}$ (Fetter, 1994). In porous media, the diffusion is slower due to longer pathways followed by the ions as they travel around mineral grains. The effective diffusion coefficient D^* can be determined from the relation

$$D^* = wD \quad (2.7)$$

where

w is an empirical coefficient determined by laboratory experiments.

Freeze and Cherry (1979) indicated that the value of w , for ions that are not adsorbed onto mineral surfaces, ranges from 0.5 to 0.01. These numbers are lower if adsorption occurs. In this case, there is retardation.

Solutes can move through the porous media even when the groundwater is not moving. In materials with low water velocities, solutes may travel faster by diffusion compared to the groundwater itself.

2.2.2.2 The Dispersion Process

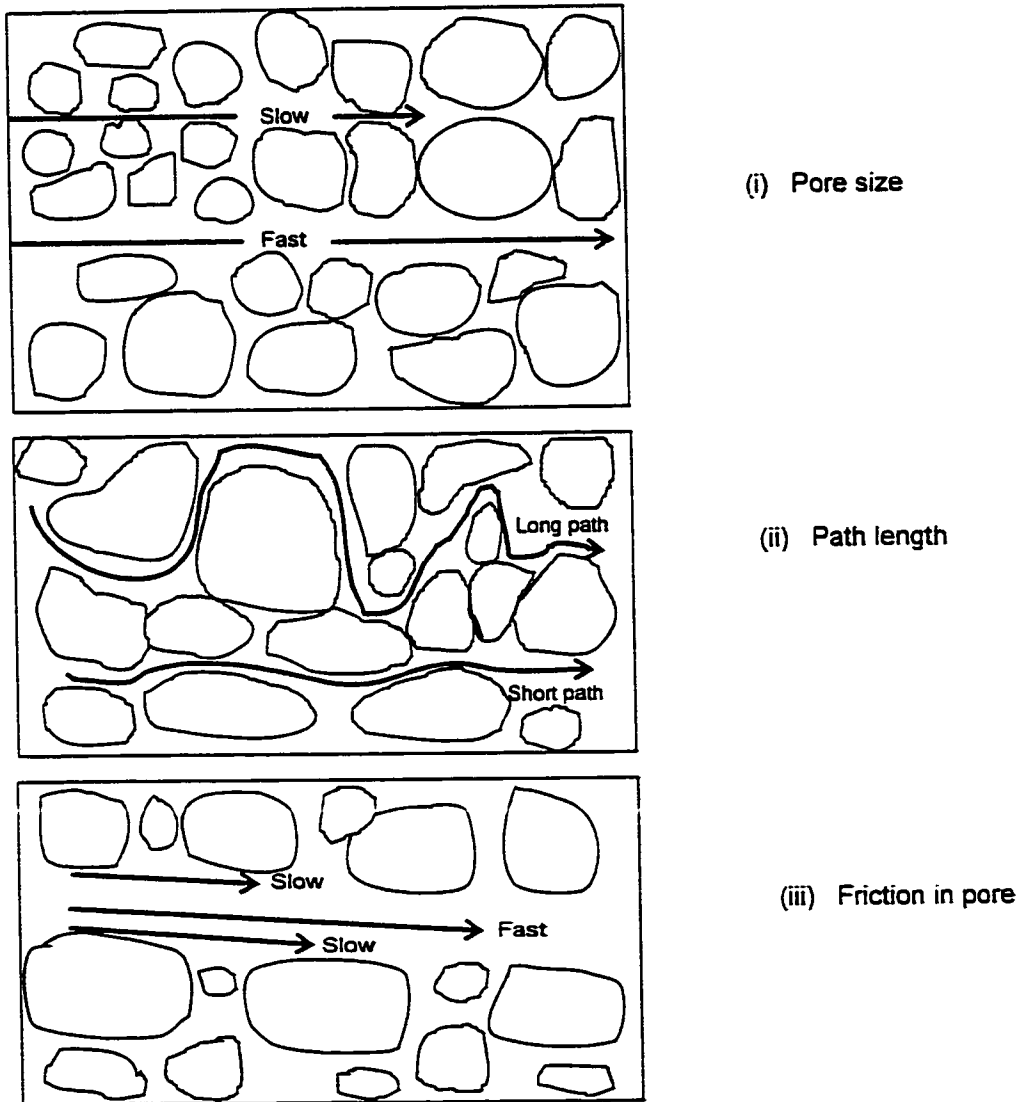
Dispersion is a mechanical process of mixing of solute with non-contaminated water as a result of deviations of actual velocity on a micro-scale from the average groundwater velocity. The mixing along the streamline of the fluid flow is called longitudinal dispersion. In cases where that mixing is normal to the pathways of the fluid flow, it is called lateral dispersion.

As illustrated in Figure 2.3, longitudinal dispersion is mainly caused by (Fetter, 1994):

- (i) fluid travelling faster through larger pores than in smaller pores;
- (ii) fluid travelling longer pathways than other fluid; and

- (iii) fluid moving faster through the center of the pore than along the edges due to the friction.

Figure 2.3 Factors causing pore-scale longitudinal dispersion (Fetter, 1994)



The longitudinal mechanical dispersion of a solution is given by the relation

$$\text{Mechanical dispersion} = \alpha_L v_x \quad (2.8)$$

where

v_x is the average linear velocity

α_L is the dynamic longitudinal dispersivity coefficient.

The dispersivity is strongly dependent on the distance over which it is measured. Neuman (1990) conducted a statistical distribution study on over 130 longitudinal dispersivities from laboratory and field tracer data in porous and fractured media published by researchers throughout the world (Lallemant-Barres and Peaudecerf, 1978; Pickens and Grisak, 1981; Gelhar, 1986; Arya, 1986; and Arya et al., 1988). He concluded that the apparent longitudinal dynamic dispersivity α_L and the flow length L could be approximated by the following equations:

$$\alpha_L = 0.0175L^{1.46} \quad \text{for } L \leq 3,500\text{m} \quad (2.9)$$

$$\alpha_L = 0.0169L^{1.53} \quad \text{for } L \leq 100\text{m} \quad (2.10)$$

Pickens and Grisak (1981) proposed that the longitudinal dispersivity can be accurately estimated by the relation

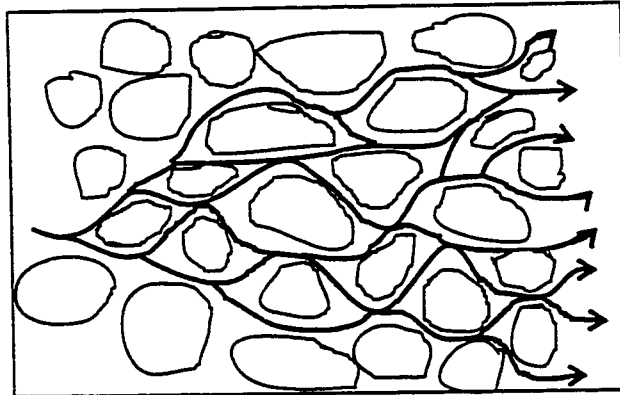
$$\alpha_L = 0.1L$$

where

L is the flow length

Lateral dispersion is related to the fact that the travelling fluid can split and branch out to the side of the regular flow paths (Figure 2.4).

Figure 2.4 Flow path causing lateral hydrodynamic dispersion (Fetter, 1994)



2.2.2.3 The Hydrodynamic Dispersion

In the field, the processes of diffusion and mechanical dispersion cannot be separated. The hydrodynamic dispersion coefficient is used to account the effects of both the molecular diffusion and the mechanical mixing. For one-dimensional flow, this is represented by the relation:

$$D_L = \alpha_L v_x + D^* \quad (2.11)$$

where

D_L is the coefficient of hydrodynamic dispersion

α_L is the dynamic dispersivity

v_x is the average linear groundwater velocity

D^* is the effective molecular diffusion coefficient defined in relation (2.7)

In three-dimensional problems, longitudinal, lateral and vertical dispersivities are considered. In transport models, the transverse and vertical dispersivities are accounted for as fractions of a fixed value of the longitudinal dispersivity. Field measurements in

granular material and data collected by Pinder (1973), Konikow and Bredehoeft (1974), Fried (1975), Robson (1978), and Wilson and Miller (1978) indicate a ratio of the lateral dispersivity over the longitudinal dispersivity varying between 0.003 and 0.3. The overall average ratio value is often considered around 0.1 according to experiments conducted by Freyberg (1986) and observations made by Bush (1988).

The ratio of the vertical dispersivity over the longitudinal is generally considered negligible (Freyberg, 1986 and Mackay et al. 1986), unless vertical velocities are significantly high compared to the longitudinal flow. In many regular field cases, the vertical hydrodynamic dispersivity is assumed equal to the molecular diffusion coefficient (Sudicky, 1983). The mechanical dispersivity term in equation (2.11) becomes negligible to the molecular diffusion term.

As far as longitudinal and lateral dispersivities are considered in the field, the molecular diffusion effect is generally secondary and negligible compared to the mechanical dispersion effect. It only becomes important when groundwater velocity is very low. In cases where the water is not flowing (very low permeability or absence of hydraulic gradient), the hydrodynamic dispersion is reduced to its molecular diffusion component.

2.2.2.4 Solute Flow by Advection

Advection is the process by which moving groundwater carries with it dissolved solutes. Advected solutes travel at the same rate as the linear velocity of ground water. The flow is governed by Darcy's law. In one dimension, this is expressed by the relation

$$v_x = \frac{k_h}{n_e} \frac{\partial h}{\partial z} \quad (2.12)$$

where

v_x is the average linear velocity

k_h is the hydraulic conductivity

n_e is the effective porosity

$\frac{\partial h}{\partial z}$ is the hydraulic gradient

For many problems involving contaminant transport, the advection term dominates. The degree of advection domination is commonly estimated by the Peclet number, which is defined as

$$P_e = \frac{|v|L}{D}$$

where

$|v|$ is the magnitude of the seepage velocity vector, $L T^{-1}$

L is a characteristic length, commonly taken as the grid cell width, L ;

D is the dispersion coefficient, $L^2 T^{-1}$

In advection dominated problems, the Peclet number has a large value. For pure advection problems, the Peclet number becomes infinite.

2.2.2.5 The Retardation Process

Retardation occurs when some ions are adsorbed on clay minerals or undergo some kind of degradation during the solute transport process. Solutes that are affected by retardation are called *reactive solutes*. On the other hand, some ions are not involved in any kind of reaction with the soil or the groundwater. These ions are termed *conservative* (Fetter, 1994).

(i) *Sorption*

Most clay minerals have an excess of imbalanced negative charges due to isomorphous replacements, broken bonds, or lattice defects (Fetter, 1994). Adsorption processes in soils involve mostly cations to satisfy the electrical balance. Adsorption is strong for shales because of their large surface area.

Models involving sorption assume equilibrium conditions between the solution and the solid. Sorption reactions are assumed to be fast enough relative to groundwater velocity so that they can be treated as instantaneous. A graphical plot of the amount of solute \bar{C} adsorbed by the soil, against the dissolved concentration C is called a *sorption isotherm*. An isotherm can be linear or non-linear. Non-linear isotherms are approximated in two ways: the Freundlich isotherm and the Langmuir isotherm.

The *linear sorption* assumes that the sorbed concentration \bar{C} is directly proportional to the dissolved concentration C as indicated by the following relation:

$$\bar{C} = K_d C \quad (2.13)$$

where

$$K_d = \frac{\partial \bar{C}}{\partial C} \text{ is the distribution coefficient, } L^3 M^{-1}.$$

The retardation factor is defined as

$$R_t = 1 + \frac{\rho_b}{\theta} \frac{\partial \bar{C}}{\partial C} = 1 + \frac{\rho_b}{\theta} K_d \quad (2.14)$$

where

ρ_b is the dry bulk mass density of the soil (M/L^3)

θ is the volumetric moisture content of the soil (dimensionless)

The Freundlich isotherm is a non-linear isotherm expressed as:

$$\bar{C} = K_f C^a \quad (2.15)$$

where

K_f is a Freundlich empirical constant, $(L^3 M^{-1})^a$

a is a Freundlich empirical exponent, dimensionless

Accordingly, the retardation factor for the Freundlich isotherm is defined as

$$R_t = 1 + \frac{\rho_b}{\theta} \frac{\partial \bar{C}}{\partial C} = 1 + \frac{\rho_b}{\theta} a K_f C^{a-1} \quad (2.16)$$

When a is equal to 1, the Freundlich isotherm is equivalent to the linear isotherm.

The Langmuir isotherm is also non-linear and defined as following

$$\bar{C} = \frac{K_l \bar{S} C}{1 + K_l C} \quad (2.17)$$

where

K_l is the Langmuir constant, $L^3 M^{-1}$

\bar{S} is the total concentration of sorption sites available, MM^{-1}

The retardation factor defined for the Langmuir isotherm is defined as

$$R_t = 1 + \frac{\rho_b}{\theta} \frac{\partial \bar{C}}{\partial C} = 1 + \frac{\rho_b}{\theta} \left[\frac{K_l \bar{S}}{(1 + K_l C)^2} \right] \quad (2.18)$$

The retardation factor might vary for different chemical species. If the contaminant source contains multiple solutes, each of them has a specific K_d and a specific solute front. The resulting plume can be complex.

(ii) *Degradation*

Degradation includes decay of the solute by chemical, biological and radioactive reactions. The rate of degradation for dissolved and adsorbed materials is expressed by the following relation

$$\text{Rate of degradation} = -\lambda \left(C + \frac{\rho_b}{\theta} \bar{C} \right) \quad (2.19)$$

where

$\lambda \left(= \frac{(\ln 2)}{t_{1/2}} \right)$ is the degradation rate constant

$t_{1/2}$ is the half-life of degradable materials.

However, for certain types of degradation, the rate constant for the dissolved and sorbed phases may be different. In this case, two rate constants are used, one for the dissolved phase (λ_1) and the other for the adsorbed phase (λ_2). The equation (2.19) becomes

$$\text{Rate of degradation} = -\lambda_1 C - \lambda_2 \frac{\rho_b}{\theta} \bar{C} \quad (2.20)$$

2.3 Laboratory Investigations

2.3.1 The Purpose of Experimental Investigations

Equation (2.11) shows that the solute flow involves the determination of two parameters: (i) the dynamic dispersivity, and (ii) the diffusion coefficient. While the dynamic dispersivity is generally approximated by Neuman's relations (2.9) and (2.10), the molecular diffusion coefficient is often determined by laboratory experiments. The main objective of the laboratory tests described in this section was to determine the molecular diffusion coefficient to be used to simulate the chloride transfer from the Colorado shale to upper Quaternary aquifers. The chloride concentration evolution was monitored in originally distilled water samples that were left in contact with the shale for a few months (Nzajibwami and Wong, 1998). The data obtained from the tests were history-matched with a chemico-osmotic model, in order to define the range of the molecular diffusion coefficient in the Colorado Shale. A study of the concentration and the pore pressure evolution during the osmotic flow process was performed as well. The tests were conducted at the Department of Civil Engineering, University of Calgary.

2.3.2 Experimental Procedures

A total of five samples of the Colorado Shale were analyzed. The size, weight and depth of analyzed samples is indicated in Table 2.1. For the first three samples (samples LP, MP and HP), a specific diffusion test apparatus was constructed as indicated in Figure 2.5. The contact with water was allowed on one side, at the bottom of the sample. For the last two samples (samples 3a and 3b), a regular swelling test apparatus was used and the sample was in contact with the sample on two faces, the bottom and the top (Figure 2.6). In both cases, the sides were never allowed to be in contact with water.

Table 2.1 Size and weight of the samples used for the laboratory tests

Sample No	Confining pressure		Weight (g)	Diameter (mm)	Height (mm)	Density (kg/m ³)	Depth (m)
	Time interval (days)	Loading (kPa)					
LP	0 - 106	0	608.3	88.19	48.61	2048.6	168.0
MP	0 - 106	500	623.3	88.06	50.38	2031.4	168.0
HP	0 - 106	1000	619.8	88.15	49.57	2048.8	168.0
3a	0 - 60	169	664.2	87.65	49.55	2221.6	303.5
	60 - 120	34					
3b	0 - 39	925	679.7	87.58	51.4	2195.1	303.5
	39 - 60	500					
	60 - 120	32					

For the first set of samples LP, MP and HP, a saturated Colorado Shale core was placed in the upper compartment of the loading cell (Figure 2.5). The size and the weight of the samples are displayed in Table 2.1. The diameter of the compartment was made to fit exactly with a 3½-inch diameter core. Confining pressures of 500 and 1000 kPa were applied to samples MP and HP during the whole monitoring program to determine if the confining pressure has any effect on the release of chlorides. The bottom and the top of the samples were lined with a thin metal screen and a filter paper. The lower compartment was filled with distilled water and air was purged to allow the water to get into contact with the bottom of the sample through a number of holes and grooves created in the cap separating the two media. The water level was limited to the bottom of the sample. The compartment was able to hold 850mL of water. A transparent tubing was set up on the side of the water compartment for chloride monitoring.

For the second set of two samples 3a and 3b, the loading varied during the test as indicated in Figure 2.7. The amount of water in the cell was 950mL.

Figure 2.5 **Equipment used for the diffusion test**

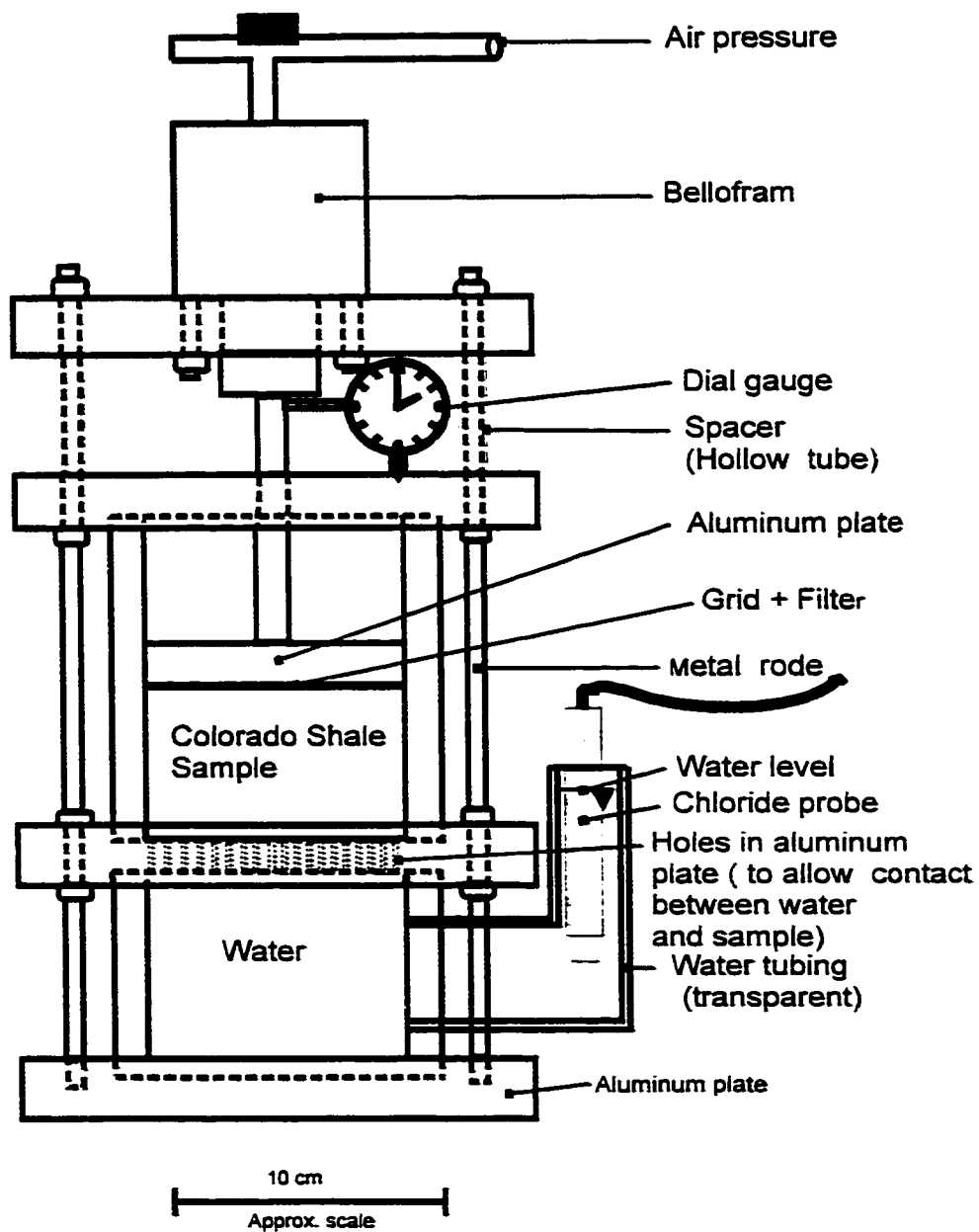


Figure 2.6 Experimental apparatus for swelling tests

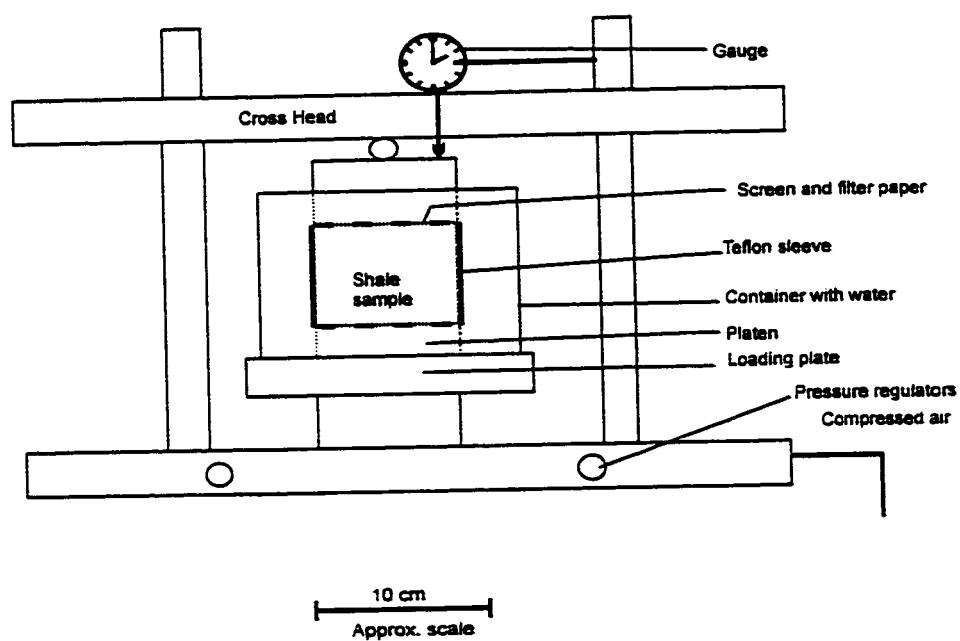
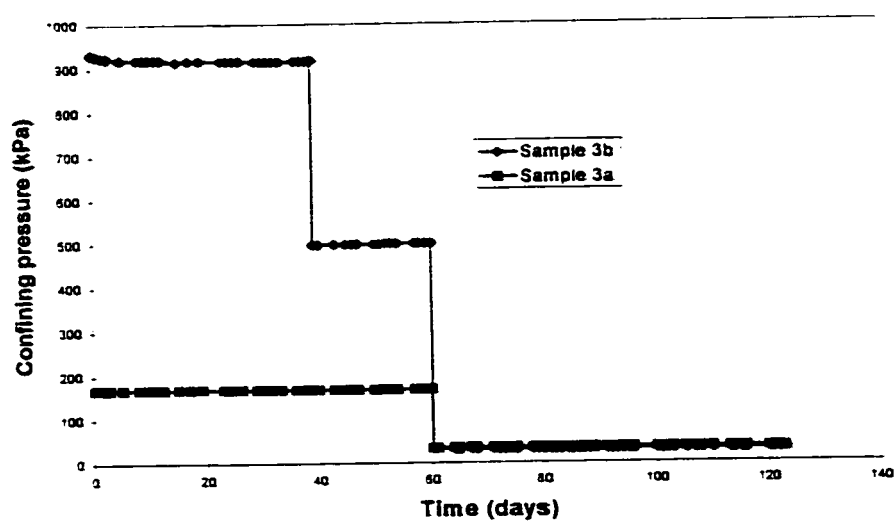
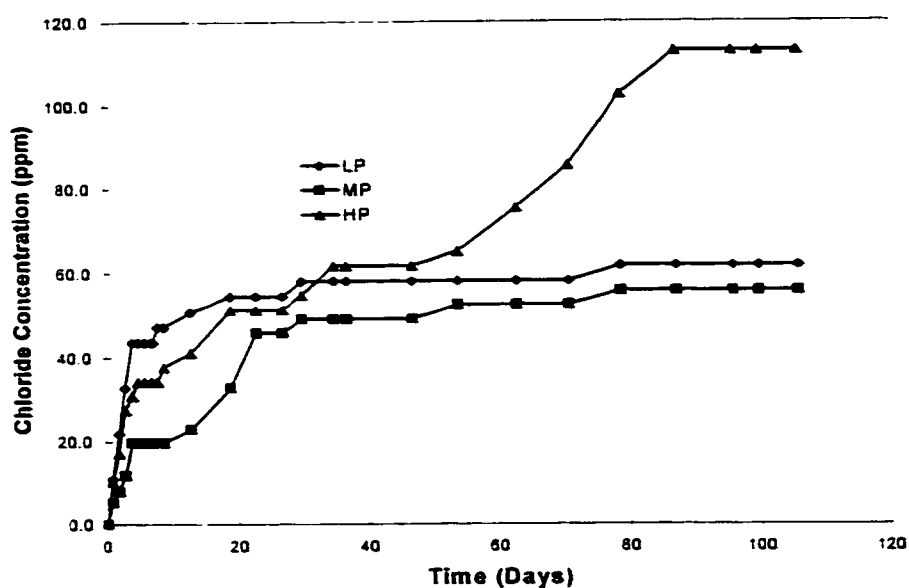


Figure 2.7 Confining pressures for swelling test on samples 3a and 3b



Chloride measurements in water were made on a regular basis for a period of 106 days for the first three samples and 110 days in the second suite of swelling tests. A VWR Chloride Electrode Cat. No. 34105-102 was used for chloride monitoring. The electrode was developed specifically for measuring chloride ions in very small quantities with minimal flow. The probe measures the electric potential, which is proportional to the amount of chloride ions into the water. Readings in millivolts were translated into mg/L of chloride using calibrations curves made with standard solutions of known chloride composition. The standards were checked and a new calibration was done for every measurement. For the first 3 samples, a magnetic stirrer allowed for the homogenization of the water before the measurements.

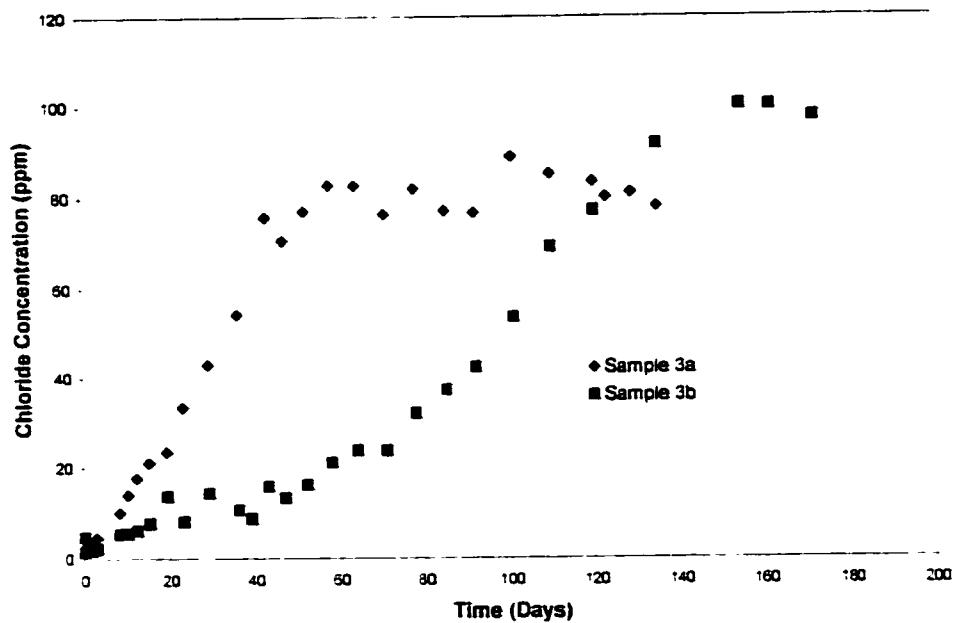
Figure 2.8 Evolution of chloride concentration with time in the water in contact with Colorado Shale samples LP, MP and HP



At the end of each test, the water samples were sent to Norwest Labs for analysis of the chloride content. For the first three samples, other elements and physical parameters were

analyzed as well. They included pH, electrical conductivity, color, turbidity, calcium, magnesium, sodium, potassium, sulfate, bicarbonate, fluoride, total alkalinity, hardness, total dissolved solids, NO_2 & $\text{NO}_3\text{-N}$, dissolved organic carbon, phenols, iron and manganese.

Figure 2.9 Evolution of chloride concentration with time in the water in contact with Colorado Shale samples 3a and 3b



The water content and its original chloride concentration in the tested samples were estimated using two other shale samples taken at the same place as the tested core samples. The original rock material was weighed and placed into an oven at 105°C for four days. The dried samples were then re-weighed to determine the water content. The water content was found to be 11.8% and 13.6% in the two samples. Their average value of 12.7% was used to estimate the original water content. For that purpose, 103.4g of finely crushed dry shale was mixed with 650g of water. The fluid content of that portion of shale was calculated at 13.1g. The mixture was left for one day to allow the water to

dissolve all the salt in the shale. The next day, water was decanted and sent for analysis at Norwest Labs. The analyses of the water indicated an amount of 61.5mg/L of chloride (Appendix 1). Considering the dilution factor of 650:13.1, the original chloride concentration in the shale was recalculated as $(61.5 \times 650) / 13.1 = 3,052\text{mg/L}$. This concentration was considered as the original chloride concentration in the samples for the model.

2.3.3 Analytical Results

Figure 2.8 displays the evolution of the chloride concentration in the water for the first set of samples LP, MP and HP. Details of analytical data are included in the Appendix 1. Analytical data for the second set of two samples 3a and 3b are given in Figure 2.9. The amounts and proportions of chloride recovered in the water at the end of the test for the two sets of samples are indicated in Table 2.2.

Table 2.2 Chloride content of water after laboratory tests

Sample →	Chloride concentration in water (mg/L)	Total amount of chloride in water (g)	Proportion of chloride released from the sample	Observations
LP	61.6	0.0570	24.90%	low swelling rate
MP	55.7	0.0515	22.52%	low swelling rate
HP	113	0.1045	45.68 %	low swelling rate, fracture during test
3a	69.18	0.0657	28.72%	high swelling rate
3b	85.15	0.0809	35.36%	high swelling rate

It appears from Figures 2.8 and 2.9 that the concentration increases rapidly at the beginning of the test and slows down considerably after a few days. Considering the size

of the sample and a water content of 12.7%, the amount of pore fluid was calculated at 75g. With a concentration of 3,052mg/L, the total amount of chloride ions in each of the samples was estimated at 0.2288g. The data displayed in Table 2.2 show that portions ranging from 22.52 % to 45.68% of chlorides were released from the samples.

A comparison of concentrations with respect to major cations in the water samples (Table 2.3) shows that the total dissolved solids content (TDS) is dominated by the chloride ion. This was also noted in chapter 1 for the water in the bedrock. However, significant amounts of carbonates and sulfates are transferred from the shale to the water at the same time. The effect of these ions on the diffusion of chlorides is assumed to be negligible and is not explored in this work.

Table 2.3 Water content in major ions after diffusion test

Water Samples →	LP	MP	HP
Total Dissolved Solids (mg/L)	165	160	285
Cl ⁻ (mg/L)	61.6	55.7	113
SO ₄ ²⁻ (mg/L)	16.1	21.1	35.0
HCO ₃ ⁻ (mg/L)	42	40	52

The swelling rate was found insignificant (less than 1%) for samples LP, MP and HP. However, it was high (more than 10%) for samples 3a and 3b (Figures 3.7 and 3.8) collected from deeper in the formation.

After the diffusion tests, Computer Aided Tomography (CAT) Scans were performed on samples LP, MP and HP (Appendix IV). Eight slices were scanned in each sample, starting from the bottom (slice 1) that was in contact with water during the experiments. During the test, fractures occurred in the samples MP and HP, probably because of the loading. For sample MP, fractures appear from slice 5 to slice 8, and they do not affect

the bottom part in contact with water. For sample HP, fractures appear from slice 1 to slice 7. In this case, the sample was fractured from the bottom at contact with water.

2.4 Application of Theoretical Concepts and Experimental Data to the Flow in the Colorado Shale

In the next two chapters, the above theoretical concepts are used to define the governing equations for the chemico-osmotic and transport models. The models will be calibrated against laboratory experimental data presented in this chapter and field observations presented in chapter 1.

Considering the chemical composition of water (see chapter 1), the main ions concerned in the Colorado shale solute flow are Cl^- , HCO_3^- and SO_4^{2-} . These ions are too large to be effectively adsorbed (Fetter, 1994). Chloride ions are larger than common ions and are often considered as the best example of conservative ions.

In this work, only chloride migration was considered. Chloride ions are predominant in the Colorado Shale as well as in the whole bedrock sedimentary column. Because these ions are conservative, the retardation phenomenon will not be considered in the models presented in the following chapters.

The interactions between the chlorides and other ions during the solute flow were assumed non-existent. However, the flow of chloride ions might be affected by the flow of the ions associated with them. In the case of the Colorado Shale, the chloride ions cannot flow faster or slower than sodium ions because of the electrical neutrality of the solute.

The chloride flow rate will depend on two main parameters, the groundwater velocity and the hydrodynamic dispersivity coefficient. As indicated earlier in this chapter, the hydrodynamic dispersivity is made up of two components, the mechanical dispersivity and the molecular diffusion. The mechanical dispersivity is dependent on the flow length (equations 2.9 and 2.10) and the water velocity (equation 2.11).

CHAPTER THREE

NUMERICAL MODELING OF THE CHEMICO-OSMOTIC FLOW IN A SHALE FORMATION

3.1 Basic Assumptions

In this chapter, chemico-osmotic flow equations are implemented to history-match the laboratory results and define the diffusion coefficient. Some basic assumptions are applied to the specificity of this case:

1. The shale is isotropic and homogeneous: spatial and time variations of hydraulic parameters are not considered;
2. The hydraulic conductivity is very low and constant;
3. The mechanical dispersivity is negligible to the molecular diffusion;
4. Volume changes can be caused by the effective stress and the osmotic pressure;
5. The change in volume corresponds to the change in porosity;
6. The change in total stress is equal to the change in pore pressure;
7. The shale is fully saturated with NaCl solution;
8. The solution is dilute enough to obey “ideal solution” relationships.

As stated in assumptions 2 and 3, the solute flow depends mainly on the molecular diffusion, given the low velocity and the low hydraulic gradient. Flow equations are derived using Darcy's and Fick's flow laws coupled with general constitutive,

equilibrium and continuity laws of continuum mechanics. The equations are designed to account for a coupled fluid and solute flowing approach in an open system under the influence of hydraulic pore pressure and solute concentration gradient.

3.2 Definition of the Governing Equation for the Fluid Flow

3.2.1 Continuity of Fluid

The law of mass conservation for a fluid flowing through an elemental volume of dimensions dx , dy and dz can be stated as follows.

$$\text{change in flow rate} = \text{flow rate in} - \text{flow rate out.}$$

Since a one-dimensional analysis is considered for the chemico-osmotic model, this is mathematically expressed as.

$$\frac{\partial V}{\partial t} = q_w dx dy - \left(q_w + \frac{\partial q_w}{\partial z} dz \right) dx dy$$

with the following resulting relation

$$\frac{\partial V}{\partial t} = - \frac{\partial q_w}{\partial z} dx dy dz \quad (3.1)$$

where

V is the volume

q_w is the flow rate

3.2.2 Constitutive Law

Small volume changes are induced by the change in pore and osmotic pressures according to the following constitutive relationship,

$$\Delta \varepsilon = \frac{\Delta V_w}{V} = M_v \Delta(\sigma - u) + M_c \Delta \pi \quad (3.2)$$

where

σ is the total stress

u is the pore pressure

π is the osmotic pressure expressed by the relation (2.4)

ε is the axial strain under the effective stress $\sigma - u$ and the osmotic pore pressure π

M_v is the coefficient of compressibility related to the change in pore pressure

M_c is the coefficient of compressibility related to the change in osmotic pressure

Assuming that the change in total stress is equal to the change in pore pressure and defining the osmotic pressure with relation (2.4), the equation (3.2) gives

$$\Delta V = (M_v \Delta u + M_c RTC) V$$

For a small volume, the constitutive law becomes

$$\frac{\partial V}{\partial t} = \left(-M_v \frac{\partial u}{\partial t} + M_c RT \frac{\partial C}{\partial t} \right) dx dy dz \quad (3.3)$$

3.2.3 Darcy's Law

Assuming that the fluid flows under pore and osmotic pressures, the one-dimensional formulation of the Darcy's law is modified as follows

$$q_w = - \left(\frac{k_h}{\gamma_w} \frac{\partial u}{\partial z} + \frac{k_c}{\gamma_w} \frac{\partial \pi}{\partial z} \right) \quad (3.4)$$

where

k_h is the hydraulic permeability coefficient (m/s)

k_c is the osmotic permeability coefficient (m/s)

γ_w is the unit weight of water

As indicated in paragraph 2.2.1.2, k_c is often considered as a fraction of k_h by the relation

$$k_c = \phi k_h \quad (3.5)$$

where

ϕ is the osmotic efficiency

3.2.4 Governing Equation for the Fluid Flow

Equating the relations (3.1) and (3.3) and replacing q_w and k_c by their values in equations (3.4) and (3.5) gives the following linear second order partial differential equation

$$\boxed{\frac{\partial u}{\partial t} - \left(RT \frac{M_c}{M_v} \right) \frac{\partial C}{\partial t} = \left(\frac{k_h}{\gamma_w M_v} \right) \frac{\partial^2 u}{\partial z^2} + \left(RT \frac{\phi k_h}{\gamma_w M_v} \right) \frac{\partial^2 C}{\partial z^2}} \quad (3.6)$$

Equation (3.6) is the governing equation for the fluid flow.

3.3 Definition of the Governing Equation for the Solute Flow

3.3.1 Continuity for the Solute

As for the fluid, the mass conservation law for the solute flowing through an elemental volume $dx dy dz$ is

$$\text{Rate of change of solute mass} = \text{Flow rate in} - \text{Flow rate out}$$

Considering C as the solute pore concentration for a volumetric element $dx dy dz$ with a porosity n , the mass of solute is

$$(nC) dx dy dz$$

and the mass conservation equation becomes,

$$\frac{\partial(nC)}{\partial t} dx dy dz = q_s dx dy - \left(q_s + \frac{\partial q_s}{\partial z} dz \right) dx dy$$

giving upon simplification,

$$\frac{\partial(nC)}{\partial t} = - \frac{\partial q_s}{\partial z}$$

where

q_s is the solute flow rate

It comes from the expansion of the above relation,

$$n \frac{\partial C}{\partial t} + C \frac{\partial n}{\partial t} = - \frac{\partial q_s}{\partial z} \quad (3.7)$$

Considering assumptions 4, 5 and 6, the porosity change can be written as follows.

$$\Delta n = \Delta \left(\frac{V_v}{V} \right) = \Delta \left(\frac{V_w}{V} \right) = M_v \Delta(\sigma - u) + M_c RT \Delta C \quad (3.7a)$$

where

V_v is the void volume equal to the water volume V_w , assuming the sample is saturated.

Differentiation of the above equation with respect to time gives,

$$\frac{\partial n}{\partial t} = -M_v \frac{\partial u}{\partial t} + M_c RT \frac{\partial C}{\partial t} \quad (3.8)$$

3.3.2 Solute Flow Law

As it was discussed in paragraph 2.2.2, the solute can be transported by

- (i) advection with the fluid moving under Darcy's law;
- (ii) diffusion governed by Fick's law, assuming that the mechanical dispersion is negligible (assumption 3. section 3.1).

In one dimension, this is written as follows

$$q_s = q_w C - nD \frac{\partial C}{\partial z}$$

where

D is the diffusion coefficient

$\frac{\partial C}{\partial z}$ is the concentration gradient

The negative sign applied to Fick's law in the equation indicates that the movement is from greater to lesser concentrations (Fetter, 1994). It comes from the above relation.

$$\frac{\partial q_s}{\partial z} = q_w \frac{\partial C}{\partial z} + C \frac{\partial q_w}{\partial z} - nD \frac{\partial^2 C}{\partial z^2} \quad (3.9)$$

3.3.3 Governing Flow Equation for the Solute

Equating relations (3.7) and (3.9) and replacing q_w by its value deduced from the equation (3.4) gives.

$$(n + M_c RTC) \frac{\partial C}{\partial t} - M_v C \frac{\partial u}{\partial t} = - \left(-nD + RTC \frac{\phi k_h}{\gamma_w} \right) \frac{\partial^2 C}{\partial z^2} - C \frac{k_h}{\gamma_w} \frac{\partial^2 u}{\partial z^2} - \frac{\phi k_h}{\gamma_w} \left(\frac{\partial C}{\partial z} \right)^2 - \frac{k_h}{\gamma_w} \frac{\partial u}{\partial z} \frac{\partial C}{\partial z}$$

It is further assumed by approximation that the term $\left[\frac{\phi k_h}{\gamma_w} \left(\frac{\partial C}{\partial z} \right)^2 \right]$ is negligible compared

to $\left(\frac{k_h}{\gamma_w} \frac{\partial u}{\partial z} \frac{\partial C}{\partial z} \right)$. Thus, the flow equation for the solute can be written as follows.

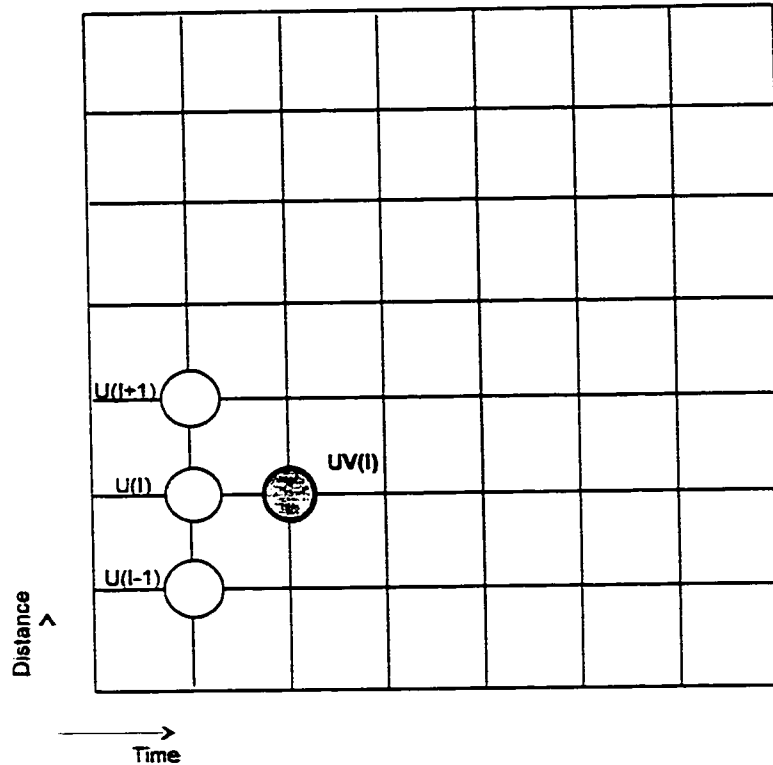
$$\boxed{M_v C \frac{\partial u}{\partial t} - (n + M_c RTC) \frac{\partial C}{\partial t} = \left(RTC \frac{\phi k_h}{\gamma_w} - nD \right) \frac{\partial^2 C}{\partial z^2} + C \frac{k_h}{\gamma_w} \frac{\partial^2 u}{\partial z^2} + \frac{k_h}{\gamma_w} \frac{\partial u}{\partial z} \frac{\partial C}{\partial z}} \quad (3.10)$$

Equation (3.10) is a nonlinear second order partial differential equation. With equation (3.6), it forms a system of equations to solve for pore pressure and concentration.

3.4 Numerical Solving

3.4.1 Explicit formulation

Figure 3.1 Grid and computational molecule for the explicit formulation



The system of equations (3.6) and (3.10) for the fluid and the solute flow, respectively, were solved numerically by the finite difference method using the explicit formulation. The unknowns to be calculated are the pore pressures and the solute concentrations at different time levels. The other parameters are estimated and adjusted in the limits fixed by the field conditions explained in chapter 1. The computational molecule for the explicit finite difference approximation is represented in Figure 3.1. For a point (I), values of the pore pressure $UV(I)$ are calculated at a time T , knowing the pore pressure

values $U(I-1)$, $U(I)$ and $U(I+1)$ calculated at a previous time $T-1$. At time $T=0$, calculations start with initial and boundary conditions. Concentrations are calculated in a similar way. Calculations are made for each time increment Δt . The sample is analyzed at a number of discrete points separated by an interval Δz . Boundary conditions are imposed at the end-points of the sample.

3.4.2 Dimensionless Governing Equations

Prior to solving numerically the problem, governing equations are written into a dimensionless form as follows:

- Dimensionless pore pressure	$U = \frac{u}{u_{\max}}$
- Dimensionless concentration	$X = \frac{C}{C_{\max}}$
- Dimensionless distance	$Z = \frac{z}{H}$
- Dimensionless time	$T = \frac{C_v t}{H^2}$

where

u_{\max} and C_{\max} are the maximum value of pore pressure and concentration, respectively, occurring in the diffusion process,

H is the drainage path length for the diffusion process and,

$C_v \left(= \frac{k_h}{\gamma_w M_v} \right)$ is the consolidation coefficient.

Writing the governing flow equations (3.6) and (3.10) into the dimensionless form gives.

$$\boxed{\frac{\partial U}{\partial T} - R_0 \frac{\partial X}{\partial T} = \frac{\partial^2 U}{\partial Z^2} + R_1 \frac{\partial^2 X}{\partial Z^2}} \quad \text{for the fluid flow} \quad (3.11)$$

and

$$R_3 X \frac{\partial U}{\partial T} - R_2 \frac{\partial X}{\partial T} = R_4 \frac{\partial^2 X}{\partial Z^2} + R_3 \frac{\partial X}{\partial Z} \frac{\partial U}{\partial Z} + R_3 X \frac{\partial^2 U}{\partial Z^2} \quad \text{for the solute flow (3.12)}$$

where

$$R_0 = \frac{M_c}{M_v} \frac{RTC_{\max}}{u_{\max}}$$

$$R_1 = \frac{\phi RTC_{\max}}{u_{\max}}$$

$$R_2 = n + M_c RTX C_{\max}$$

$$R_3 = M_v u_{\max}$$

$$R_4 = C_{\max} \phi RT M_v X - \frac{nD}{C_v}$$

3.4.3 Numerical Approximations

Considering the explicit formulation used for numerical solving of equations (3.11) and (3.12), the following approximations were used:

For the pore pressure

$$\frac{\partial U}{\partial T} = \frac{UV(I) - U(I)}{\Delta T}$$

$$\frac{\partial U}{\partial Z} = \frac{U(I+1) - U(I-1)}{2\Delta Z}$$

$$\frac{\partial^2 U}{\partial Z^2} = \frac{U(I+1) - 2U(I) + U(I-1)}{\Delta Z^2}$$

Similarly, for the concentration

$$\begin{aligned}\frac{\partial X}{\partial T} &= \frac{XV(I) - X(I)}{\Delta T} \\ \frac{\partial X}{\partial Z} &= \frac{X(I+1) - X(I-1)}{2\Delta Z} \\ \frac{\partial^2 X}{\partial Z^2} &= \frac{X(I+1) - 2X(I) + X(I-1)}{\Delta Z^2}\end{aligned}$$

After substitution of above approximations into differential equation (3.11) the fluid flow equation becomes

$$\begin{aligned}\frac{UV(I) - U(I)}{\Delta T} - R_0 \frac{XV(I) - X(I)}{\Delta T} &= \frac{U(I+1) - 2U(I) + U(I-1)}{\Delta Z^2} \\ &+ R_1 \frac{X(I+1) - 2X(I) + X(I-1)}{\Delta Z^2}\end{aligned}$$

which gives after re-arrangements

$$\begin{aligned}UV(I) &= R_0 XV(I) + U(I) - R_0 X(I) \\ &+ \frac{\Delta T}{\Delta Z^2} (U(I+1) - 2U(I) + U(I-1)) \\ &+ R_1 \frac{\Delta T}{\Delta Z^2} (X(I+1) - 2X(I) + X(I-1))\end{aligned}\tag{3.13}$$

Similarly, the solute flow equation (3.12) is numerically approximated as follows

$$\begin{aligned}R_3 X(I) \frac{UV(I) - U(I)}{\Delta T} - R_2 \frac{XV(I) - X(I)}{\Delta T} &= R_4 \frac{X(I+1) - 2X(I) + X(I-1)}{\Delta Z^2} \\ &+ R_3 \left(\frac{X(I+1) - X(I-1)}{2\Delta Z} \right) \left(\frac{U(I+1) - U(I-1)}{2\Delta Z} \right) \\ &+ R_3 X(I) \frac{U(I+1) - 2U(I) + U(I-1)}{\Delta Z^2}\end{aligned}$$

which gives after re-arranging

$$\begin{aligned}
 XV(I) = & \frac{R_3}{R_2} X(I)UV(I) + X(I) - \frac{R_3}{R_2} X(I)U(I) \\
 & - \frac{\Delta T}{\Delta Z^2} \frac{R_4}{R_2} (X(I+1) - 2X(I) + X(I-1)) \\
 & - \frac{\Delta T}{\Delta Z^2} \frac{R_3}{4R_2} (X(I+1) - X(I-1))(U(I+1) - U(I-1)) \\
 & - \frac{\Delta T}{\Delta Z^2} \frac{R_3}{R_2} X(I)(U(I+1) - 2U(I) + U(I-1))
 \end{aligned} \tag{3.14}$$

Equations (3.13) and (3.14) were used for the numerical simulation of the one-dimensional flow in the samples.

3.4.4 Initial and Boundary Conditions

A FORTRAN algorithm (Appendix 3) using equations (3.13) and (3.14) was written to analyze the one-dimensional flow of solute and fluid in a shale sample. The flow process was simulated by history-matching the laboratory data presented in section 2.3. The pore pressure and the concentration distributions in the sample were calculated at different time levels.

For samples LP, MP and HP, water was allowed to contact the bottom of the samples only (Figure 2.5). The thickness of the samples was considered as equal to H and the dimensionless thickness equal to 1. For the model, each sample was divided into 10 intervals, resulting in a dimensionless interval Δz equal 0.10. These samples did not swell during the diffusion test. Therefore, the swelling pressure was assumed to be 0 at the beginning of the test. Boundary and initial conditions for the dimensionless pore pressure U and the dimensionless concentration X were fixed as follows:

$$t = t; \quad z = 0 \rightarrow U = 0$$

X = chloride concentration in the water; this boundary condition changes with time.

$$t = 0; \quad z = z \rightarrow U = 0$$

$$X = 1$$

For samples 3a and 3b, the water contact was allowed on both sides of the samples (Figure 2.6). Assuming that the flow was symmetrical with respect to the middle of the sample, H was considered as the thickness of one half of the sample, meaning a thickness of $2H$ for the whole sample. Each sample was also divided into 10 intervals, with a dimensionless interval Δz equal 0.20. Samples 3a and 3b showed a significant swelling behavior during the swelling tests where they were subject to different confining pressures (Figure 2.7, Table 2.1). The maximum swelling pressure was assumed equal to 1,200 kPa, consistent with results from swelling tests on the Colorado Shale at the Department of Civil Engineering, University of Calgary. For the first loading, an excess pore pressure, equal to the difference between the maximum pore pressure and the prevalent confining pressure, develops in the sample. That excess pore dissipates after some time. For a subsequent loading, the excess pore pressure is calculated as the difference between the previous and the new confining pressure (Table 3.1). The obtained excess pore pressures are used as initial conditions for every loading cycle.

Table 3.1 Excess pore pressures in swelling samples 3a and 3b for different confining pressures, for a maximum swelling pressure of 1,200 kPa

	Loading interval (days)	Confining pressure (kPa)	excess pore pressure (kPa)
Sample 3a	0 – 60	169	1,031
	60 – 120	34	135
Sample 3b	0 – 39	925	275
	39 – 60	500	425
	60 – 120	32	468

Therefore, using the dimensionless pore pressure and concentration, the boundary and initial conditions for samples 3a and 3b were set up as:

$$\begin{aligned}
 t = t; \quad z = 0 \text{ and } z = 2H &\quad \rightarrow \quad U = 0 \\
 &\quad X = \text{chloride concentration in the water; this} \\
 &\quad \text{boundary condition changes with time.} \\
 t = 0; \quad z = z &\quad \rightarrow \quad U = 1 \\
 &\quad X = 1
 \end{aligned}$$

3.4.5 Parameters Used for the Simulation

For the model, hydraulic and consolidation parameters were assumed as follows:

hydraulic conductivity coefficient k_h	$1.2 \times 10^{-11} \text{ m/s}$
osmotic conductivity coefficient k_c	$0.005 k_h$
pore pressure compressibility coefficient M_v	$1.0 \times 10^{-5} \text{ kPa}^{-1}$
osmotic pressure compressibility coefficient M_c	$1.0 \times 10^{-6} \text{ kPa}^{-1}$
porosity	20%
temperature	300°K

These values are commonly observed in clays and shales (Barbour and Fredlund, 1989; Haddad, 1998). The value of the hydraulic conductivity coefficient is consistent with values obtained for similar rocks in the bedrock.

3.5 Simulation Results

3.5.1 Calculation of the Molecular Diffusion Coefficient

Figures 3.2 to 3.6 show the results of the history match of the chloride concentrations measured in the laboratory and presented earlier in Figures 2.8 and 2.9. The simulation assumed an initial chloride concentration of 3,052mg/L in all the samples, as calculated in subsection 2.3.3. The diffusion coefficient was found to be the only parameter affecting the solute flow rate. As indicated in paragraph 3.1.1, the hydrodynamic dispersion expressed by the relation (2.11) is reduced to its molecular diffusion component, given that the mechanical dispersivity is negligible. A small change in the diffusion coefficient has a considerable impact on the shape of the simulation curve.

The interpretation of the results conducted to the definition of a range for the diffusion coefficient. The history match required an empirical variation of the diffusion coefficient between $1.7 \times 10^{-11} \text{ m}^2/\text{s}$ and $1.27 \times 10^{-10} \text{ m}^2/\text{s}$. The solute flow rate is important in the early stage of the test, indicating a relatively high diffusion coefficient. It slows down in the late stage of the test, attesting of a lower diffusion coefficient. Samples 3a and 3b indicated a high swelling rate, with maxima of 13.4% and 9% respectively. The diffusion coefficient ranges between $1.7 \times 10^{-11} \text{ m}^2/\text{s}$ and $1.16 \times 10^{-10} \text{ m}^2/\text{s}$ for sample 3a and between $1.7 \times 10^{-11} \text{ m}^2/\text{s}$ and $7.46 \times 10^{-11} \text{ m}^2/\text{s}$ for sample 3b. Despite the swelling behavior in these samples, the variation intervals for the diffusion coefficient are similar to those obtained for samples LP, MP and HP. The reason for the diffusion coefficient variation is not well understood at this stage. No significant correlation was found between the swelling of the samples and the variation of the diffusion coefficient, as shown in Figures 3.7 and 3.8.

The situation for sample HP appears complex. The solute flow rate increases rapidly at the beginning of the test and slows down after a few days like in samples LP and MP. However, it increases again due presumably to a fracture occurring in the sample at that

time (see CAT Scan, Appendix IV). The range for the diffusion coefficient in sample HP is comparable to the other samples.

The lowest value for the diffusion coefficient that is characteristic of the late stage of the solute flow process was estimated at $1.7 \times 10^{-11} \text{ m}^2/\text{s}$ in all the samples. This value was considered as the steady state value for the diffusion coefficient in the Colorado Shale. This value should be used in situ for non-fractured shale. For the top 20 to 30m of fractured Colorado Shale, the diffusion coefficient should be increased to a higher value depending on the density, the orientation, the rate of connection and the length of the fractures.

Figure 3.2 Sample LP - solute flow rate

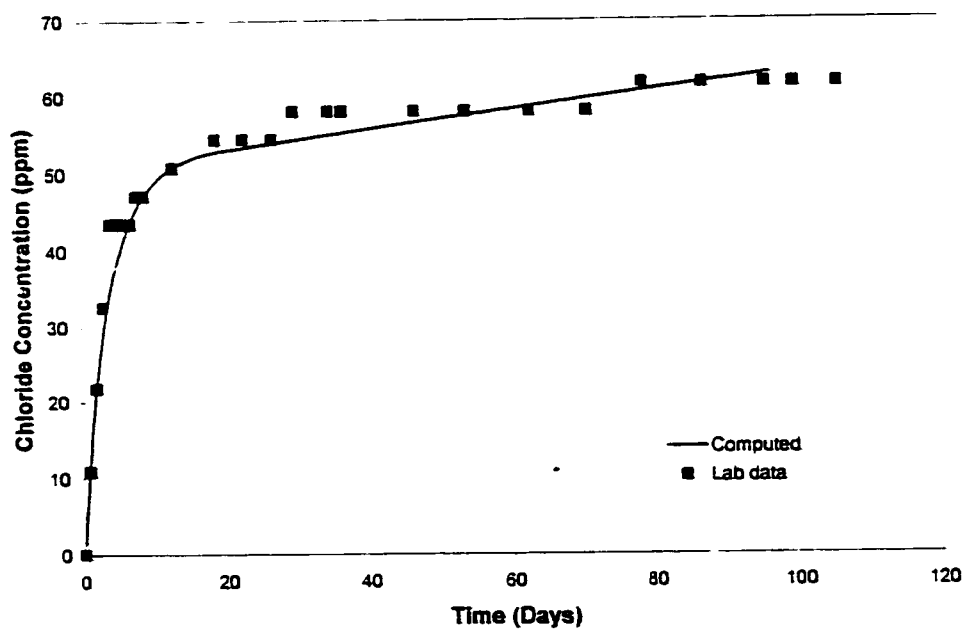


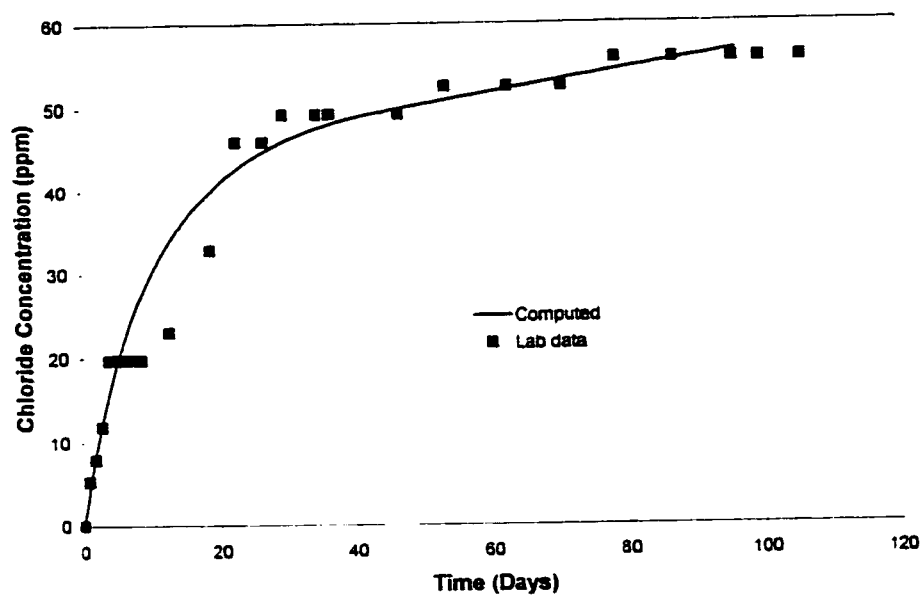
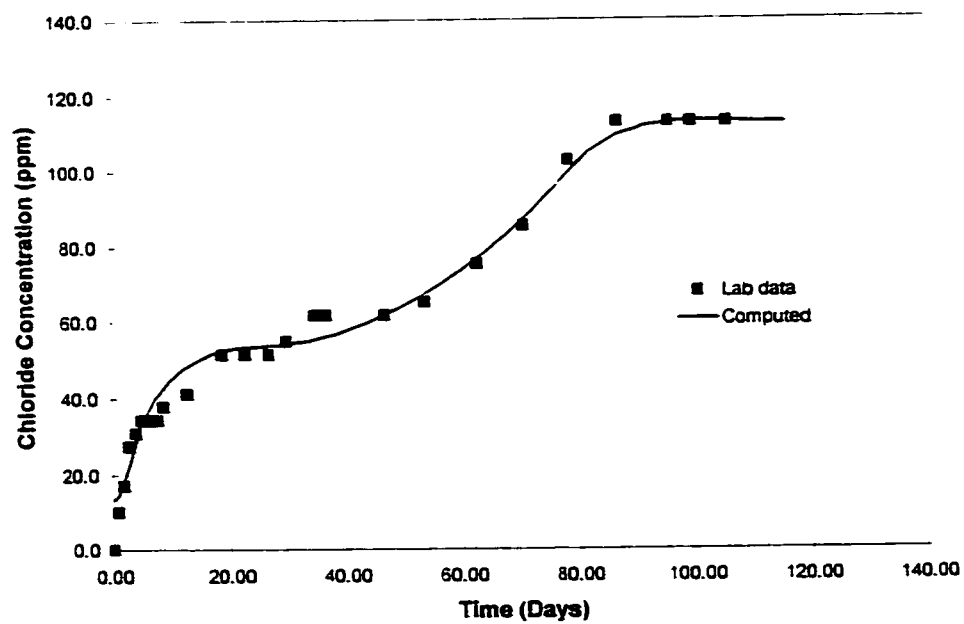
Figure 3.3 Sample MP - solute flow rate**Figure 3.4 Sample HP - solute flow rate**

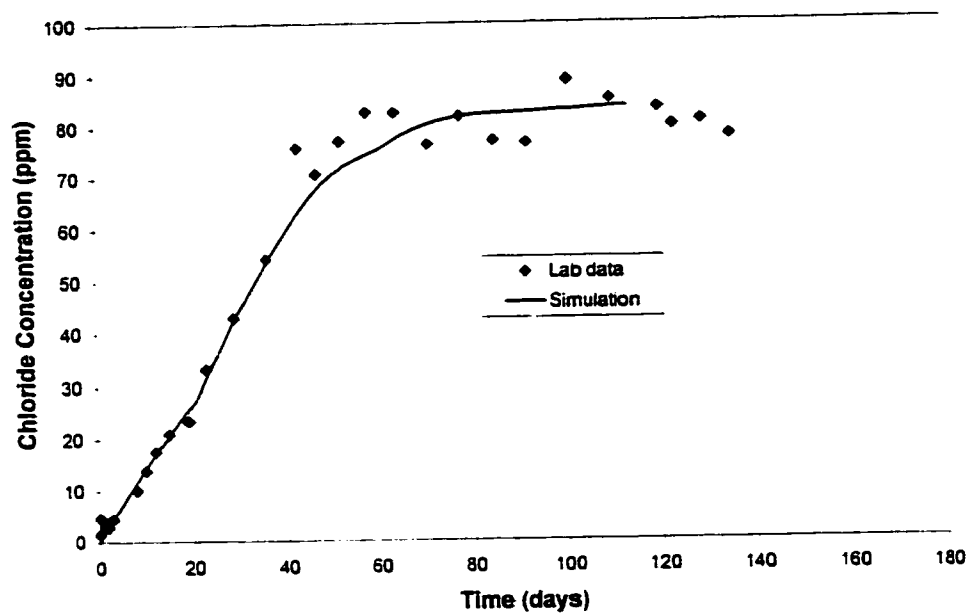
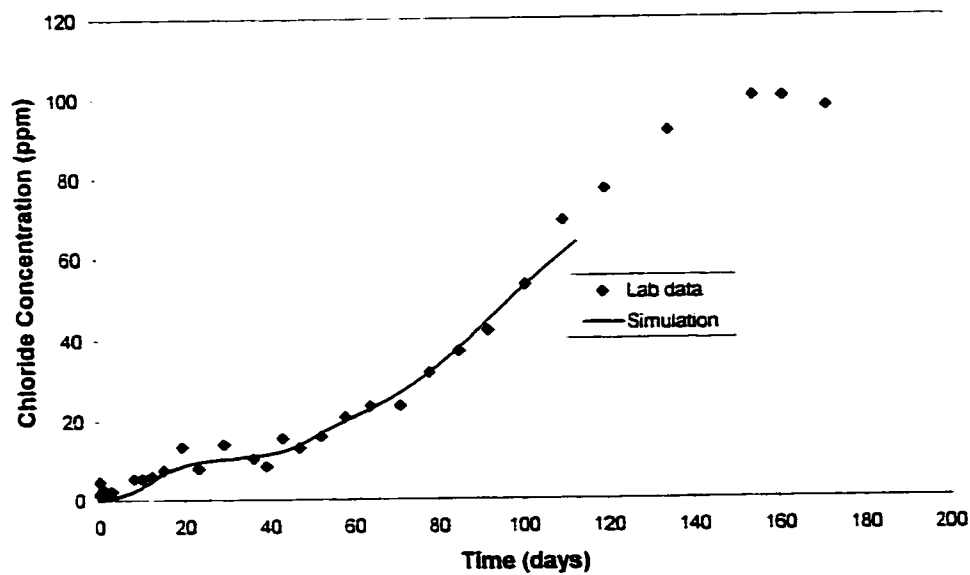
Figure 3.5 Sample 3a - solute flow rate**Figure 3.6 Sample 3b - solute flow rate**

Figure 3.7 Sample 3a - variation of the diffusion coefficient in comparison with the swelling of the sample

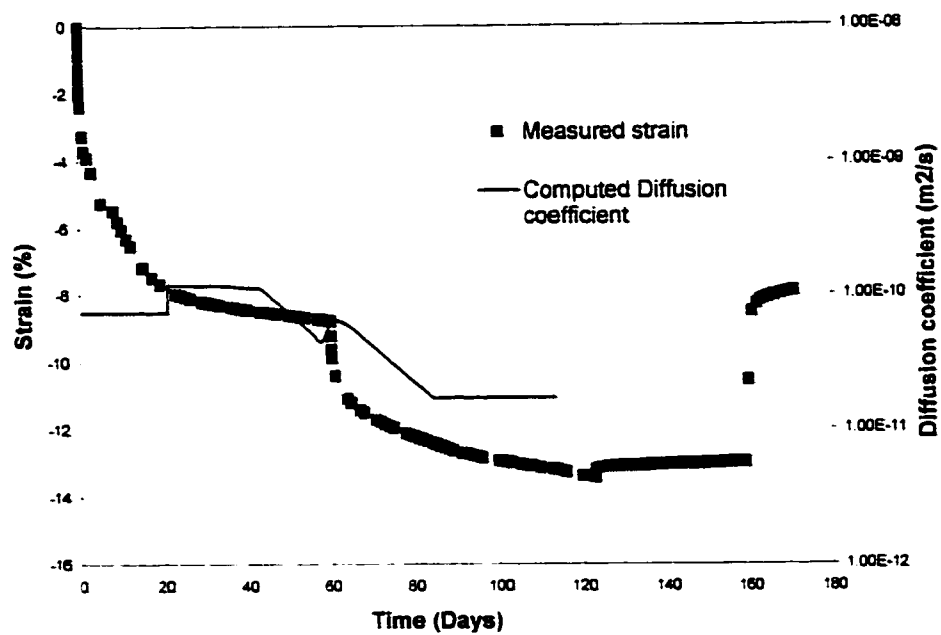
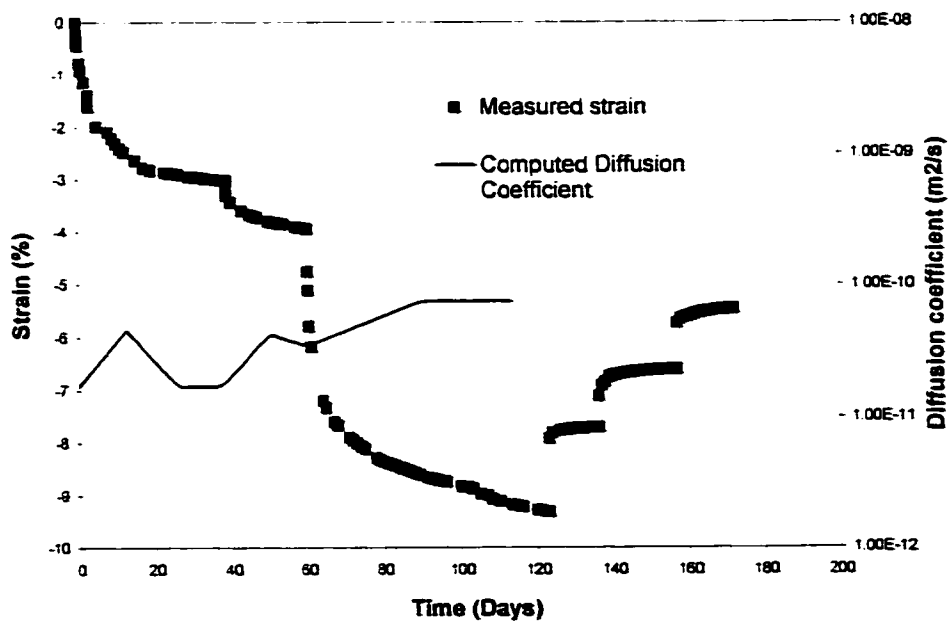


Figure 3.8 Sample 3b - variation of the diffusion coefficient in comparison with the swelling of the sample



3.5.2 Chloride Concentration Distribution

Chloride concentration changes within the samples were also calculated with the model. The evolution of concentration isochrones for the five samples is displayed in Figures 3.9 to 3.13. The drainage was done on one side for samples LP, MP and HP, and on both sides for samples 3a and 3b. The figures confirm that the chloride outflow is important in the early stage of the test and slows down thereafter at steady state. Figure 3.11 shows a higher chloride outflow because of the fractures in sample HP.

3.5.3 Pore Pressure Distribution

Figures 3.14 to 3.18 show the evolution of the pore pressure isochrones with time. Samples LP, MP and HP did not swell during the test. From an initial pore pressure equal to zero, a negative pore pressure due to osmotic suction develops throughout the sample. At the beginning of the test, the depletion of the pore pressure is maximum at the contact with the water. A trend to equalization followed by a slow dissipation of the pore pressure takes place later. Similar features were observed by Mitchell et al. (1973).

Samples 3a and 3b showed a significant swelling behaviour during the test. As indicated in Figure 2.7 and Table 3.1, the samples were subject to different loadings during the test. From a maximum swelling pressure measured at 1200 kPa, the initial excess pore pressures for each loading were calculated in Table 3.1. Figures 3.17 and 3.18 show the excess pore pressure distribution pattern for one loading interval. It appears that, for the simulation conditions indicated in subsection 3.4.5, the excess pore pressure dissipates in the sample after a few hours to a value of 0 kPa. The pore pressure can be calculated anywhere in the sample at any time by multiplying the dimensionless fraction with the corresponding initial excess pore pressure.

3.5.4 Sensitivity Analysis

3.5.4.1 The Chloride Outflow

A sensitivity study indicated that the chloride outflow rate depends solely on the value of the diffusion coefficient. Figure 3.19 shows a comparison of chloride flow rates in the conditions of the model for three different diffusion coefficients $10^{-11}\text{m}^2/\text{s}$, $10^{-8}\text{m}^2/\text{s}$ and $10^{-9}\text{m}^2/\text{s}$. The solute flow rate increases significantly with diffusion coefficient. The variation of any other parameter has no significant effect on the release of the chloride out of the sample.

3.5.4.2 The Pore Pressure

The study suggested that the pore pressure distribution is very sensitive to the osmotic efficiency of the porous media ϕ defined by equation 2.3, subsection 2.2.1.1. The results displayed in Figures 3.17 and 3.18 were obtained in the base case with $\phi=0.005$. Figures 3.20 and 3.21 show the pore pressure distribution for $\phi=0.1$ and $\phi=0.4$, respectively. They show that for higher osmotic efficiency values, the osmotic pore pressure becomes more important and develops in the sample a negative suction proportional to the value of ϕ . The dissipation of the osmotic pressure is much slower than the excess pore pressure due to loading.

The change in porosity was simulated for samples 3a and 3b (Figures 3.22 and 3.23) to study the effect of the swelling process on the model. These samples display a significant change in porosity during the swelling tests. The strain measured in the laboratory was history-matched, using the relation 3.7a. However, it appeared that the impact of the porosity change on the model was negligible and can be assumed constant (Haddad, 1998).

3.5.4.3 Effect of the Pore Pressure Variation on the Chloride Outflow

The sensitivity study indicated that the variation of the diffusion coefficient affects considerably the chloride outflow, but has no effect on the pore pressure. On the other side, the chloride outflow is insensitive to parameters that have an impact on the pore pressure. This suggests that, in the context of these experiments, the chloride release is not dependent on the pore pressure distribution. This observation suggests that the governing equations (3.6) for the fluid flow and (3.10) for the solute flow are not apparently coupled.

Figure 3.9 Sample LP - concentration isochrones at different times

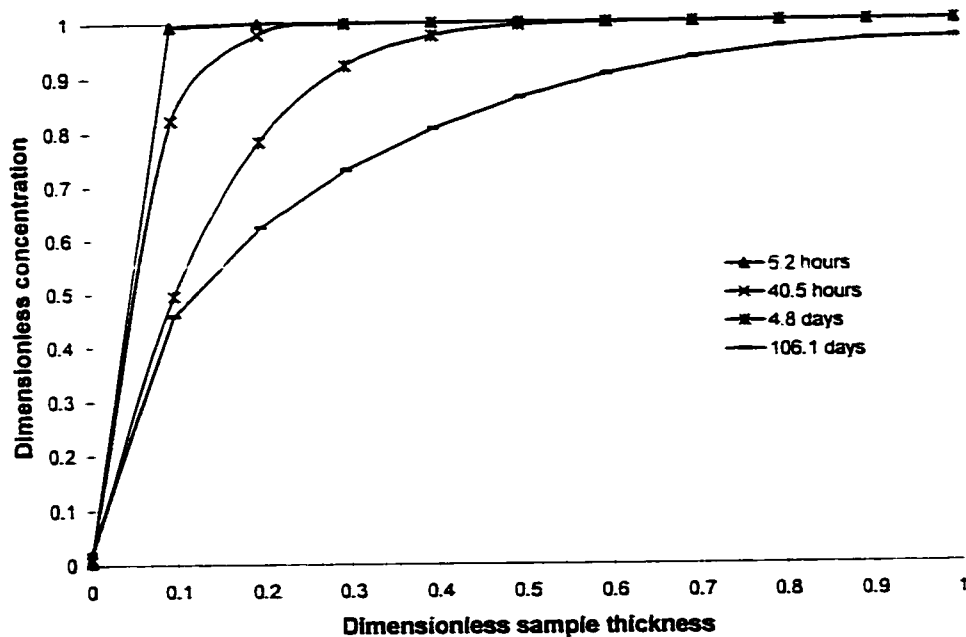


Figure 3.10 Sample MP - concentration isochrones at different times

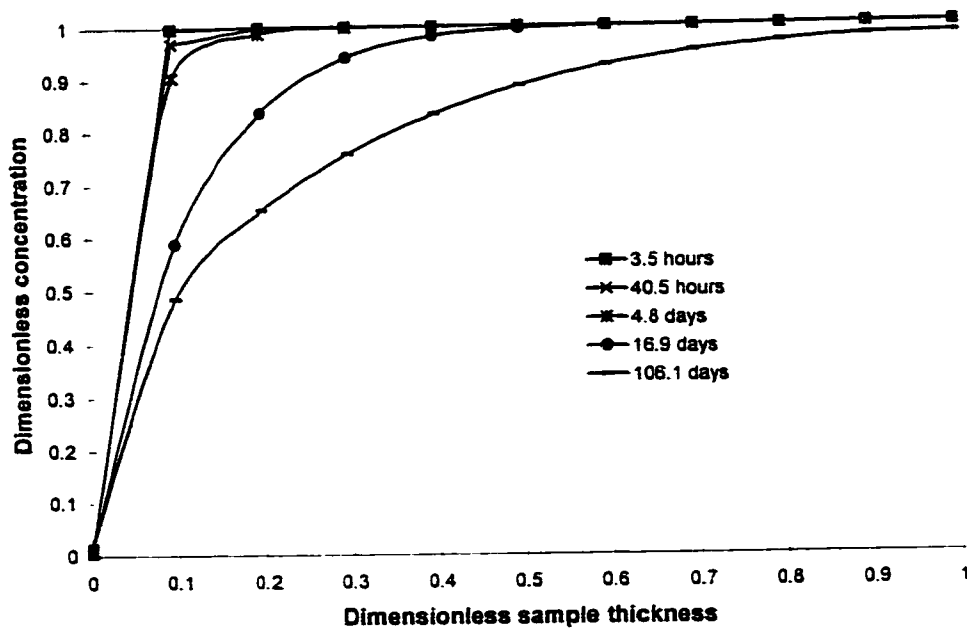


Figure 3.11 Sample HP - concentration isochrones at different times

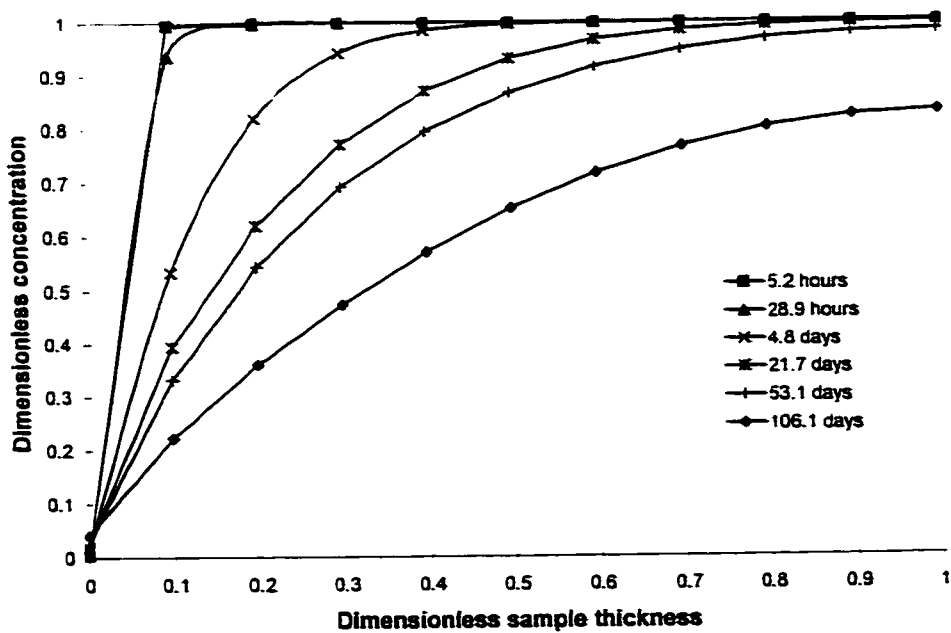


Figure 3.12 Sample 3a - concentration isochrones at different times during swelling test

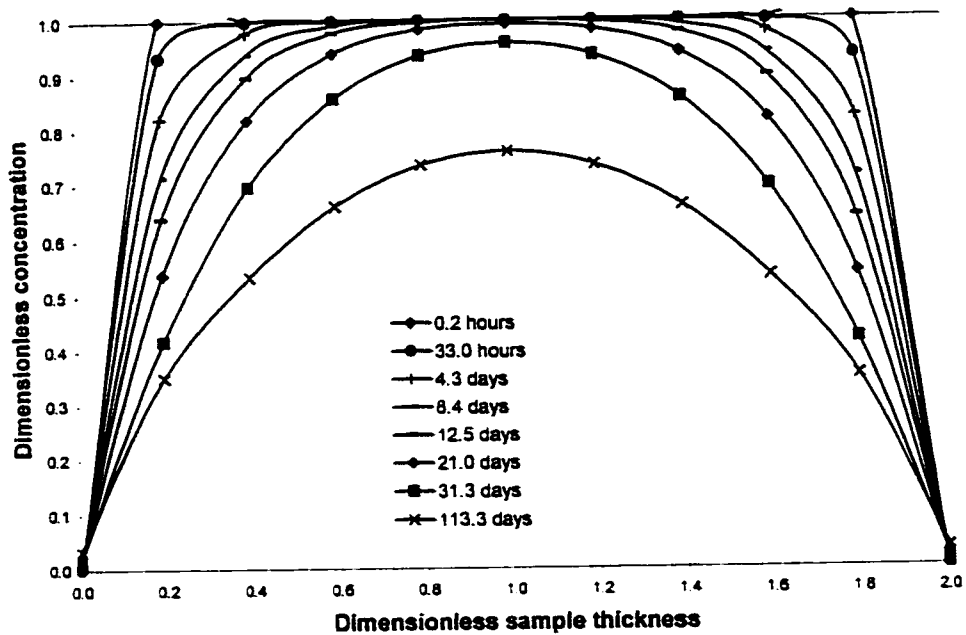


Figure 3.13 Sample 3b - concentration isochrones at different times during swelling test

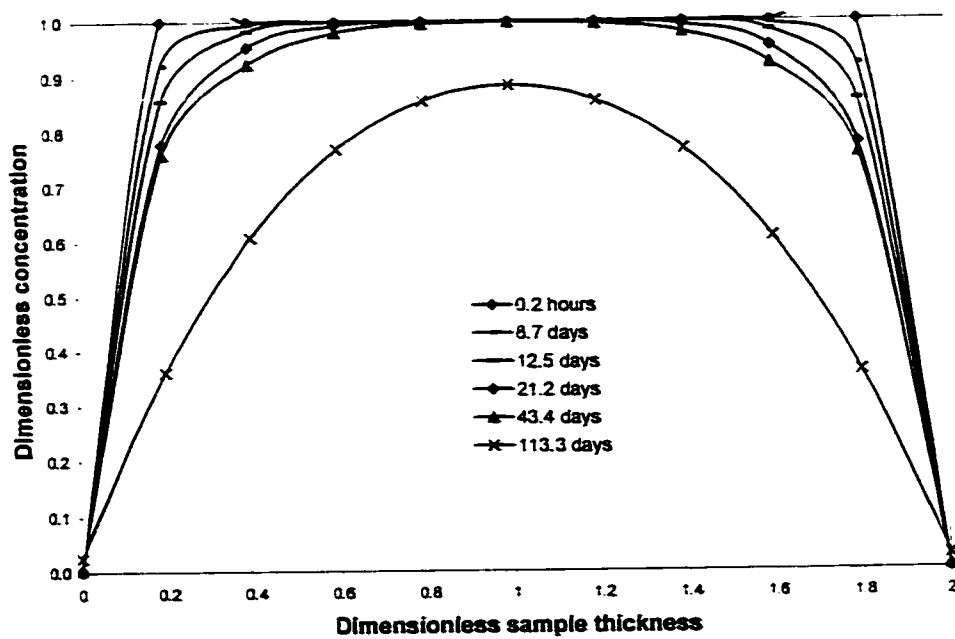


Figure 3.14 Sample LP - pore pressure isochrones at different times

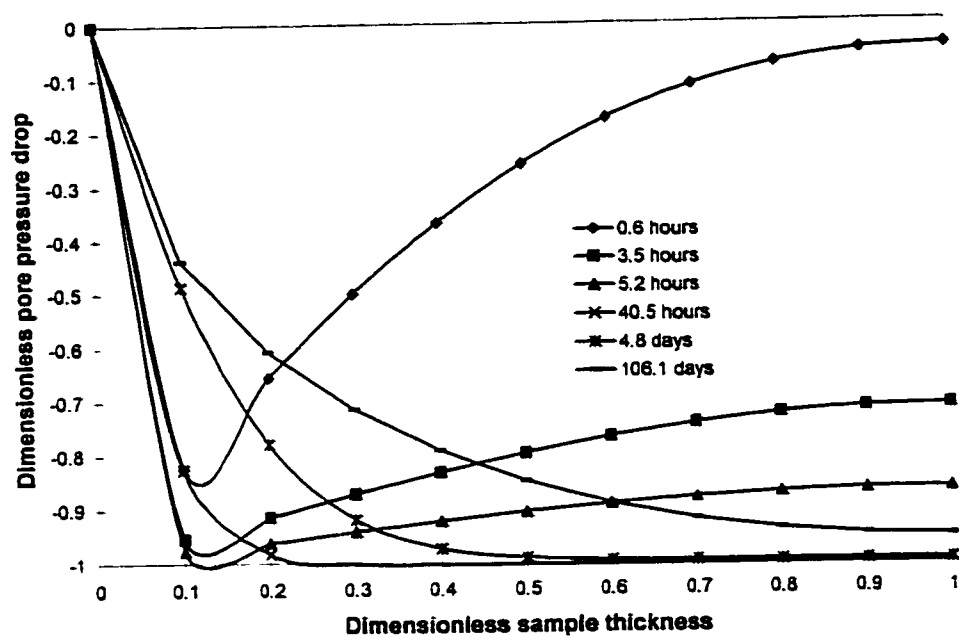


Figure 3.15 Sample MP - pore pressure isochrones at different times

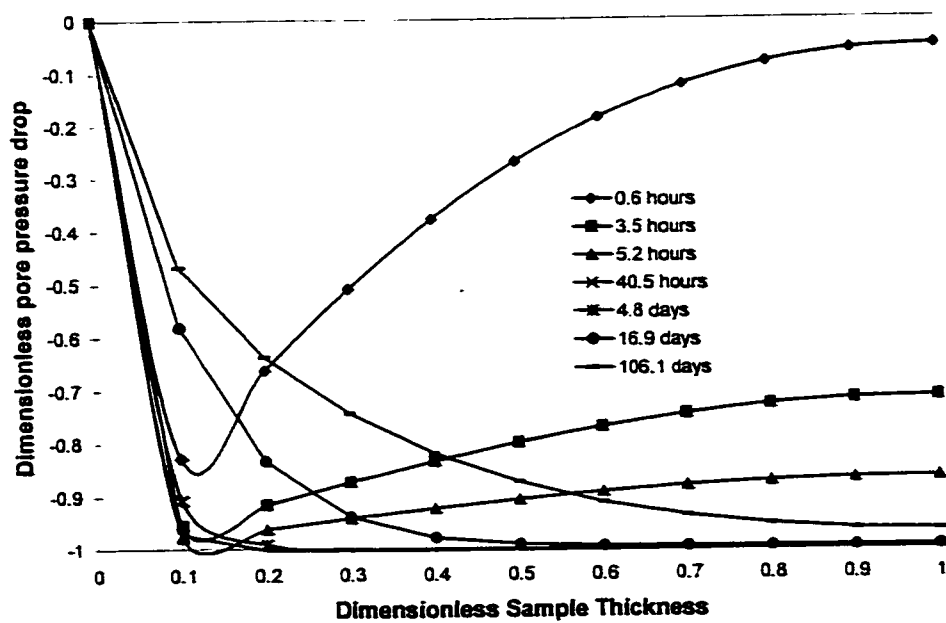


Figure 3.16 Sample HP - pore pressure isochrones at different times

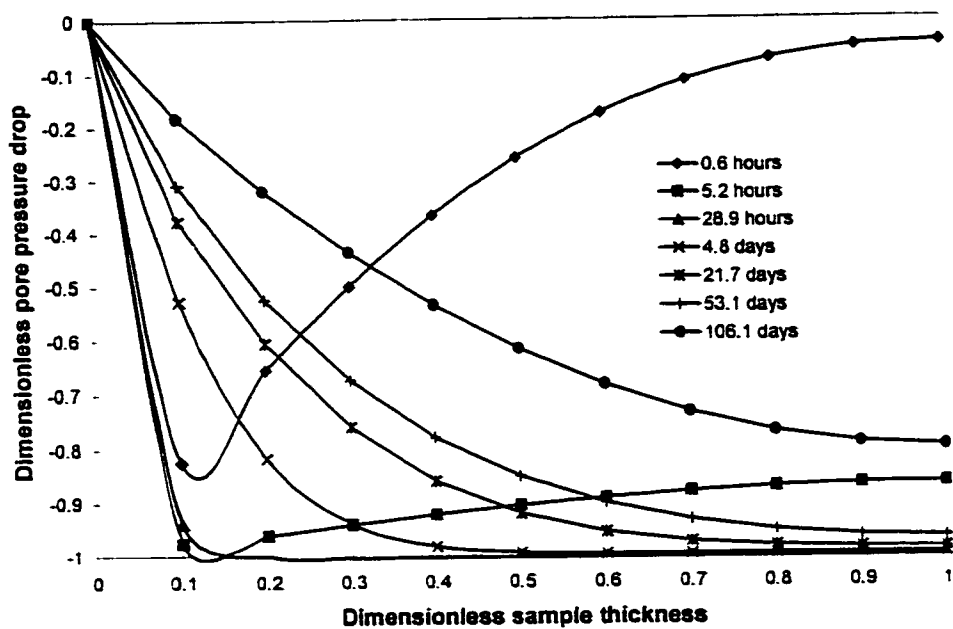


Figure 3.17 Sample 3a - pore pressure isochrones at different times during swelling test for one loading interval

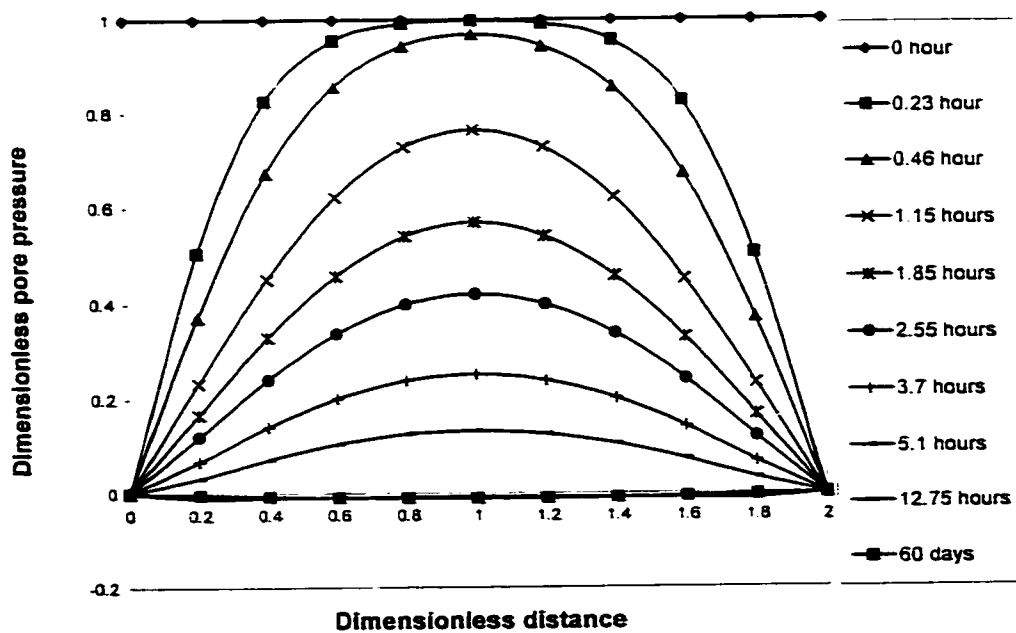


Figure 3.18 Sample 3b - pore pressure isochrones at different times during swelling test for one loading interval

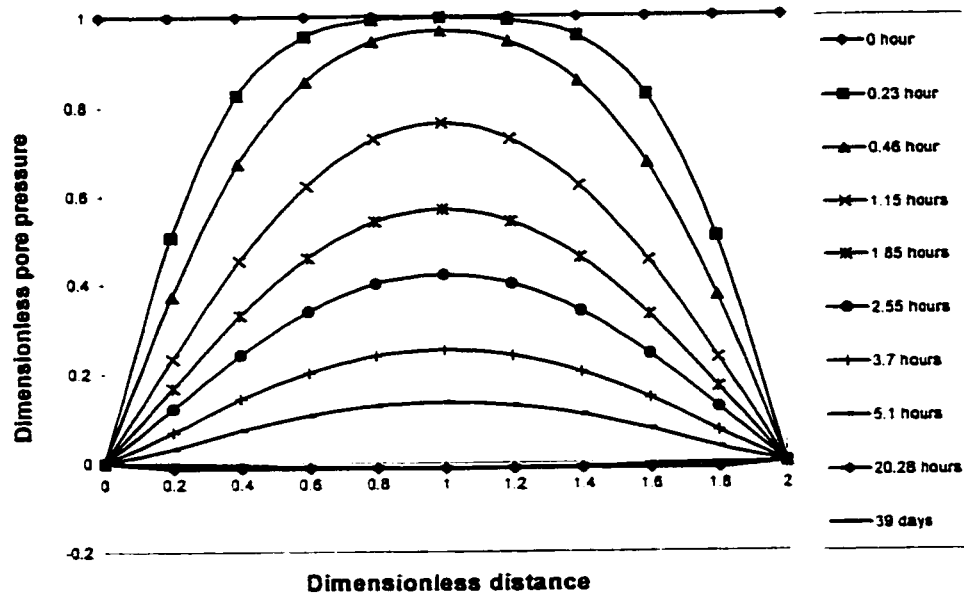


Figure 3.19 Chloride flow rate variation with the diffusion coefficient

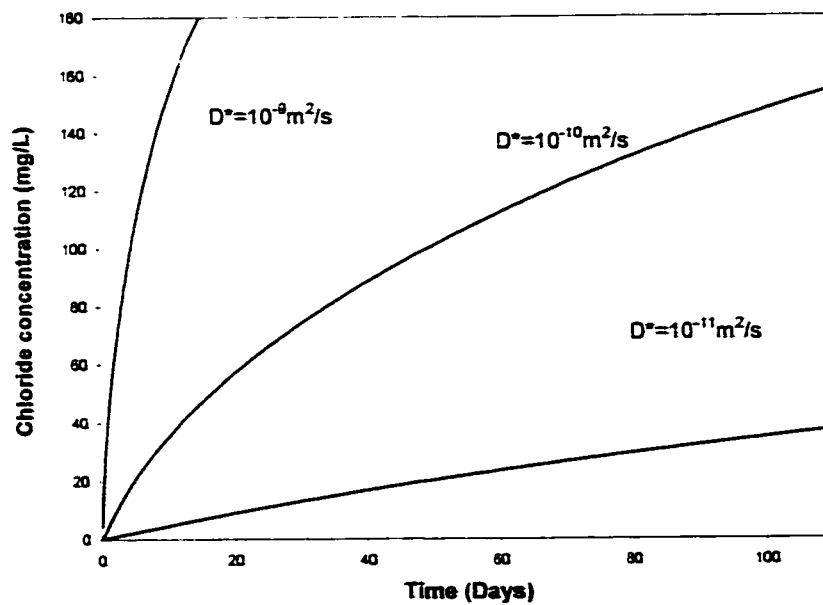


Figure 3.20 Sample 3a - pore pressure isochrones for an osmotic efficiency $\phi = 0.1$

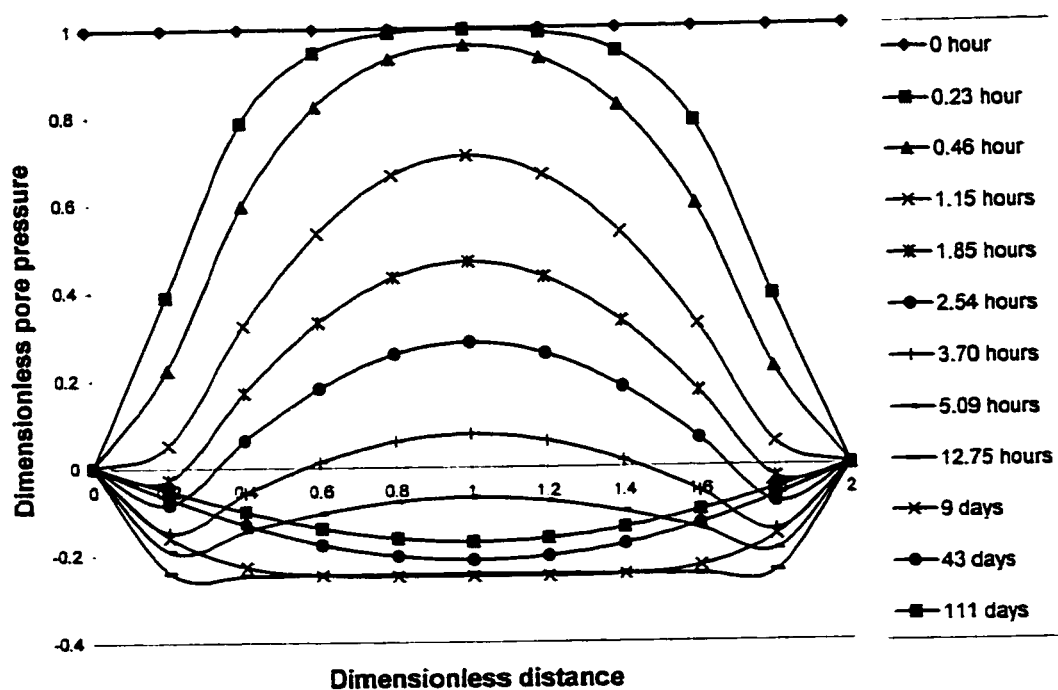


Figure 3.21 Sample 3a - pore pressure isochrones for an osmotic efficiency $\phi = 0.4$

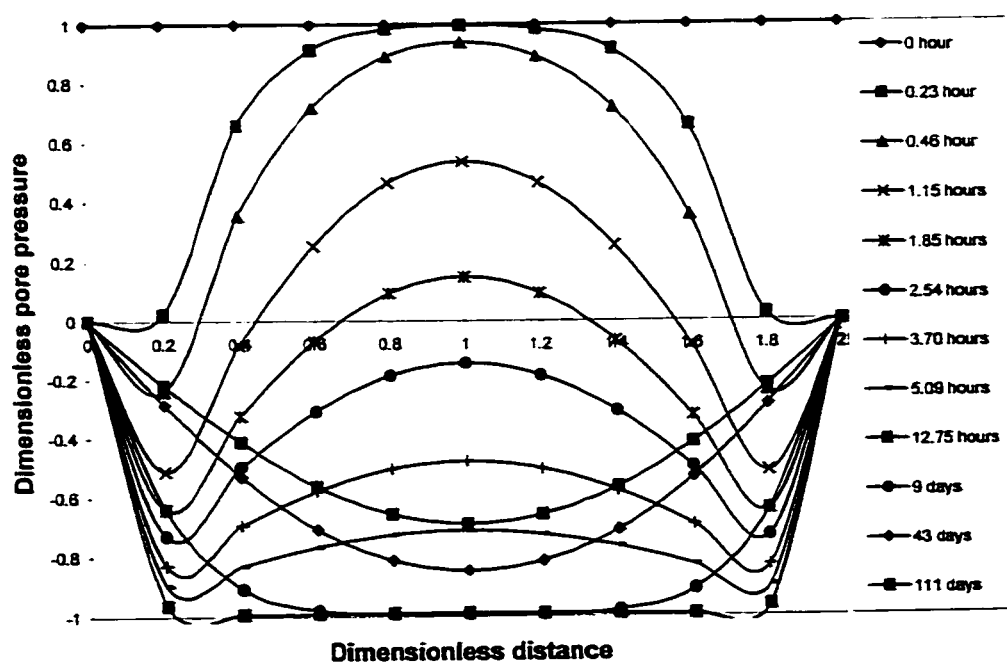


Figure 3.22 Sample 3a - Porosity change during swelling test

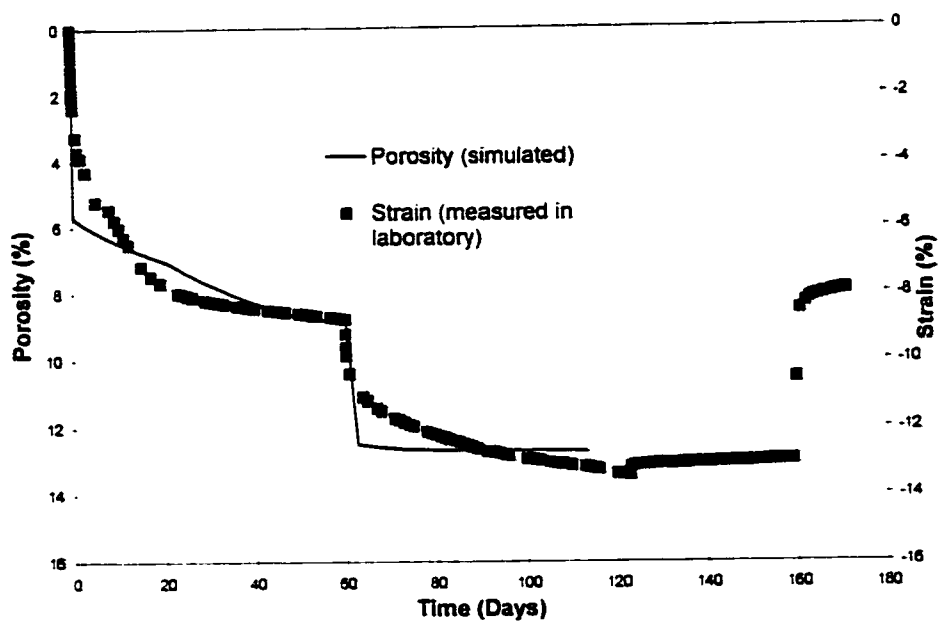
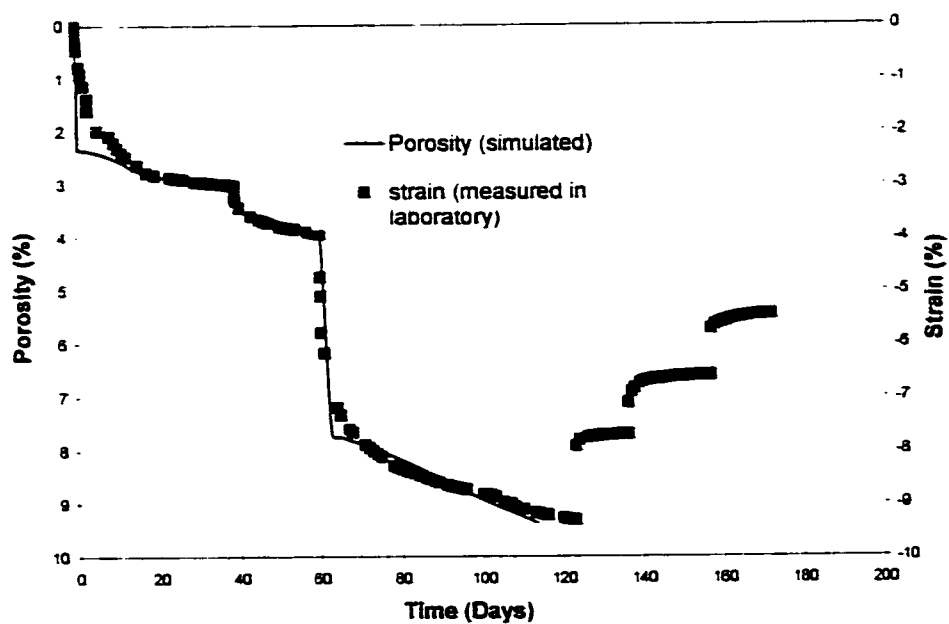


Figure 3.23 Sample 3b - Porosity change during swelling test



CHAPTER FOUR

NUMERICAL SIMULATION OF CHLORIDE TRANSPORT IN THE COLD LAKE AREA

4.1 Introduction

MT3D was used to model chloride migration in the field. MT3D is a public domain, three-dimensional, finite-difference contaminant transport simulator written by Zheng (1990) for the U.S. Environmental Protection Agency. The model uses a modular structure similar to that implemented in the U.S. Geological Survey modular three-dimensional finite-difference groundwater flow model, commonly known and referred to as MODFLOW (McDonald and Harbaugh, 1988). MT3D is used in conjunction with a flow model. In this case, hydraulic heads implemented in MT3D were calculated with MODFLOW. VISUAL MODFLOW, a commercial package of Waterloo Hydrogeologic Inc. combining MT3D and MODFLOW, was used for the simulation.

As it was indicated earlier in section 2.2.2.6, only chloride was considered for the simulation. For the present study, the simulation was run in two dimensions.

4.2 Governing Equation

The general partial differential equation for three-dimensional solute transport used in MT3D was derived from the mass balance principle [Bear (1979), Istok (1989), Javandel et al. (1984), Yu and Singh (1995)] as

$$R_t \frac{\partial C}{\partial t} = \frac{\partial}{\partial x_i} \left(D_{ij} \frac{\partial C}{\partial x_j} \right) - \frac{\partial}{\partial x_i} (v_i C) + \frac{q_{ws}}{\theta} C - \lambda \left(C + \frac{\rho_b}{\theta} \bar{C} \right) \quad (4.1)$$

where

R_t is the retardation factor, dimensionless, defined by relations (2.14), (2.16) and (2.18);

C is the solute concentration, ML^{-3} ;

t is the time, T ;

x_i is the distance along the respective Cartesian coordinate axis, L ;

D_{ij} is the hydrodynamic dispersion coefficient, L^2T^{-1} , defined by relation (2.11) in one dimension;

v_i is the linear pore water velocity, LT^{-1}

q_{ws} is the volumetric flux of water per unit volume of aquifer representing sources (positive) and sinks (negative), T^{-1} ;

C_s is the concentration of the sources or sinks, ML^{-3} ;

θ is the total porosity of the porous medium, dimensionless;

\bar{C} is the solute concentration sorbed on the porous medium, MM^{-1} ;

ρ_b is the bulk density of the porous medium, ML^{-3} ;

λ is the first order rate reaction constant, T^{-1} , defined by relation (2.19).

The right side of this equation comprises four terms describing successively the dispersion, the advection, the sink or the source and the chemical reaction. The reaction term will not be considered here because the chloride is a conservative ion (see subsection 2.2.2.5) and is therefore not affected by the chemical during the transport.

4.3 The Advection Term

4.3.1 Partial Differential Equations for Velocity Calculation

The advection term $\frac{\partial}{\partial x_i}(v_i C)$, second on the right hand side of equation (4.1), describes the transport of miscible contaminants at the same velocity as groundwater. The velocity included in the advection term is calculated with the flow equation through the relationship:

$$v_i = -\frac{K_{ii}}{\theta} \frac{\partial h}{\partial x_i} \quad (4.2)$$

where

K_{ii} is a principal component of the hydraulic conductivity tensor, LT^{-1} ;
 h is the hydraulic head, L.

The hydraulic head is in turn calculated numerically by MODFLOW from the mass balanced groundwater flow partial-differential equation (McDonald and Harbaugh, 1988):

$$\frac{\partial}{\partial x_i} \left(K_{ii} \frac{\partial h}{\partial x_i} \right) - q_{ws} = S_s \frac{\partial h}{\partial t} \quad (4.3)$$

where

S_s is the specific storage of the porous material (L^{-1}); in other terms, it is the volume of water that can be injected or withdrawn per unit volume of aquifer material per unit change in head;

q_{ws} is the volumetric flux per unit volume representing sources and sinks of water (T^{-1});

t is the time (T).

The continuity equation given by the relation (4.3) is the expression of the balance of flow, assuming that the density of ground water is constant (McDonald and Harbaugh, 1988).

4.3.2 Numerical Calculation of Hydraulic Heads by MODFLOW

In a 2-D cartesian coordinate system, the expansion of equation (4.3) gives:

$$\frac{\partial}{\partial x} \left(K_x \frac{\partial h}{\partial x} \right) + \frac{\partial}{\partial y} \left(K_y \frac{\partial h}{\partial y} \right) - q_{ws} = S_s \frac{\partial h}{\partial t} \quad (4.4)$$

Considering the cells adjacent to cell (i,j) (Figure 4.1), the flux through the cell (i,j) can be numerically written according to Darcy's law as follows:

$$q_{i,j-1/2} = K_{i,j-1/2} \Delta y_i \frac{(h_{i,j-1} - h_{i,j})}{x_j - x_{j-1}} \quad \text{is the flux through the interface between cells}$$

(i,j-1) and (i,j) and $K_{i,j-1/2}$ is the weighted average of the hydraulic conductivities between the two cells (Collins, 1961).

$$q_{i,j+1/2} = K_{i,j+1/2} \Delta y_i \frac{(h_{i,j+1} - h_{i,j})}{x_{j+1} - x_j} \text{ is the flux between cells (i,j) and (i,j+1)}$$

$$q_{i-1/2,j} = K_{i-1/2,j} \Delta x_j \frac{(h_{i-1,j} - h_{i,j})}{y_i - y_{i-1}} \text{ is the flux between cells (i-1,j) and (i,j)}$$

$$q_{i+1/2,j} = K_{i+1/2,j} \Delta x_j \frac{(h_{i+1,j} - h_{i,j})}{y_{i+1} - y_i} \text{ is the flux between cells (i,j) and (i+1,j)}$$

The flow equation for cell (i,j) can be expressed in 2-D finite difference approximation as

$$\begin{aligned} & K_{i,j-1/2} \Delta y_i \frac{(h_{i,j-1} - h_{i,j})}{x_j - x_{j-1}} + K_{i,j+1/2} \Delta y_i \frac{(h_{i,j+1} - h_{i,j})}{x_{j+1} - x_j} + K_{i-1/2,j} \Delta x_j \frac{(h_{i-1,j} - h_{i,j})}{y_i - y_{i-1}} \\ & + K_{i+1/2,j} \Delta x_j \frac{(h_{i+1,j} - h_{i,j})}{y_{i+1} - y_i} + W_{i,j} = Ss_{i,j} \Delta x_j \Delta y_i \frac{\Delta h_{i,j}}{\Delta t} \end{aligned}$$

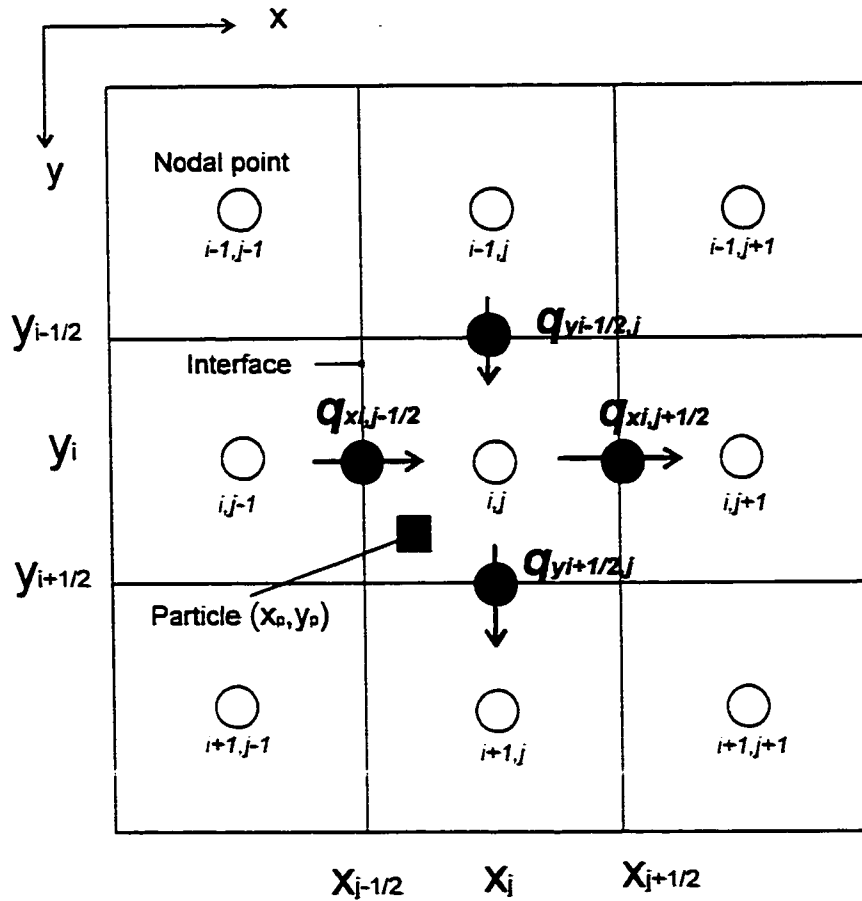
In time, the above equation is solved for the hydraulic heads by MODFLOW using a backward difference as follows:

$$\begin{aligned} & K_{i,j-1/2} \Delta y_i \frac{(h_{i,j-1}^m - h_{i,j}^m)}{x_j - x_{j-1}} + K_{i,j+1/2} \Delta y_i \frac{(h_{i,j+1}^m - h_{i,j}^m)}{x_{j+1} - x_j} + K_{i-1/2,j} \Delta x_j \frac{(h_{i-1,j}^m - h_{i,j}^m)}{y_i - y_{i-1}} \\ & + K_{i+1/2,j} \Delta x_j \frac{(h_{i+1,j}^m - h_{i,j}^m)}{y_{i+1} - y_i} + W_{i,j} = Ss_{i,j} \Delta x_j \Delta y_i \frac{h_{i,j}^m - h_{i,j}^{m-1}}{t_m - t_{m-1}} \end{aligned} \quad (4.5)$$

In the equation (4.5), only the hydraulic heads h^m at time level m are unknown. The different coefficients are known as well as the head h^{m-1} at the previous time level. Since there is one unknown per cell, writing the above equation for each cell gives a system of n equations with n unknown. The system of equations is then solved simultaneously for the

hydraulic heads h^m by MODFLOW. In a steady state case, the right hand side of the equation is equal to zero.

Figure 4.1 Numerical interpolations used to solve the advection term in MT3D



4.3.3 Velocity Numerical Interpolation

The x- and y-components of the pore water velocity at an arbitrary point (x_p, y_p) within a cell (i,j) are obtained as follows (Figure 4.1):

$$\begin{aligned}
 v_x(x_p, y_p) &= \frac{q_x(x_p, y_p)}{\theta_{i,j}} \\
 v_y(x_p, y_p) &= \frac{q_y(x_p, y_p)}{\theta_{i,j}}
 \end{aligned} \tag{4.6}$$

where

$\theta_{i,j}$ is the total porosity value at cell (i,j)

$$q_x(x_p, y_p) = (1 - \alpha_x)q_{i,j-1/2} + \alpha_x q_{i,j+1/2}$$

$$q_y(x_p, y_p) = (1 - \alpha_y)q_{i-1/2,j} + \alpha_y q_{i+1/2,j}$$

with

$$\alpha_x = \frac{x_p - x_{j-1/2}}{\Delta x_j} \text{ and } \alpha_y = \frac{y_p - y_{i-1/2}}{\Delta y_i} \text{ are linear interpolation factors for the}$$

x- and y- components

4.3.4 Numerical Solution for the Advection Term

With the velocity field known, MT3D allows different numerical techniques to solve for the solute concentration due to advection alone. The methods used are subdivided in two groups: the finite difference method and the particle tracking methods.

4.3.4.1 The Finite Difference Method

The finite difference method solves the advection term as follows:

$$\frac{\partial}{\partial x_i}(v_i C) = \frac{v_{x_{j+1/2}} C_{i,j+1/2} - v_{x_{j-1/2}} C_{i,j-1/2}}{\Delta x_j} + \frac{v_{y_{i+1/2,j}} C_{i+1/2,j} - v_{y_{i-1/2,j}} C_{i-1/2,j}}{\Delta y_i} \tag{4.7}$$

This method is suitable for diffusion-dominated problems. It is computationally efficient and have a small mass balance discrepancy. However, for advection-dominated problems, the solution of the transport equation by many standard numerical methods is plagued by numerical dispersion and artificial oscillation, particularly for problems with sharp concentration fronts. For this reason, particle tracking techniques have been included in MT3D to solve advection related problems. These methods are virtually free of numerical dispersion and artificial oscillation and are capable of handling the entire range of Peclet numbers from 0 to ∞ .

4.3.4.2 The Particle Tracking Methods

(i) Eulerian-Lagrangian Equations

The particle methods implemented in MT3D transport model are based on mixed Eulerian-Lagrangian equations. While the Eulerian scheme works in a fixed frame, the pure Lagrangian method involves continuously deforming coordinates or grids that follow the fluid motion. The advection term of the governing equation can be expanded according to the chain rule as follows:

$$\frac{\partial}{\partial x_i}(v_i C) = v_i \frac{\partial C}{\partial x_i} + C \frac{\partial v_i}{\partial x_i} = v_i \frac{\partial C}{\partial x_i} + C \frac{q_{ws}}{\theta} \quad (4.8)$$

By substitution of the above equation into the governing equation (4.1) and dividing both sides by the retardation factor, one gets:

$$\frac{\partial C}{\partial t} = \frac{1}{R_t} \frac{\partial}{\partial x_i} \left(D_{ij} \frac{\partial C}{\partial x_j} \right) - \bar{v}_i \frac{\partial C}{\partial x_i} - \frac{q_{ws}}{R_t \theta} (C - C_s) - \frac{\lambda}{R_t} \left(C + \frac{\rho_b}{\theta} \bar{C} \right) \quad (4.9)$$

where

$\bar{v}_i = \frac{v_i}{R_i}$ is the retarded velocity of a contaminant particle.

The above relation can be expressed in the Lagrangian form as

$$\frac{DC}{Dt} = \frac{1}{R_i} \frac{\partial}{\partial x_i} \left(D_{ij} \frac{\partial C}{\partial x_j} \right) - \frac{q_{ws}}{R_i \theta} (C - C_s) - \frac{\lambda}{R_i} \left(C + \frac{\rho_b}{\theta} \bar{C} \right) \quad (4.10)$$

where

the substantial derivative $\frac{DC}{Dt} = \frac{\partial C}{\partial t} + \bar{v}_i \frac{\partial C}{\partial x_i}$ indicates the rate of change in solute concentration calculated along the particle pathline (or a characteristic curve of the velocity field).

Introducing the finite difference, the substantial derivative (a Lagrangian concept) in a fixed (Eulerian) grid system becomes

$$\frac{DC}{Dt} = \frac{C_m^{n+1} - C_m^{n*}}{\Delta t} \quad (4.11)$$

In finite difference, this gives for the governing equation:

$$C_m^{n+1} = C_m^{n*} + \Delta t * RHS \quad (4.12)$$

where

C_m^{n+1} is the average solute concentration for cell m at the new time level (n+1);

C_m^{n*} is the average solute concentration for cell m at the new time level (n+1) due to the advection alone;

Δt is the time increment between the old time level (n) and the new time level (n+1);

RHS represents the finite difference approximation of the terms on the right hand side of the equation 4.10.

The equation (4.12) constitutes the basic algorithm of mixed Eulerian-Lagrangian method used in MT3D transport model.

Three particle tracking numerical methods are used in MT3D. Depending on the use of different Lagrangian techniques to approximate the advection term, the Eulerian-Lagrangian method may be classified as: the method of characteristics (Gardner et al., 1964), the modified method of characteristics (Cheng et al., 1984) and the hybrid method of characteristics, a combination of the two (Farmer, 1987).

(ii) *The Method of Characteristics (MOC)*

The method of characteristics involves both a stationary grid and a set of moving particles. To start the calculations, a set of moving points is uniformly distributed in the flow field either randomly or with a fixed pattern. A concentration and a position in the Cartesian coordinate system are associated with each of these particles. Considering a two-dimensional rectangular grid (x,y) , let p be the index number identifying a point, and n the time-step number (Figure 4.2). Initial coordinates (x_p^0, y_p^0) and an initial concentration C_p^0 are assigned to each point p . Particles are tracked forward through the flow field using a small time increment. Each particle has its own characteristic curve. At the end of each time increment Δt , a new position of the moving point is approximated knowing the velocity field. After a certain time n , the position of the particle is calculated as follows:

$$\begin{aligned}x_p^{n+1} &= x_p^n + \Delta t \left[v_x(x_p^n, y_p^n) \right] \\y_p^{n+1} &= y_p^n + \Delta t \left[v_y(x_p^n, y_p^n) \right]\end{aligned}\tag{4.13}$$

where

the superscripts n and $n+1$ indicate the old and the new time level, respectively.

The average concentration C_m^{n*} due to advection alone is evaluated as the sum of the concentrations of the particles that happen to be located within cell m after the time increment Δt (Figure 4.2):

$$C_m^{n*} = \frac{1}{NP} \sum_{l=1}^{NP} C_l^n \tag{4.14}$$

where

NP is the number of particles within cell m ;

C_l^n is the concentration of the l_{th} particle at the old time level n .

After the evaluation of C_m^{n*} for all cells, a weighted concentration \hat{C}_m^n is calculated based on the new and the old time level is calculated as follows:

$$\hat{C}_m^n = \omega C_m^{n*} + (1 - \omega) C_m^n \tag{4.15}$$

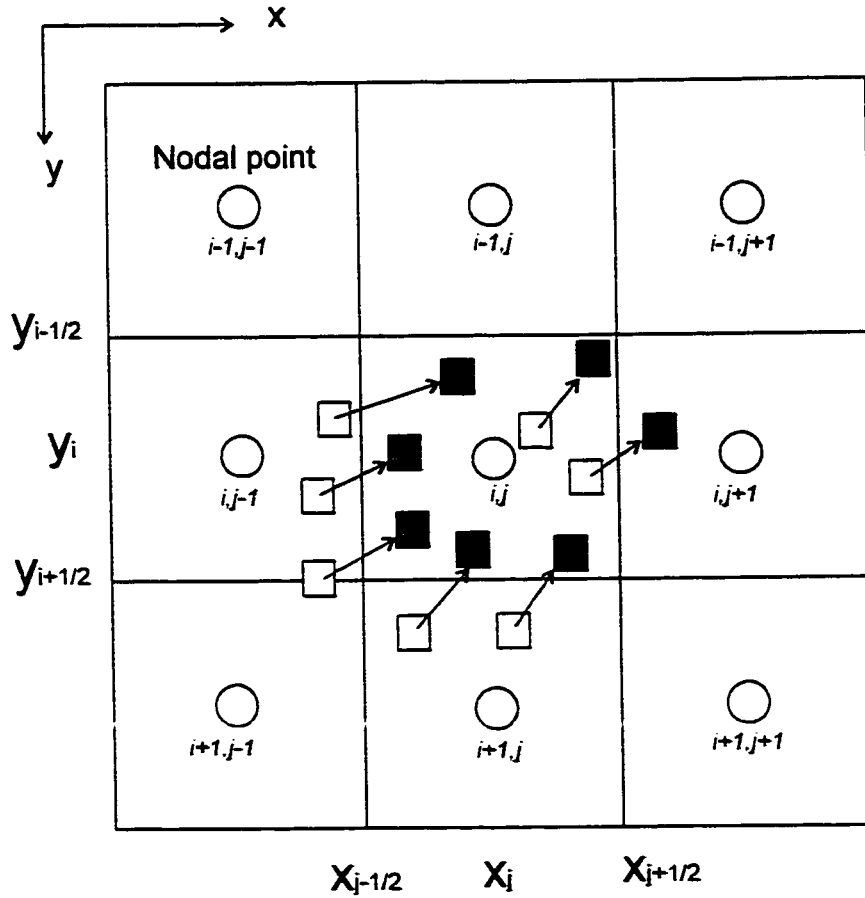
where

ω is a weighting factor between 0 and 1.

\hat{C}_m^n is then used to calculate the RHS terms of the equation (4.12), in other words, the changes in concentration due to dispersion, sink / source and chemical reaction terms:

$$\Delta C_m^{n+1} = \Delta t * RHS\left(C_m^n\right) \quad (4.16)$$

Figure 4.2 Illustration of moving particles used in the method of characteristics



The use of the weighted concentration in equation (4.16) represents an averaged approach because the processes of dispersion, sink/source, and/or chemical reactions occur throughout the time increment Δt . The concentration C_m^{n+1} for cell m at the new time level $(n+1)$ is then approximated as

$$C_m^{n+1} = C_m^{n*} + \Delta C_m^{n+1} \quad (4.17)$$

The concentrations of all moving particles are also updated to reflect the change due to the RHS terms. The procedure is repeated until the end of the desired time period.

Unlike many standard numerical schemes, the MOC technique is virtually free of numerical dispersions. However, it can lead to large mass balance discrepancies under certain situations because it is not entirely based on the principle of mass conservation. This can be overcome to a large extent by the use of consistent velocity interpolation schemes and higher order interpolation as the fourth-order Runge-Kutta method. On the other side, the MOC method can be slow due to the large amount of computer memory required to track to keep track of a large number of moving particles. In MT3D transport model, the use of the dynamic approach for particle distribution allows to reduce dramatically the computer memory requirement.

(iii) *The Modified Method of Characteristics (MMOC)*

The MMOC technique requires a much smaller memory because it uses one particle for each finite-difference cell.

To introduce the modified method of characteristics, let us consider a two-dimensional Eulerian grid system where a characteristic curve PQ indicates the particle pathline due to advection only (Figure 4.3). Assuming that the principal axes of the dispersion tensor are in the streamwise and transverse directions and neglecting the sink/source and reaction terms for simplicity, the advection-dispersion equation becomes

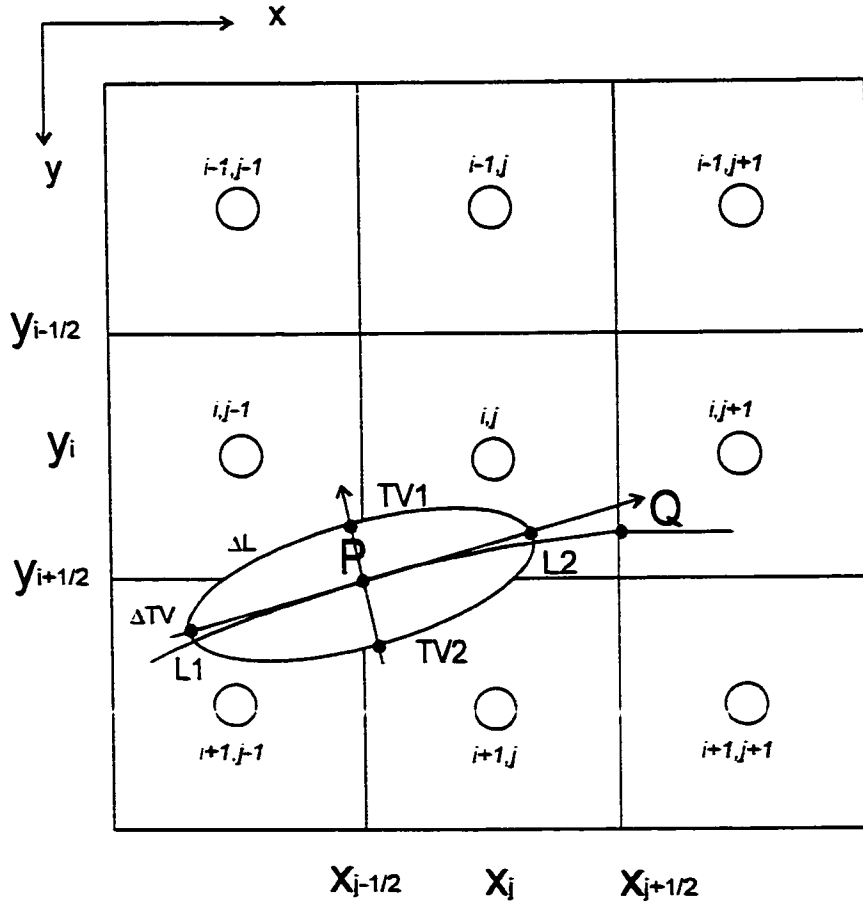
$$\frac{DC}{Dt} = \frac{\partial}{\partial L} \left(D_L \frac{\partial C}{\partial L} \right) - \frac{\partial}{\partial TV} \left(D_{TV} \frac{\partial C}{\partial TV} \right) \quad (4.18)$$

where

L and TV are the streamwise and normal coordinates;

D_L and D_{TV} are the longitudinal and transverse dispersion coefficients.

Figure 4.3 Illustration of the modified method of characteristics



In finite difference approximation, for a particle moving from P to Q during the time interval Δt , the equation (4.18) gives

$$\frac{C^{n+1}(Q) - C^n(P)}{\Delta t} = D_L \frac{C^n(L_1) - 2C^n(P) + C^n(L_2)}{(\Delta L)^2} + D_n \frac{C^n(TV_1) - 2C^n(P) + C^n(TV_2)}{(\Delta TV)^2}$$

where

$C^{n+1}(Q)$ is the concentration at point Q at time level $(n+1)$

$C^n(P)$ is the concentration at point P at time level n

ΔL and ΔTV are the spatial differences in the L and TV directions and L_1, L_2

TV_1 and TV_2 are points defined in Figure (4.3).

Therefore, the concentration at point Q at time level $(n+1)$ can be approximated as

$$C^{n+1}(Q) = C^n(P) + \frac{\Delta t D_L}{(\Delta L)^2} [C^n(L_1) - 2C^n(P) + C^n(L_2)] + \frac{\Delta t D_{TV}}{(\Delta TV)^2} [C^n(TV_1) - 2C^n(P) + C^n(TV_2)] \quad (4.19)$$

The equation (4.19) indicates that the concentration at point Q at level $(n+1)$ is the concentration at point P at time level n , which is convected to Q subjected to the perturbation of the dispersion. In a general case, the sink/source and reaction terms can be added to the right hand side. The anisotropic dispersion in a time span between $n \Delta t$ and $(n+1) \Delta t$ is expressed as the difference between the values of C at points L_1, L_2, TV_1 and TV_2 at point P . In other words, the region encompassed by points L_1, L_2, TV_1, TV_2 is an effective mixing zone centred at P (Cheng et al, 1984). Adopting notations used in equations (4.13),

$$C^{n*}(x_Q) = C^n(x_P) = C^n(x_Q - d) \quad (4.20)$$

where

x_p is the position of P or a position which a particle starting from nodal point Q reaches when it is tracked backward along the reverse pathline over the time increment Δt ;

x_Q is the position vector of nodal point Q

d is the characteristic nodal displacement, or the distance along a particle path from x_p to x_Q ;

$C''(x_p)$ is the concentration at position x_p at the old time level (n), generally interpolated from the concentrations at neighbouring nodal points.

$C''(x_Q)$ is the concentration at nodal point Q at new time level due to advection only.

The MMOC technique places one fictitious particle at the nodal point of the fixed grid at each new time level ($n+1$). Knowing the velocity field, the particle is tracked backward to find its position at old time level (n). The concentration associated with that position, interpolated from the concentrations at neighbouring nodal points, is used to approximate the $C''(x_Q)$ term. The dispersion term is treated in a similarly to the MOC method.

The MMOC technique is also free of numerical dispersion for advection-dominated problems. In addition, it uses a much smaller computer memory than the MOC method. However, with the use of lower-order interpolation in schemes adopted in MT3D, the MMOC technique can be plagued by some numerical dispersions for sharp front problems.

(iv) *The Hybrid Method of Characteristics (HMOC)*

The hybrid method of characteristics was introduced to combine the strengths of both the MOC and the MMOC methods (Neuman, 1984) by an automatic adaptive scheme. In presence of sharp concentration fronts, the advection term is solved by the MOC technique. Away from such fronts, the advection term is solved by the MMOC method. The selection of an appropriate criterion to control the switch between the MOC and the MMOC schemes can provide accurate solutions to transport problems over the entire range of Peclet numbers from 0 to ∞ with virtually no numerical dispersions.

4.4 The Dispersion Term

The dispersion and diffusion process in porous media were explained in sections 2.2.2.1, 2.2.2.2 and 2.2.2.3. The dispersion term includes two main components, the mechanical dispersion and the molecular diffusion. In the field, the molecular diffusion effect is generally secondary and negligible compared to the mechanical dispersion effect. It only becomes important when groundwater velocity is very low.

MT3D transport model supports a hydrodynamic dispersion tensor allowing the use of two transverse dispersivities, a horizontal transverse dispersivity (α_{TH}) and a vertical transverse dispersivity (α_{TV}) (Burnett and Frind, 1987). In a two-dimensional case involving a longitudinal and a vertical dispersivity, the hydrodynamic dispersity is given by the relation:

$$\begin{aligned}
D_{xx} &= \alpha_L \frac{v_x^2}{|v|} + \alpha_{TV} \frac{v_y^2}{|v|} + D^* \\
D_{yy} &= \alpha_L \frac{v_y^2}{|v|} + \alpha_{TV} \frac{v_x^2}{|v|} + D^* \\
D_{xy} &= (\alpha_L - \alpha_{TV}) \frac{v_x v_y}{|v|}
\end{aligned} \tag{4.21}$$

Expanding the dispersion term of the governing equation (4.1) in two dimensions, one gets:

$$\frac{\partial}{\partial x_i} \left(D_{ij} \frac{\partial \mathcal{C}}{\partial x_j} \right) = \frac{\partial}{\partial x} \left(D_{xx} \frac{\partial \mathcal{C}}{\partial x} \right) + \frac{\partial}{\partial x} \left(D_{xy} \frac{\partial \mathcal{C}}{\partial y} \right) + \frac{\partial}{\partial y} \left(D_{yx} \frac{\partial \mathcal{C}}{\partial x} \right) + \frac{\partial}{\partial y} \left(D_{yy} \frac{\partial \mathcal{C}}{\partial y} \right) \tag{4.22}$$

In MT3D, the equation (4.22) is solved with a fully explicit central finite-difference method as follows:

$$\begin{aligned}
& D_{xx, j-1/2} \frac{C_{i,j+1}^n - C_{i,j}^n}{\Delta x_j (0.5\Delta x_j + 0.5\Delta x_{j+1})} - D_{xx, j+1/2} \frac{C_{i,j}^n - C_{i,j-1}^n}{\Delta x_j (0.5\Delta x_{j-1} + 0.5\Delta x_j)} \\
& + D_{xy, i-1/2, k} \frac{\omega_{x_{j+1/2}} C_{i+1,j}^n + (1 - \omega_{x_{j+1/2}}) C_{i+1,j+1}^n - \omega_{x_{j+1/2}} C_{i-1,j}^n - (1 - \omega_{x_{j+1/2}}) C_{i-1,j+1}^n}{\Delta x_j (0.5\Delta y_{i-1} + \Delta y_i + 0.5\Delta y_{i+1})} \\
& - D_{xy, i+1/2, k} \frac{\omega_{x_{j-1/2}} C_{i+1,j-1}^n + (1 - \omega_{x_{j-1/2}}) C_{i+1,j}^n - \omega_{x_{j-1/2}} C_{i-1,j-1}^n - (1 - \omega_{x_{j-1/2}}) C_{i-1,j}^n}{\Delta x_j (0.5\Delta y_{i-1} + \Delta y_i + 0.5\Delta y_{i+1})} \\
& + D_{yx, j-1/2} \frac{\omega_{y_{i+1/2}} C_{i,j+1}^n + (1 - \omega_{y_{i+1/2}}) C_{i+1,j+1}^n - \omega_{y_{i+1/2}} C_{i,j-1}^n - (1 - \omega_{y_{i+1/2}}) C_{i+1,j-1}^n}{\Delta y_i (0.5\Delta x_{j-1} + \Delta x_j + 0.5\Delta x_{j+1})} \\
& - D_{yx, j+1/2} \frac{\omega_{y_{i-1/2}} C_{i-1,j+1}^n + (1 - \omega_{y_{i-1/2}}) C_{i,j+1}^n - \omega_{y_{i-1/2}} C_{i-1,j-1}^n - (1 - \omega_{y_{i-1/2}}) C_{i,j-1}^n}{\Delta y_i (0.5\Delta x_{j-1} + \Delta x_j + 0.5\Delta x_{j+1})} \\
& + D_{yy, i+1, l} \frac{C_{i+1,j}^n - C_{i,j}^n}{\Delta y_j (0.5\Delta y_j + 0.5\Delta y_{j+1})} - D_{yy, i-1, l} \frac{C_{i,j}^n - C_{i-1,j}^n}{\Delta y_i (0.5\Delta y_{i-1} + 0.5\Delta y_i)}
\end{aligned} \tag{4.23}$$

where

$\dot{C}_{i,j}^n$ is the weighted concentration defined earlier in relation (4.15)

D_{xx} , D_{xy} , D_{yx} and D_{yy} are the components of the hydrodynamic dispersion coefficient, evaluated at cell interfaces and given by the relation (4.2);

Subscripts i and j indicate the position of the cell in the grid;

ω_x and ω_y are cell interface weighting factors used to compute the concentration value at cell interface; they are given by the following formula:

$$\begin{aligned}\omega_x &= \frac{x - x_{j-1}}{0.5\Delta x_j + 0.5\Delta x_{j-1}} \\ \omega_y &= \frac{y - y_{i-1}}{0.5\Delta y_i + 0.5\Delta y_{i-1}}\end{aligned}\quad (4.24)$$

with

x located between x_{j-1} and x_j and y between y_{i-1} and y_i .

Accordingly, the longitudinal and vertical dispersivities are interpolated using the cell weighting factors:

$$\begin{aligned}\alpha_{L,i+0.5} &= \alpha_{L,i} \omega_{x,i+0.5} + \alpha_{L,i+1} (1 - \omega_{x,i+0.5}) \\ \alpha_{TV,i+0.5} &= \alpha_{TV,i} \omega_{x,i+0.5} + \alpha_{TV,i+1} (1 - \omega_{x,i+0.5})\end{aligned}\quad (4.25)$$

Therefore, the values of D_{xx} , D_{yy} , D_{xy} and D_{yx} at cell interfaces given by the relation (4.2) are approximated as follows:

$$\begin{aligned}
D_{xx_{i,j+1/2}} &= \alpha_{L_{i,j+1/2}} \frac{v_{x_{i,j+1/2}}^2}{v_{i,j+1/2}} + \alpha_{TV_{i,j+1/2}} \frac{v_{y_{i,j+1/2}}^2}{v_{i,j+1/2}} \\
D_{yy_{i,j+1/2}} &= \alpha_{L_{i+1/2,j}} \frac{v_{y_{i+1/2,j}}^2}{v_{i+1/2,j}} + \alpha_{TV_{i+1/2,j}} \frac{v_{x_{i+1/2,j}}^2}{v_{i+1/2,j}} \\
D_{xy_{i,j+1/2}} &= \left(\alpha_{L_{i,j+1/2}} - \alpha_{TH_{i,j+1/2}} \right) \frac{v_{x_{i,j+1/2}} v_{y_{i,j+1/2}}}{v_{i,j+1/2}} \\
D_{yx_{i+1/2,j}} &= \left(\alpha_{L_{i+1/2,j}} - \alpha_{TH_{i+1/2,j}} \right) \frac{v_{x_{i+1/2,j}} v_{y_{i+1/2,j}}}{v_{i+1/2,j}}
\end{aligned} \tag{4.26}$$

4.5 Sinks and Sources

Sinks and sources represent solute mass dissolved in water entering the simulated domain through sources, or solute mass dissolved in water leaving the simulated domain through sinks. Sinks or sources can be areally distributed or point sinks or sources. Point sinks or sources include wells, drains and rivers. Constant head (i.e. lakes) and general head boundaries are also treated in the flow model as point sink or sources.

For sources, it is necessary to specify the concentration of source water. For sinks, the concentration of sink water is generally equal to the concentration of groundwater in the aquifer and should not be specified. The exception is evapotranspiration, which may be assumed to take only pure water away from the aquifer so that the concentration of the evapotranspiration flux is zero.

4.6 Chemical Reactions

Chemical reactions included in the MT3D transport model are equilibrium-controlled linear or non-linear sorption and first-order irreversible rate reactions, most commonly radioactive decay or biodegradation (see paragraph 2.2.2.5). For a conservative ion such as chloride, the chemical reaction term of equation 4.1 is not used.

4.7 Geological Data for the Model

An 8.500m long section was chosen in the southern part of the Cold Lake Production Projects (CLPP) of Imperial Oil for the simulation of the chloride transport in the field. The simulated section is situated south of the groundwater mound characterizing the hydrogeological pattern in the Quaternary aquifers (Figures 1.9, 1.10 and 1.11).

The simulation involved a section where the Empress Formation Unit 3 aquifer is in contact with the Colorado Shale. The section includes wells situated at locations GEW97-3 and GEW97-9 respectively in the southern and the northern part of the section (Figure 1.6). The two locations are separated by a distance of about 5.700m. The stratigraphy, the logs and the instrumentation data collected by Imperial Oil (1998) are indicated in Appendix 2. Three wells were drilled and installed at the GEW97-3 location. They were completed in different layers: the Bonnyville Formation Unit 1, the Empress Formation Unit 3 and the Colorado Shale. Only one well was completed at location GEW97-9, in the Empress Formation Unit 3.

The borehole data indicate that the Empress Formation Unit 3 aquifer has an average thickness of about 20m. The aquifer is in direct contact with the Colorado Shale. At location GEW97-3, the aquifer is confined by 15m of silty clay of the Bronson Lake

formation. The confining layer is reduced to about 2 to 3m at location GEW97-9. In both wells, the Empress Formation Unit 3 aquifer was monitored through a 6m screen placed at the bottom of the aquifer, near the contact with the bedrock.

The section between the two wells is characterised by a flow consistently directed from north to south. The hydraulic heads for the Empress Formation Unit 3 were measured at 593.86m at location GEW97-9 in the northern part of the section and 555.41m at location GEW97-3 situated in south. The calculated lateral hydraulic gradient averages 0.0069. This value is consistent with the local gradient of 0.007 measured at location GEW97-3 (Table 1.7). Piezometric measurements show that the aquifer recharges in the northern part of the section and discharges in the south.

During the monitoring period from December 20, 1997 to May 25, 1998, the chloride content analyses in the Empress Formation Unit 3 at GEW97-9 indicated values between 1.5 and 8.3mg/L (Table 1.7) with an average of 5.1mg/L. Measurements at location GEW97-3 from November 3, 1997 to June 1, 1998 showed values between 664 and 777mg/L with an average of 708.9mg/L for the same aquifer. It appears that chloride levels increase from the recharge area to the discharging zone. Chloride measurements in the surrounding area (Figure 4.4) show a similar spatial trend.

Analyses of two water samples at the base of the fractured Colorado Shale at location GEW97-3 indicated a chloride content of 5,100 - 5,150mg/L.

4.8 Model Set Up

The model was set up to simulate a two-dimensional transfer of chlorides from the Colorado Shale to the Empress Formation Unit 3 aquifer. It was calibrated with data

collected from boreholes GEW97-3 and GEW97-9. The simulation was done for a period of 15,000 years, assuming that the Quaternary sediment deposition was complete at that time and the hydrogeological conditions were comparable to those observed today.

The section was simulated with four layers including, from bottom to top: the non-fractured Colorado Shale, the fractured Colorado Shale, the Empress formation Unit 3 Aquifer and the confining layer (Figure 4.5). The thickness of the non-fractured Colorado Shale was set at 80m. It was considered important enough to provide sufficient amount of chloride ions required for the flow modeling process. This requirement is dictated by the fact that the bedrock is considered as an endless source of chlorides (see geological conditions in chapter 1). The thickness of the fractured Colorado Shale was taken as 30m, consistent with the field data. A thickness of 20m was adopted for the Empress Formation Unit 3 Aquifer, in accordance with the data from boreholes GEW97-3 and GEW97-9. The confining layer was given an average thickness of 10m. The model was limited to a total thickness of 140m for a section 8,500m long. In Figure 4.5 and other figures representing the section, the vertical scale was exaggerated 40 times to the horizontal scale for the clarity of the model.

A grid was applied to the section with a horizontal interval of 100m (Figure 4.5). Most of the time, the vertical interval was varied from 2.5m to 10m. However, preliminary tests indicated that a finer grid improved significantly the accuracy of the results around the contact between the fractured Colorado Shale and the Empress Formation Unit 3 aquifer. For this reason, the vertical interval was refined to 0.625m in that zone.

Figure 4.4 Chloride levels for Empress Formation Unit 3 (Imperial Oil, 1998)

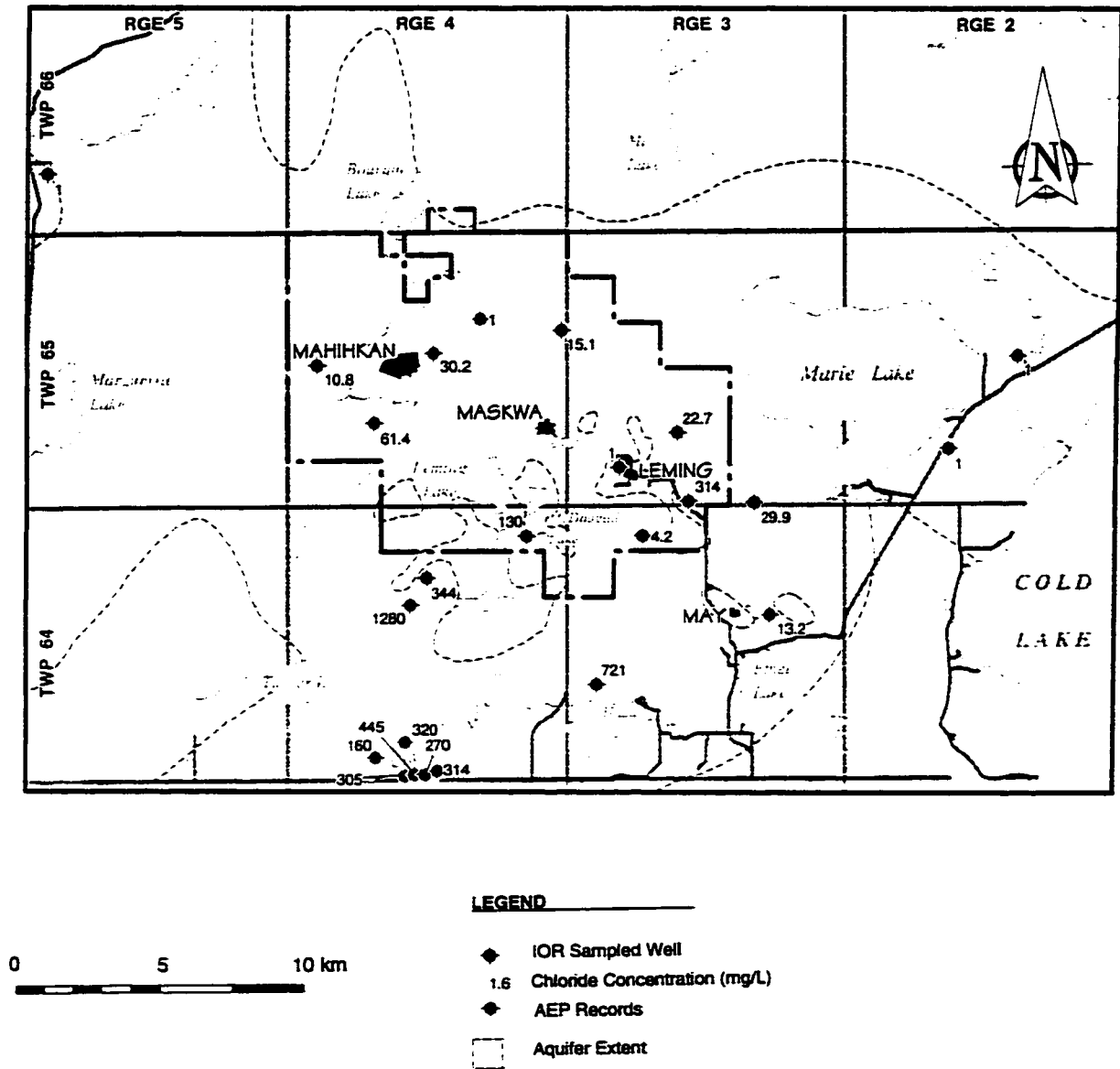
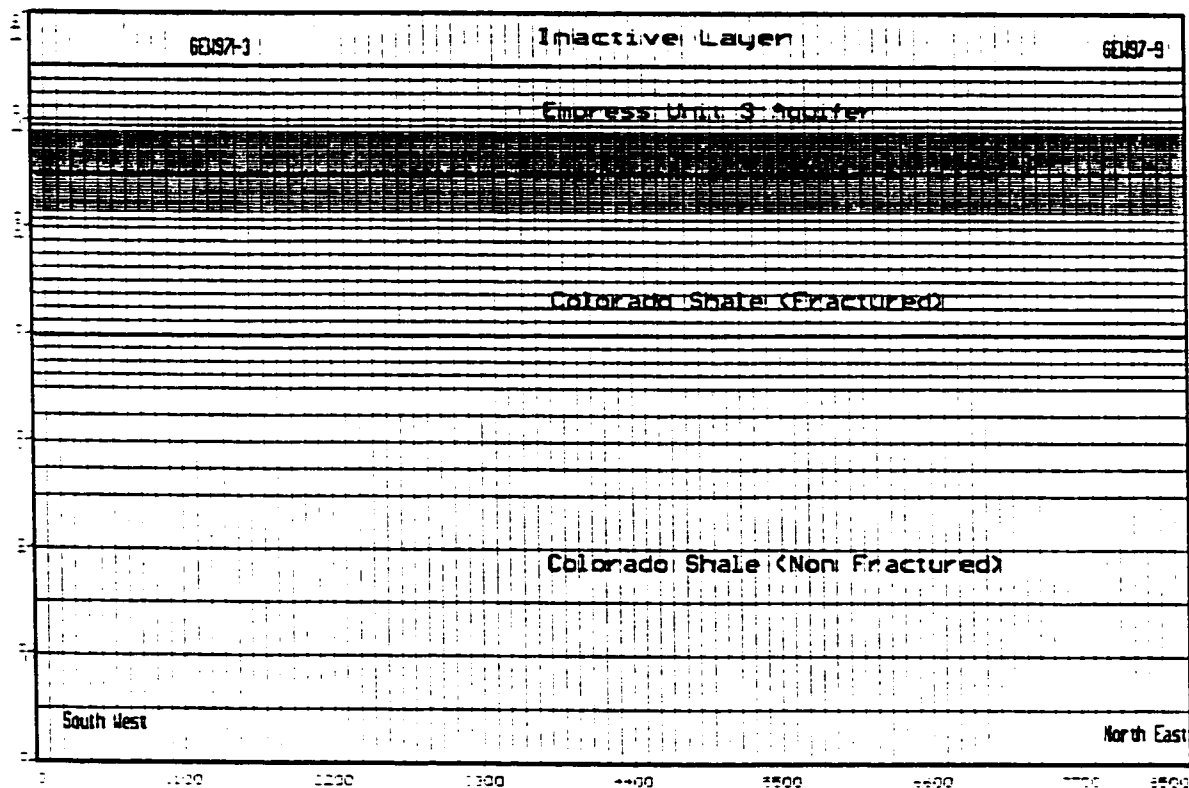


Figure 4.5 Grid setup for the transport model



4.9 Initial and Boundary Conditions

4.9.1 The Initial Chloride Content

The initial chloride content was set at 0 mg/L for the Empress Formation Unit 3, given the continental origin of Quaternary aquifers. For the initial chloride concentration in the Colorado Shale, three cases were considered for the simulation, 5,500mg/L, 10,000mg/L and 20,000mg/L. The value of 5,500mg/L is consistent with the analysis obtained from

the borehole located at GEW97-3. The value of 20,000mg/L represents the average chloride concentration for the sea water. As indicated in chapter 1, the chloride concentration decreases from about 40,000mg/L at the bottom of the Colorado Shale to about 5,000mg/L or less in the upper part. The initial chloride concentration in the shale at the contact with the Quaternary sediments depends partly on the level reached by the pre-Cretaceous erosion.

4.9.2 The Hydraulic Head Boundary

A hydraulic head boundary was imposed at both ends of the model in the Empress 3 Formation Unit 3. Hydraulic heads of 600m and 542m were adopted respectively for the north and south edges of the section. These values were adapted so that the hydraulic heads calculated from the model match exactly those observed at locations GEW97-3 and GEW97-9.

4.9.3 The Flow Boundary

A no flow boundary was imposed at the contact between the Empress Formation Unit 3 and the confining layer. The no flow boundary was assumed considering that the confining inactive layer is composed of silty clay with very low hydraulic conductivities compared to the aquifer layer. The borders of the Colorado Shale (not included the contact with the Quaternary aquifer) were implicitly considered as no flow boundaries, as the flow is governed by hydraulic heads fixed only in the Empress formation Unit 3.

4.10 Simulation of the Base Case

For the base case, the model was calibrated against site observations and data collected from wells at locations GEW97-3 and GEW97-9. The hydraulic parameters used for that case are displayed in Table 4.1.

Table 4.1 Properties used for the simulation of the base case

	Empress Formation Unit 3	Fractured Colorado Shale	Non-Fractured Colorado Shale
Horizontal hydraulic conductivity K_h (m/s)	2.0×10^{-6}	1.0×10^{-7}	1.0×10^{-11}
Specific storage coefficient	0.003	0.003	0.003
Total porosity	0.25	0.2	0.2
Effective porosity	0.25	0.07	0.03
Horizontal dispersivity coefficient (m)	15	15	15
Molecular diffusion coefficient (m^2/s)	1.0×10^{-9}	1.0×10^{-10}	1.7×10^{-11}

The horizontal hydraulic conductivity for the Empress formation Unit 3 was fixed at $2.0 \times 10^{-6} m/s$ for the base case. Hydraulic conductivities for the Colorado Shale were approximated at $1.0 \times 10^{-7} m/s$ and $1.0 \times 10^{-11} m/s$ for the fractured and the non-fractured layers, respectively. The ratio between the vertical and horizontal hydraulic conductivities was always considered as 0.1 for this study. The specific storage coefficient was set up at 0.003 for all the layers. These values are consistent with field data indicated in chapter 1 and average hydraulic conductivities measured in wells around the simulated area.

Total and effective porosities were used in the model. The total porosity accounts for all the voids in the porous material, while the effective porosity considers only connected

voids filled with gravity water that can flow under a hydraulic gradient. The total porosity was fixed at 0.25 for the Empress formation Unit 3 and 0.2 for the Colorado Shale. These values are consistent with field observations and literature data (Hitchon et al. 1989). Effective porosities were assumed at 0.07 and 0.03 for the fractured and the non-fractured Colorado Shale. Effective porosities are used when velocities are calculated with MODFLOW. However, velocities calculated with MT3D involve the total porosity because the diffusion and dispersion processes include not only gravity water, but also adsorbed water and ions electrically bound in the structure of the porous media.

The longitudinal dispersivity was approximated at 15m by the use of the relation 2.9, considering the adopted grid interval of 100m for the model. The vertical dispersivity is generally considered insignificant compared to the horizontal component. The vertical/horizontal dispersivity ratio is expected to be very low as indicated in subsection 2.2.2.3. For this work, it was estimated between 10^{-3} and 10^{-6} , considering the negligible vertical velocity compared to the longitudinal velocity. The molecular diffusion coefficient taken for the non-fractured Colorado Shale was previously calculated with the laboratory experiments at $1.7 \times 10^{-11} \text{ m}^2/\text{s}$. This value was increased to $1.0 \times 10^{-10} \text{ m}^2/\text{s}$ for the fractured layer of the Colorado Shale as suggested by the laboratory experiments. The diffusion coefficient of the Empress Formation Unit 3 was fixed at $1.0 \times 10^{-9} \text{ m}^2/\text{s}$. This value is often considered for the diffusion of the major ions in water (Fetter, 1994).

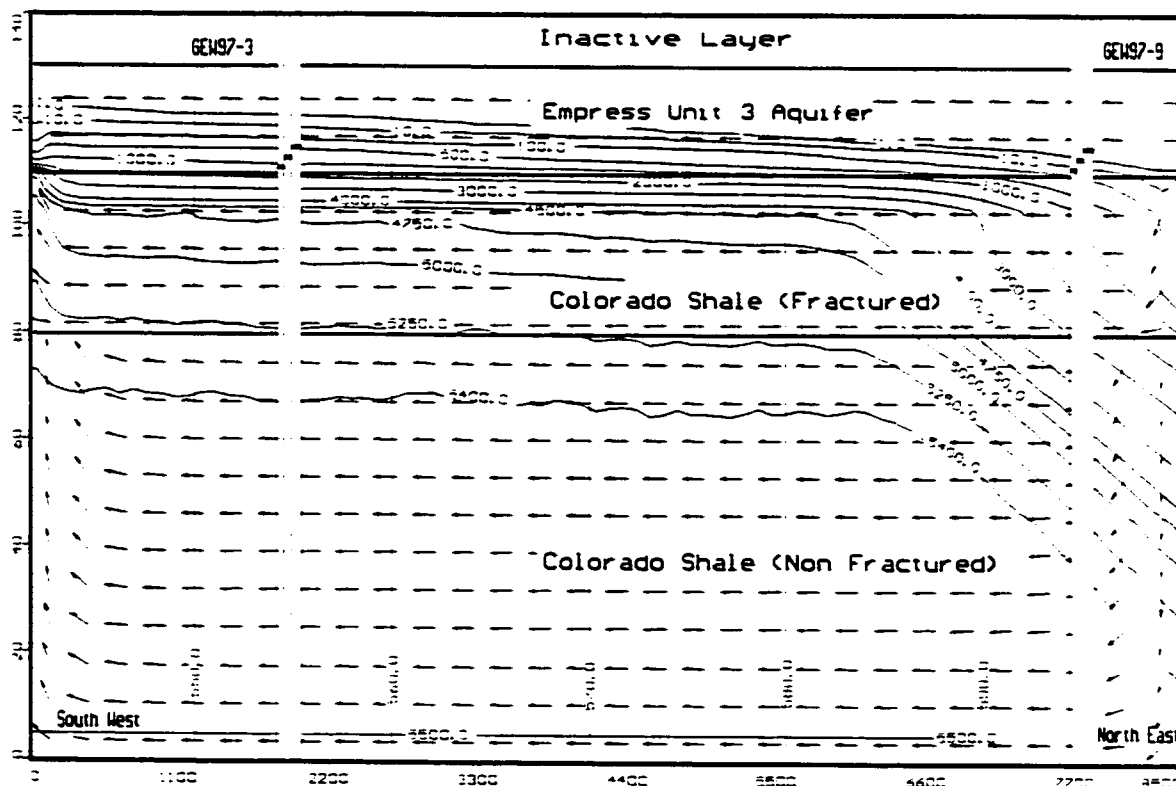
The results of the simulation are presented in two figures. Figure 4.6a represents the present simulated situation after running the model for a period of 15,000 years. A southwest-northeast section is displayed with the four layers representing the non-fractured Colorado Shale, the fractured Colorado Shale, the Empress Formation Unit 3 and the inactive layer, respectively from the bottom to the top. The hydraulic heads were calculated by MODFLOW in steady state conditions from the boundary heads imposed in the model. The hydraulic heads of 555.3m and 594.6m observed respectively at locations

GEW97-3 and GEW97-9 for the Empress formation Unit 3 are matched in the model.

The flow directions calculated with MODFLOW suggest a recharge at the northeast end of the section (near GEW97-9) and a discharge at its southwest end (near GEW97-3), in accordance with field observations.

Chloride concentration isochrones are also represented in Figure 4.6a. They were calculated with MT3D from the transport equation (4.1) with numerical approximations explained earlier in this chapter. A chloride concentration of 5,100-5,150mg/L was measured at the base of the fractured Colorado Shale at location GEW97-3. This value was history matched by considering an initial chloride content of 5,500mg/L. Figure 4.6a shows the extent of chloride introduced into the Empress Formation Unit 3 aquifer. The extent of chloride impact in the Empress Formation Unit 3, calculated from the contact with the Colorado Shale, increases progressively from 1 to 3m in the recharge area to about 13m in the discharge zone. At a comparable level from the contact, the chloride concentration decreases from the discharge to the recharge area. The chloride content also decreases from the bottom of the Empress Formation Unit 3 to the top of the contaminated zone. In the discharge area, the chloride exceeds 1,000mg/L at the bottom of the aquifer. It decreases to 370mg/L, 10mg/L and 1mg/L at 5m, 10m and 13m, respectively from the bottom. In the recharge area, the chloride concentration is low, less than 10mg/L, even near the contact with the Colorado Shale.

Figure 4.6a Simulated chloride contours, hydraulic heads and flow directions for the base case¹

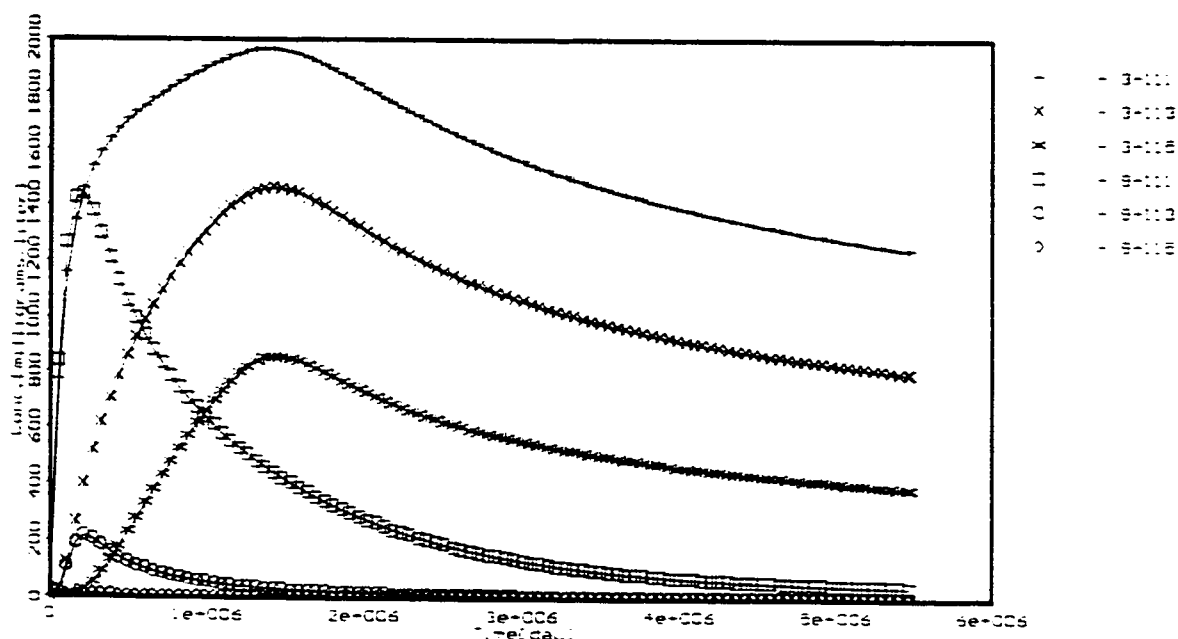


The evolution of chloride concentrations with time was simulated at 3 distinct locations in each of the two wells, GEW97-3 and GEW97-9, completed in the Empress formation Unit 3. The monitoring points were chosen at 1m, 3m and 5m from the contact of the Quaternary aquifer with the Colorado Shale (Figure 4.6a). This interval is assumed to

¹ The location of monitored points at locations GEW97-3 and GEW97-9 are indicated. The vertical scale is exaggerated 40 times to the horizontal scale.

represent the screened level of the well where water samples were collected during the field investigations.

Figure 4.6b Simulated chloride evolution with time for the base case²



The evolution of chloride concentrations with time at monitored points is represented in Figure 4.6b. The chloride concentration increases sharply to a maximum in the early stage of the model. This early fast increase was also observed with the release of chloride in laboratory samples (Figures 3.2 to 3.6). The rate of chloride content increase and the maximum reached by the peak depend on the distance of the monitored point from the

² The numbers in the legend stand for the last digit for the location (3 for GEW97-3 and 9 for GEW97-9) and the vertical position of the simulated point (111, 113 and 115 are at 1, 3 and 5m from the contact Quaternary aquifer / Colorado Shale).

contact with the Colorado Shale. They are higher for points close to the bottom. The rate of increase is similar for the two wells at monitoring points located at the same level from the bottom. However, the concentration peak is always lower for monitoring points located at GEW97-9, close to the recharge area.

Figure 4.7a Simulated chloride contours, hydraulic heads and flow directions for a groundwater velocity of 0 m/year in the Quaternary aquifer

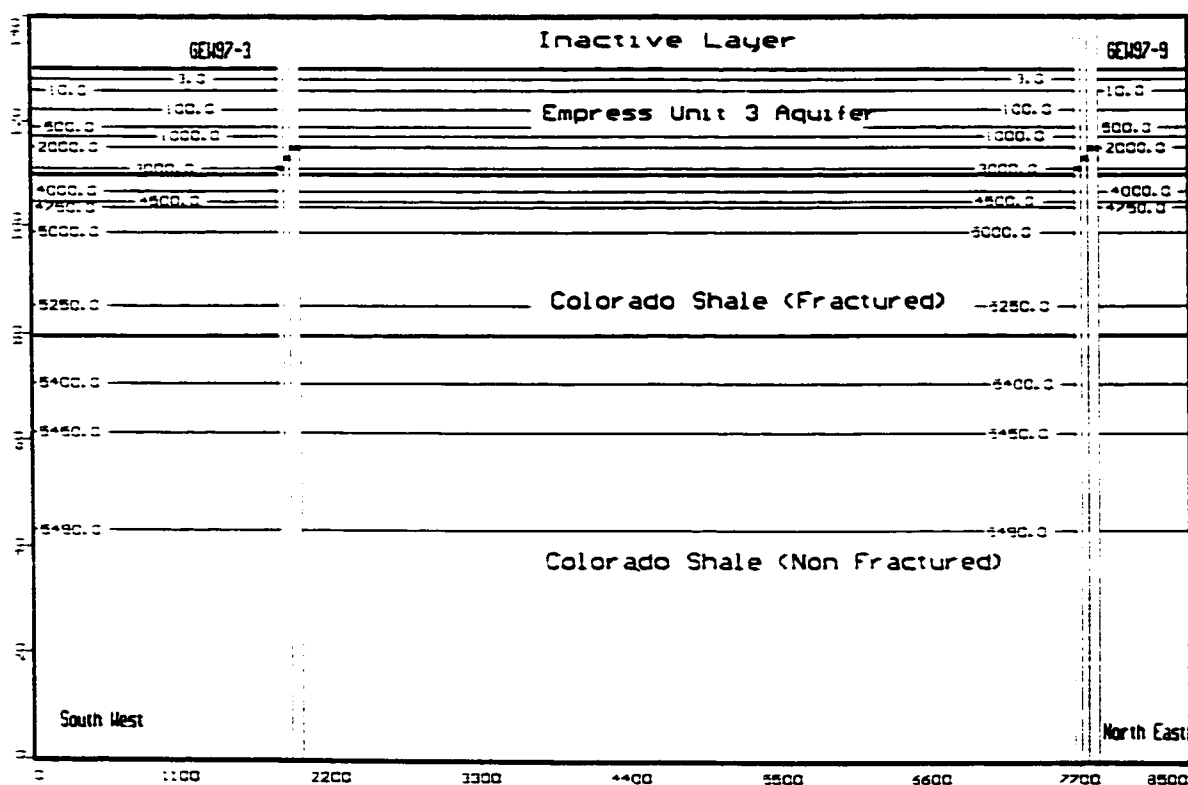


Figure 4.7b Simulated chloride evolution with time for a groundwater velocity of 0m/year in the Quaternary aquifer

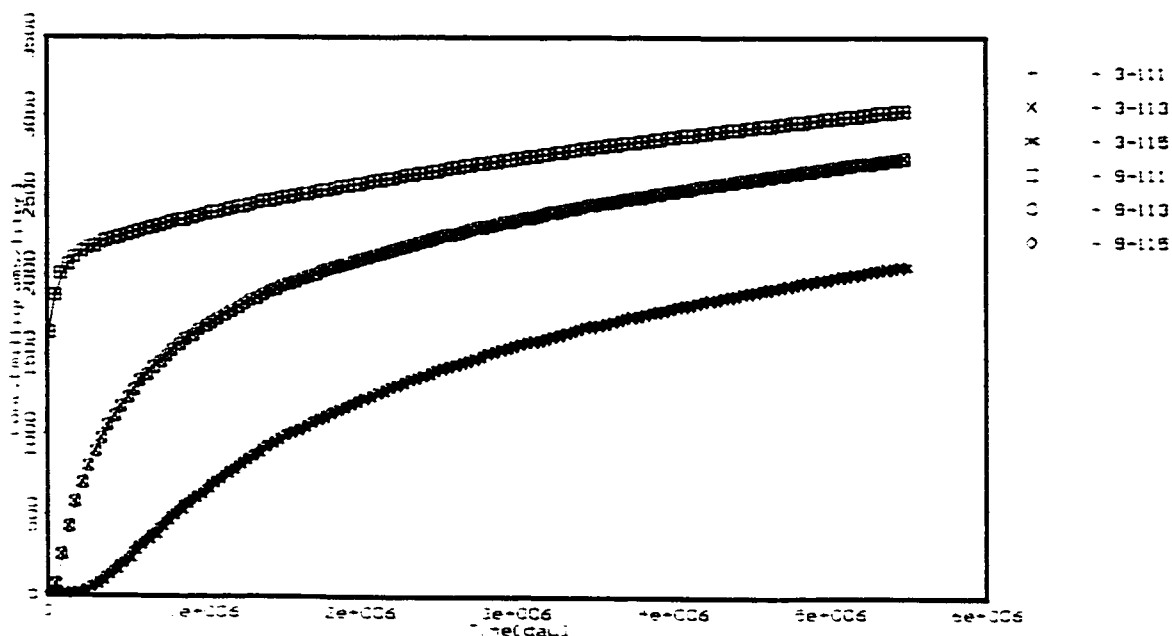
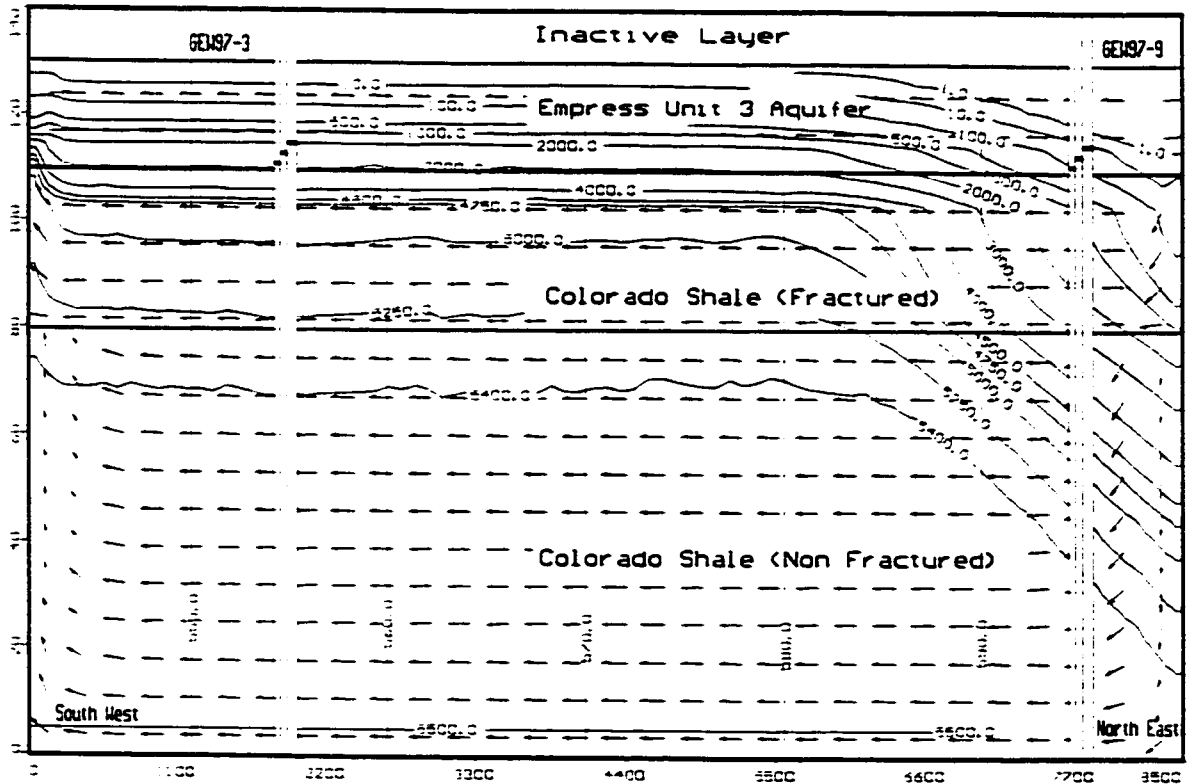


Table 4.2 Comparison between simulated and analytical chloride concentrations for the base case

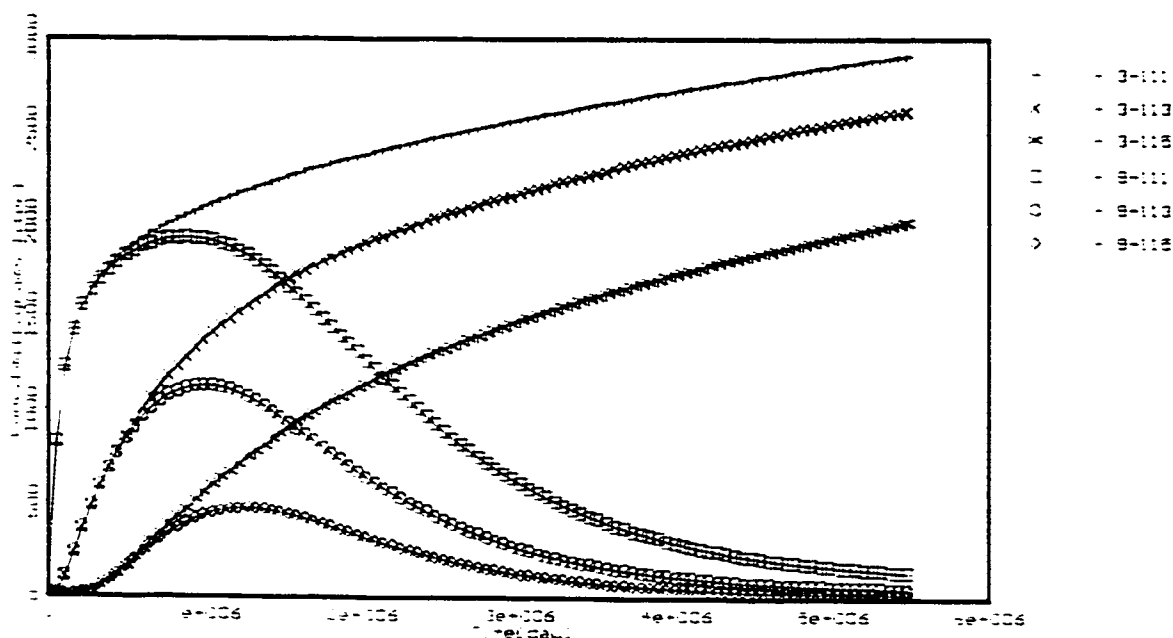
	GEW97-3	GEW97-9
Simulated chloride concentration at <u>1m</u> from the contact with the bedrock	1200mg/L	0mg/L
Simulated chloride concentration at <u>3m</u> from the contact with the bedrock	800mg/L	0mg/L
Simulated chloride concentration at <u>5m</u> from the contact with the bedrock	370mg/L	15mg/L
Average simulated chloride concentration	790mg/L	5mg/L
Average analytical results	721mg/L	4.2mg/L

Figure 4.8a Simulated chloride contours, hydraulic heads and flow directions for a groundwater velocity of 0.17 m/year in the Quaternary aquifer



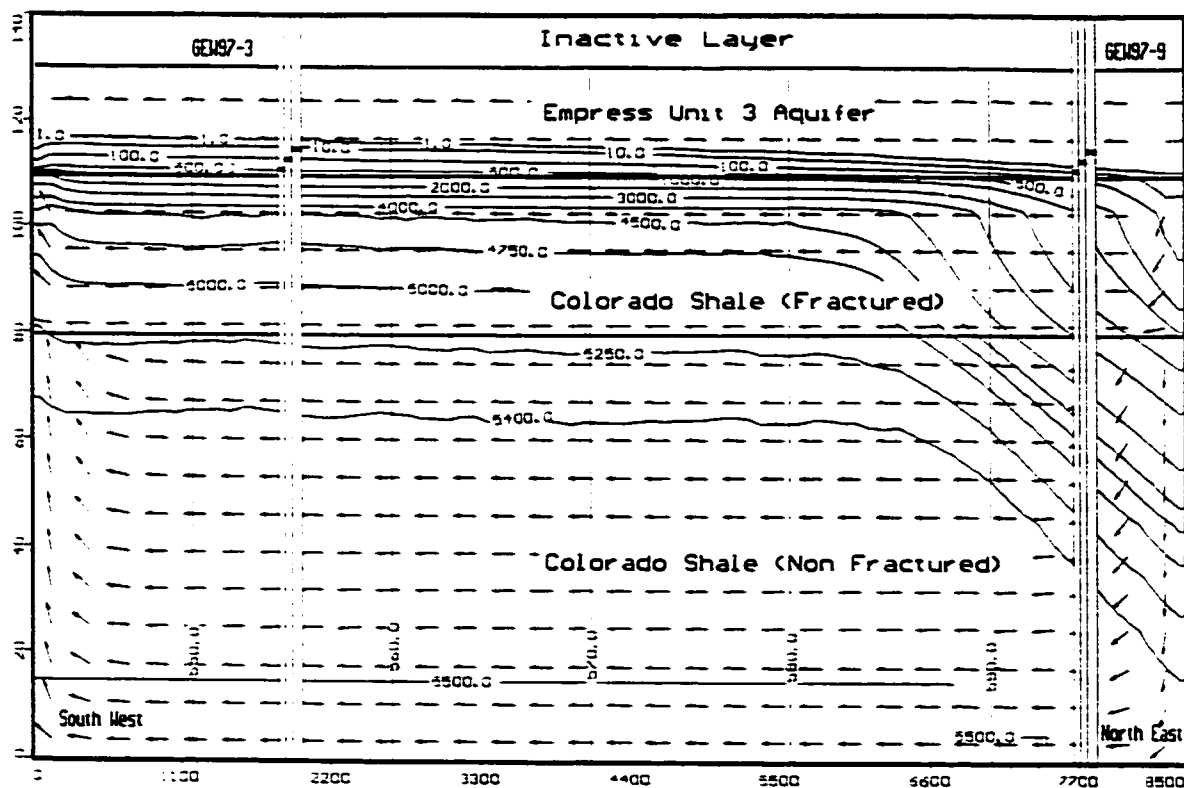
After the early increase, the chloride content decreases to stabilize at a steady chloride level. The decrease begins earlier in time and proceeds at a higher rate as monitoring points get closer to the recharge area. The introduction of fresh water from the recharge area has the effect of enhancing the removal of chlorides out of the system, causing a depression of the concentration isochrones toward the recharge zone. The overall net resultant is a balance between the amount of chloride brought into the aquifer by the solute flow process, and the amount of chloride swept out of the system by the flush of fresh water from the recharge area.

Figure 4.8b Simulated chloride evolution with time for a groundwater velocity of 0.17m/year in the Quaternary aquifer



Chloride concentrations obtained for the 3 monitoring points at the end of the simulation were averaged. The resulting value was assumed to represent the average chloride content of the aquifer water at the level of the screen area, and was compared to analytical results of water samples collected during field investigations. The simulated chloride contents obtained in the base case are 790mg/L for GEW97-3 and 5mg/L for GEW97-9 (Table 4.2). These values are comparable to the concentrations of 721mg/L and 4.2mg/L obtained analytically for the same well (Figure 4.4).

Figure 4.9a Simulated chloride contours, hydraulic heads and flow directions for a groundwater velocity of 8.7 m/year in the Quaternary aquifer

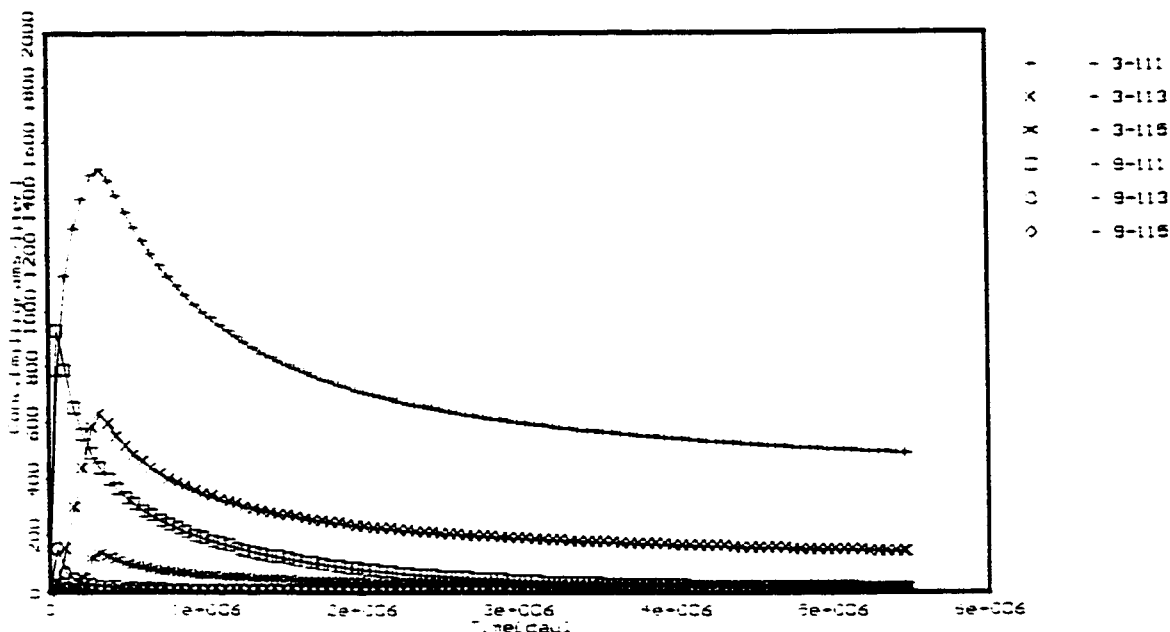


4.11 Effect of Groundwater Velocity in the Quaternary Aquifer

The study of the base case shows clearly that the prevalent average hydraulic and chemical conditions allowed a significant amount of chloride to be transferred from the Colorado Shale to the Quaternary Empress Formation Unit 3 aquifer during the 15,000 years of the model. Chloride concentrations reached about 2,000mg/L in the early stage of the simulation (Figure 4.6b). However, the amount of chloride present today in the

Quaternary aquifer depends on the efficiency of chloride removal from the system by fresh water originated from the recharging area.

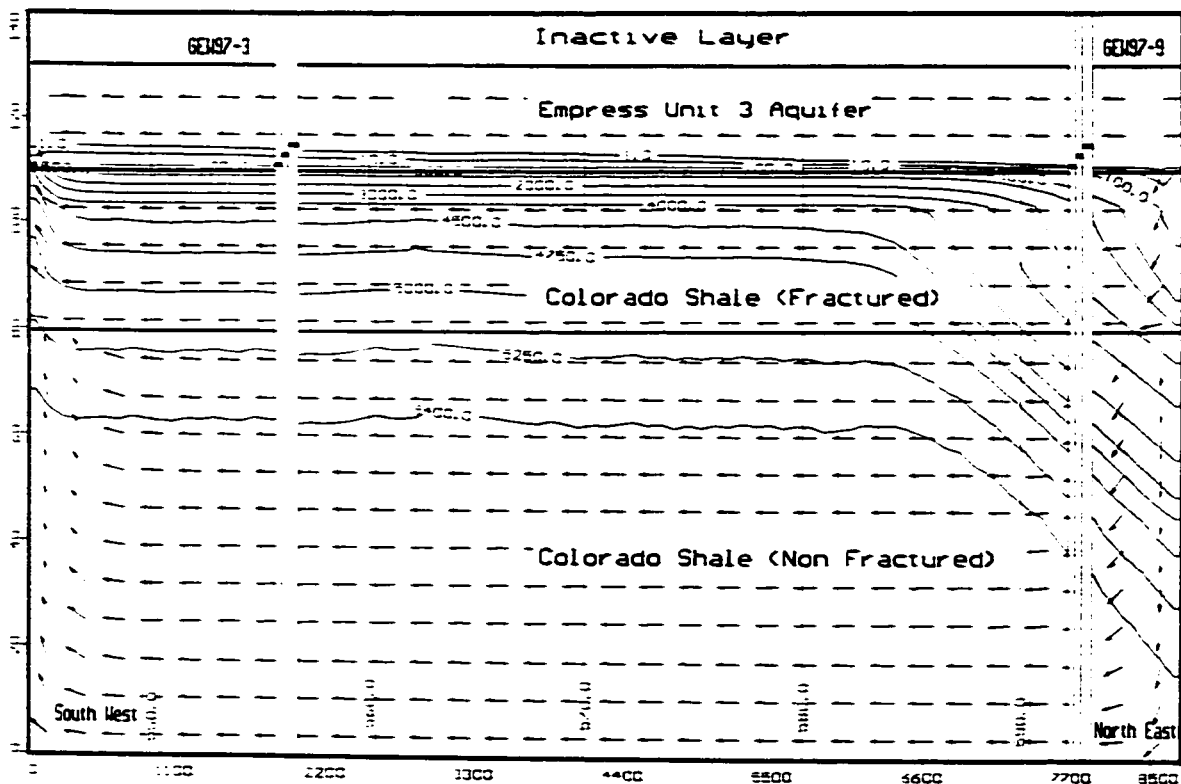
Figure 4.9b Simulated chloride evolution with time for a groundwater velocity of 8.7m/year in the Quaternary aquifer



A sensitivity study indicated that the amount of chloride remaining in the system depends mainly on the velocity of fresh water transiting through it. In the base case, the groundwater velocity was calculated at 1.74m/year. A higher groundwater velocity in the Quaternary aquifer is expected to leave, at the end of the simulation time, a smaller amount of chloride in the system. To simulate the effect of the groundwater velocity in the Quaternary aquifer, the hydraulic conductivity in the Empress formation Unit 3 was varied in the interval between 2.0×10^{-7} m/s and 1.0×10^{-4} m/s. This interval represents the range of hydraulic conductivities measured in the field for that layer. A zero velocity case

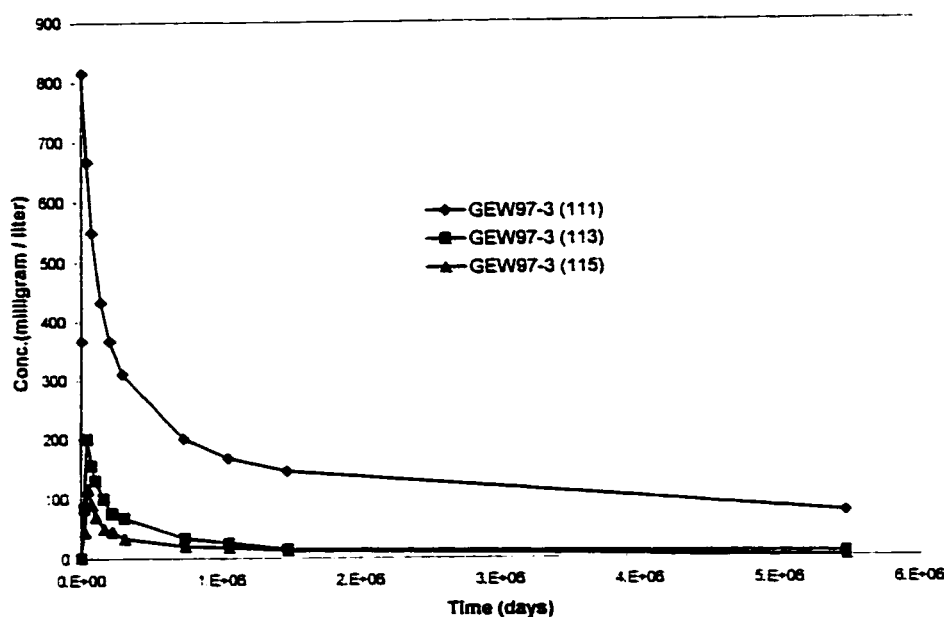
was also simulated, by allowing a zero hydraulic gradient. The concentration isochrones resulting from different velocities are shown in Figures 4.6a, 4.7a, 4.8a, 4.9a and 4.10a, and the end results are summarized in Table 3. These figures clearly show an important drop in remaining amounts of chloride as the velocity increases. For well location GEW97-3, the average amount of chloride decreases from 2,500mg/L to less than 100mg/L when the groundwater velocity varies from 0 to 87m/year. The chloride concentration decreases from 2,500 to 0mg/L for the same velocity variation at location GEW97-9.

Figure 4.10a Simulated chloride contours, hydraulic heads and flow directions for a groundwater velocity of 87 m/year in the Quaternary aquifer



The corresponding chloride concentration evolution with time is displayed in Figures 4.6b, 4.7b, 4.8b, 4.9b and 4.10b. When the groundwater velocity is equal to 0, the amount of chloride released from the Colorado Shale increases continuously in the Quaternary aquifer system (Figure 4.7b) under the effect of the molecular diffusion. The rate of increase, high at the beginning, slows down to stabilize at a steady state lower rate. A similar phenomenon was observed for the laboratory tests (Figures 3.2 to 3.6).

Figure 4.10b Simulated chloride evolution with time for a groundwater velocity of 87m/year in the Quaternary aquifer



At very low velocities, represented in this case by a velocity of 0.17m/s, the effect of the chloride flush by fresh groundwater is visible only near the recharge area, at location GEW97-9 (Figure 4.8b). The chloride level in the recharge area drops from about 2500 to 60mg/L near the recharge area when the velocity varies slightly from 0 to 0.17m/s.

Conversely, such a small velocity variation doesn't affect the chloride concentration in the discharge area, at location GEW97-3 (Figure 4.8b).

The reduction of remaining chloride in the discharge area becomes significant at low to medium velocities represented here by 1.74m/year (Figure 4.6b) and 8.7m/year (Figure 4.9b).

Figure 4.11a Simulated chloride contours, hydraulic heads and flow directions for a hydraulic conductivity of 10^{-8} m/s in the fractured Colorado Shale

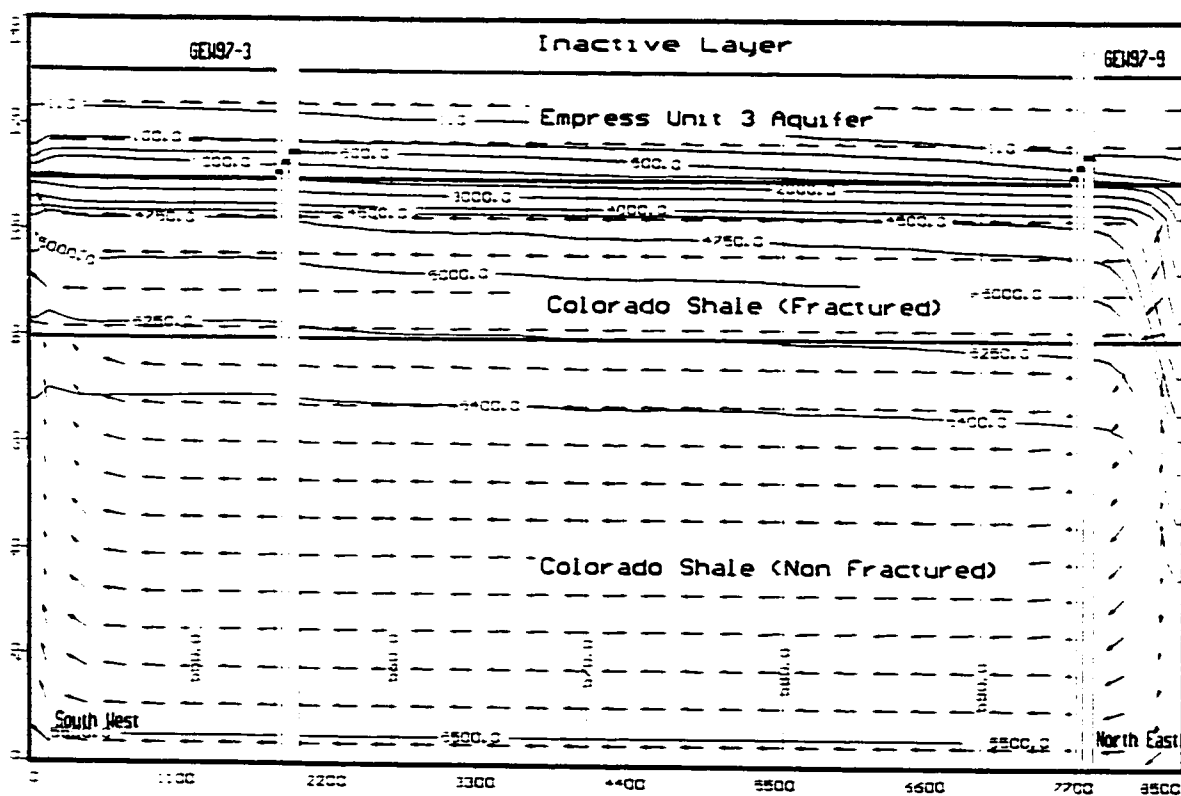
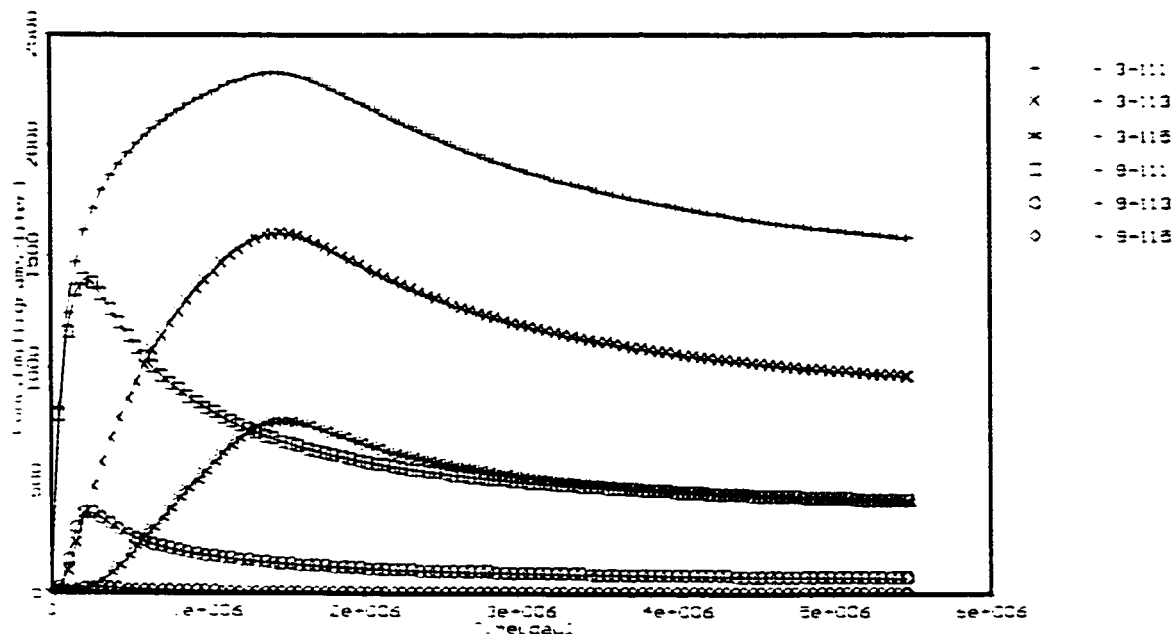


Figure 4.11b Simulated chloride evolution with time for a hydraulic conductivity of 10^{-8} m/s in the fractured Colorado Shale



At high velocities represented by 87m in this study (Figure 4.10b, Table 3), almost the entire amount of chloride released from the bedrock is removed out of the Quaternary aquifer, and only fresh water, possibly with negligible chloride contents, is found everywhere, even in the discharge area.

This study strongly suggests that the amount of chloride found today in the Empress Formation Unit 3, depends primarily on the groundwater velocity in the Quaternary aquifer and the position of the sampling point with respect to the recharge zone. Higher chloride concentrations are likely to be found in the discharging areas and in areas where the groundwater velocities in the Quaternary aquifer are low. Chloride concentrations are

likely to decrease as one proceeds closer to the recharging area and for increasing groundwater velocities.

Figure 4.12a Simulated chloride contours, hydraulic heads and flow directions for a hydraulic conductivity of 5×10^{-7} m/s in the fractured Colorado Shale

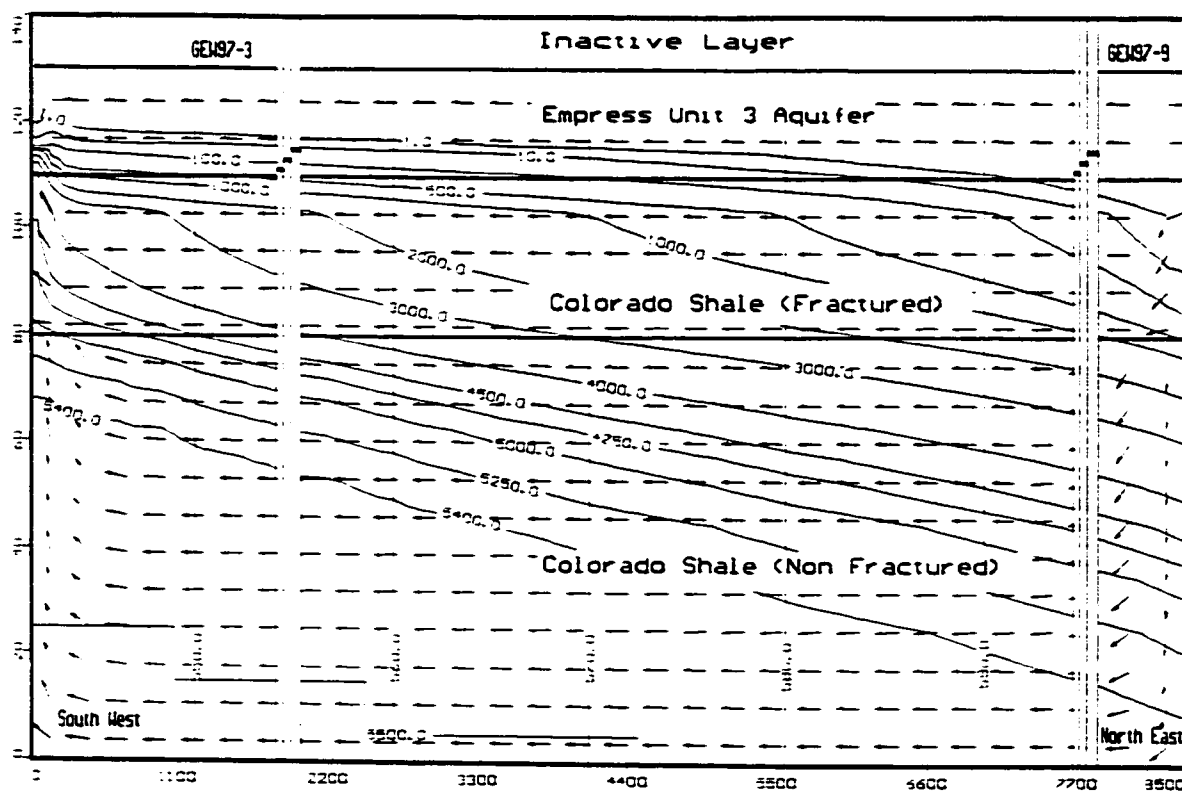


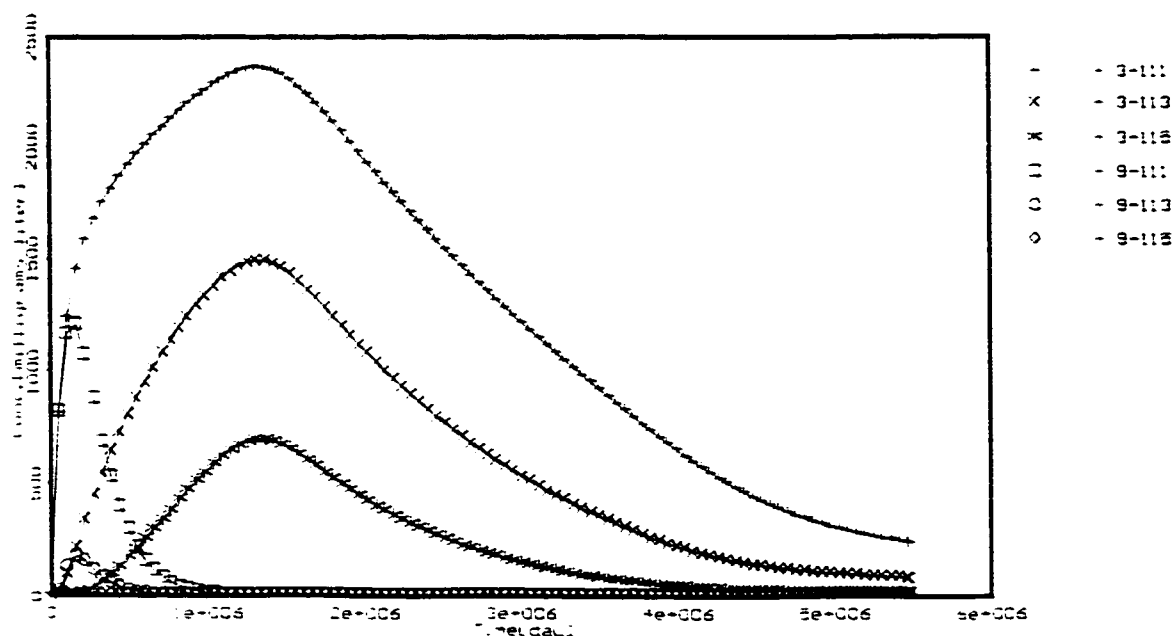
Table 4.3 Impact of the velocity in the Quaternary aquifer on the amount of chloride remaining in the system

Hydraulic properties of the Empress formation Unit 3 aquifer		Simulated average chloride concentrations remaining in the Quaternary aquifer at sampled locations after 15000 years		
Hydraulic conductivity (m/s)	Groundwater velocity (m/year)	GEW97-3 (mg/L)	GEW97-9 (mg/L)	Reference figures
	0.00	2500	2500	4.7a, 4.7b
2×10^{-7}	0.17	2470	60	4.8a, 4.8b
2×10^{-6}	1.74	790	5	4.6a, 4.6 b (base case)
1.0×10^{-5}	8.70	225	3	4.9a, 4.9b
1.0×10^{-4}	87.04	25	1	4.10a, 4.10b

4.12 The Effect of the Variation of the Hydraulic Conductivity in the Fractured Colorado Shale Layer

The release of chloride ions in the Quaternary aquifer was simulated at different groundwater velocities in the fractured Colorado Shale layer. This was done by varying the hydraulic conductivities in the shale within the range of variations measured in the field, from 10^{-8} m/s to 5×10^{-7} m/s. Velocities corresponding to different case studies are indicated in Table 4.4. These velocities were calculated using a total porosity value of 0.2. The effective porosity was not used to calculate velocities because diffusion and dispersion processes involve not only gravity pore water or water in the fractures, but also water and ions bound by electrical charges in the clay structure. A hydraulic gradient equal to 0 was used to simulate the case of a zero groundwater velocity. For this sensitivity study, the other hydraulic parameters remained similar to the base case (Table 4.1).

Figure 4.12b Simulated chloride evolution with time for a hydraulic conductivity of 5×10^{-7} m/s in the fractured Colorado Shale



A comparison of the simulation results for different bedrock velocities shows that the chloride level in the Quaternary aquifer depends also on the groundwater velocity in the fractured Colorado Shale (Figures 4.11a, 4.11b, 4.12a and 4.12b; Table 4.4). Smaller velocities in the bedrock allow less recharging fresh water to get into the shale. Lesser amounts of chloride are swept out of the system by fresh water and more chloride ions are involved in the dispersion - diffusion process. In this case, a decrease of the hydraulic conductivity from 10^{-7} to 10^{-8} m/s resulted in a constant average increase of 140mg/L all over the section in the Quaternary aquifer (Figures 4.11a and 4.11b, Table 4.4). This can explain how significant amounts of chloride can sometimes be found in the recharge area. The isochrones get more horizontal, particularly in the shale. It was generally noted that velocity decrease, especially in the Colorado shale, reduces the gap between the recharge

and the discharge area, in terms of the amount of chloride ions moving to the Quaternary aquifer.

Figure 4.13a Simulated chloride contours, hydraulic heads and flow directions for a bedrock initial chloride concentration of 10,000mg/L

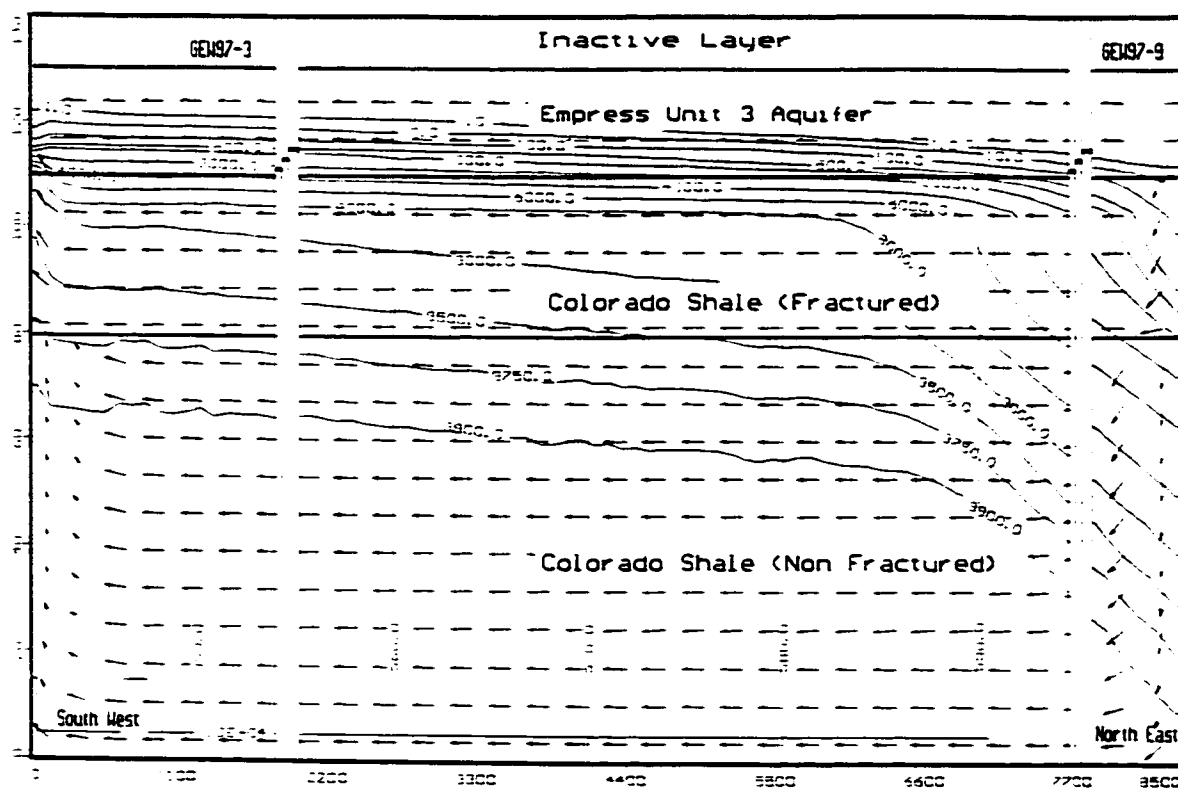


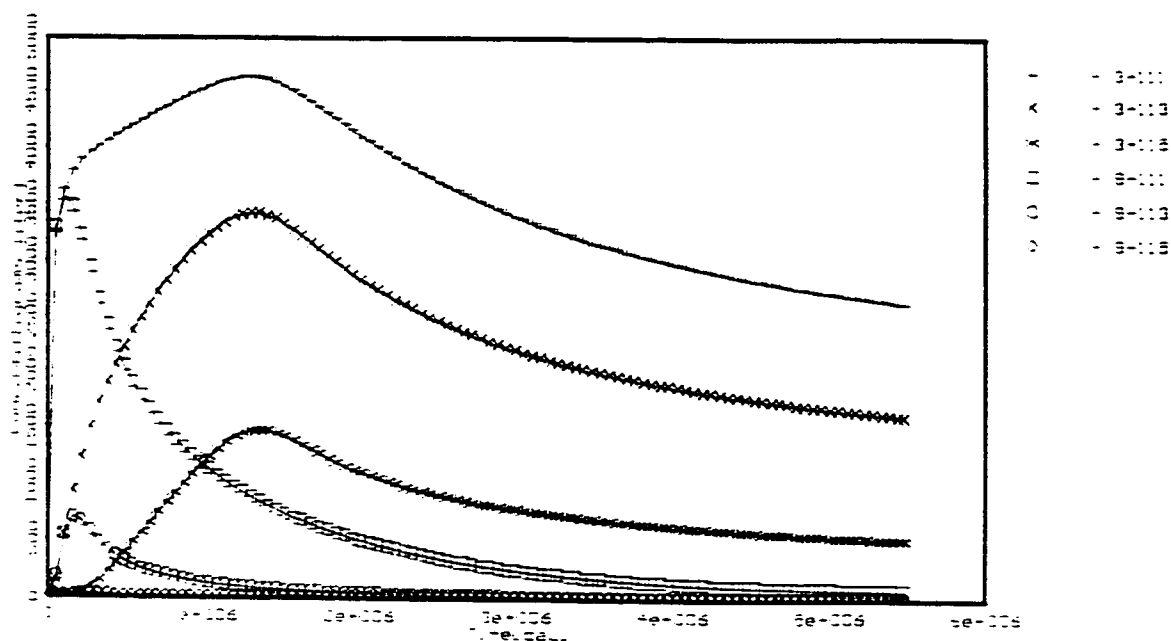
Table 4.4 Influence of the velocity in the fractured Colorado Shale on the chloride concentration in the Quaternary aquifer

Hydraulic properties of the fractured Colorado Shale		Simulated average chloride concentrations remaining in the Quaternary aquifer at sampled locations after 15,000 years		
Hydraulic conductivity (m/s)	Groundwater velocity (m/year)	GEW97-3 (mg/L)	GEW97-9 (mg/L)	Reference figures
	0.00	2500	2500	4.7a, 4.7b
1.0×10^{-8}	0.01	930	145	4.11a, 4.11b
1.0×10^{-7}	0.11	790	5	4.6a, 4.6 b (base case)
5×10^{-7}	0.54	100	0	4.12a, 4.12b

Conversely, higher velocities ($k_h = 5 \times 10^{-7}$ m/s) in the Colorado Shale allow more fresh water into the shale and therefore, a larger amount of chloride ions to be swept out of the system through the horizontal flow, even before the ions have time to get involved in the dispersion-diffusion processes. Chloride isochrones are significantly depressed in the shale towards the recharge area (Figure 4.12a). The amount of chloride in the Quaternary aquifer is considerably reduced due the combined effect of the velocity in the Empress formation Unit 3 and the increased velocity in the shale (Figure 4.12b).

The velocities involved here for the Colorado shale are very small. Considering a groundwater hydraulic conductivity of 5×10^{-7} m/s in the shale and the prevalent hydraulic gradient, a particle moving downgradient from the recharge area would take 15,740 years to get out of the system. Fresh water injected in the recharge area would have barely enough time to reach the other end of the model given the 15,000 years considered in the simulation. Even though, the influence of such small velocities, continuously sustained in the whole system for a period as long as 15,000 years, is considerable.

Figure 4.13b Simulated chloride evolution with time for a bedrock initial chloride concentration of 10,000mg/L



4.13 The Effect of the Initial Chloride Concentration in the Bedrock

The base case was run for an initial chloride concentration of 5,500mg/L in the Colorado Shale. The simulation was also run for bedrock initial concentrations of 10,000mg/L (Figure 4.13a and 4.13b) and 20,000mg/L (Figure 4.14a and 4.14b), the other conditions remaining the same as in the base case. The results show that the amount of chloride ions transferring to the Quaternary aquifer is directly proportional to the initial concentration in the bedrock (Table 4.5). In case the initial chloride content in the bedrock varies from place to place, the chloride content in the Quaternary aquifer can be affected accordingly.

Table 4.5 Effect of the initial bedrock concentration on the chloride concentration in the Quaternary aquifer

Bedrock initial concentration (mg/L)	Simulated average chloride concentrations remaining in the Quaternary aquifer at sampled locations after 15000 years		
	GEW97-3 (mg/L)	GEW97-9 (mg/L)	Reference figures
5,500	790	5	4.6a, 4.6b (base case)
10,000	1,580	20	4.13a, 4.13b
20,000	3,160	40	4.14a, 4.14b

Figure 4.14a Simulated chloride contours, hydraulic heads and flow directions for a bedrock initial chloride concentration of 20,000mg/L

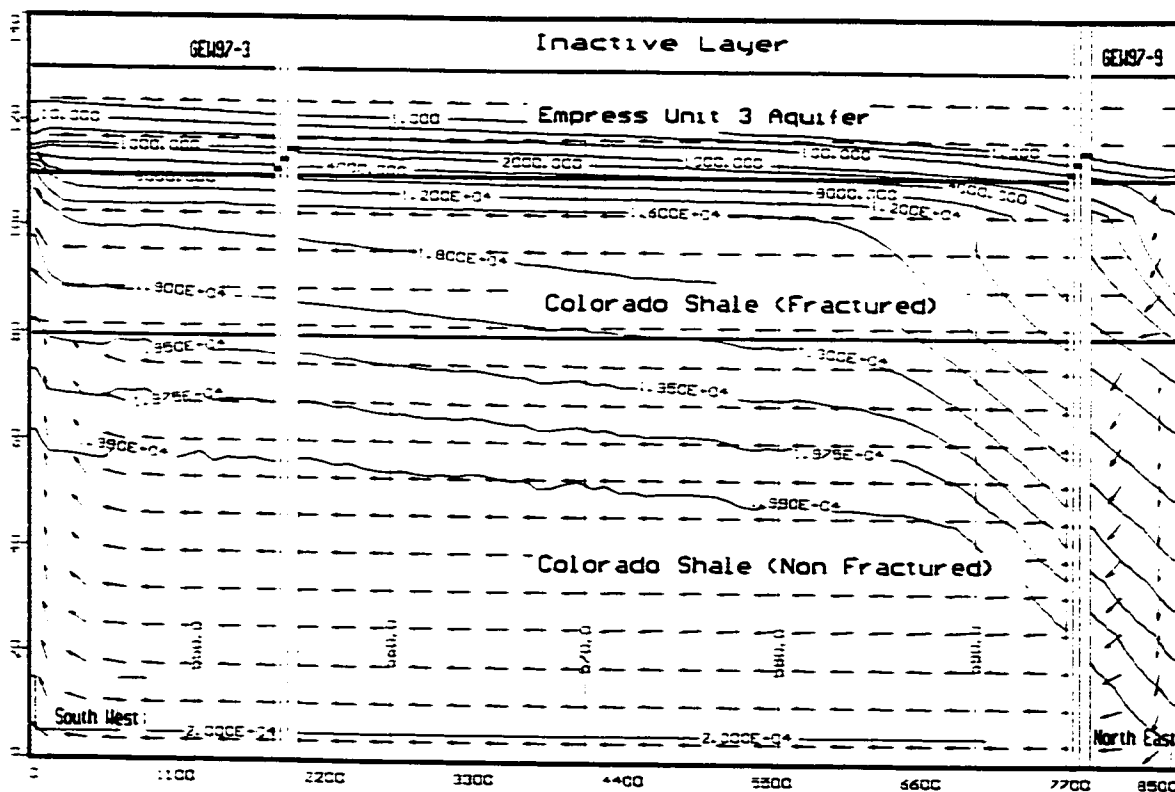
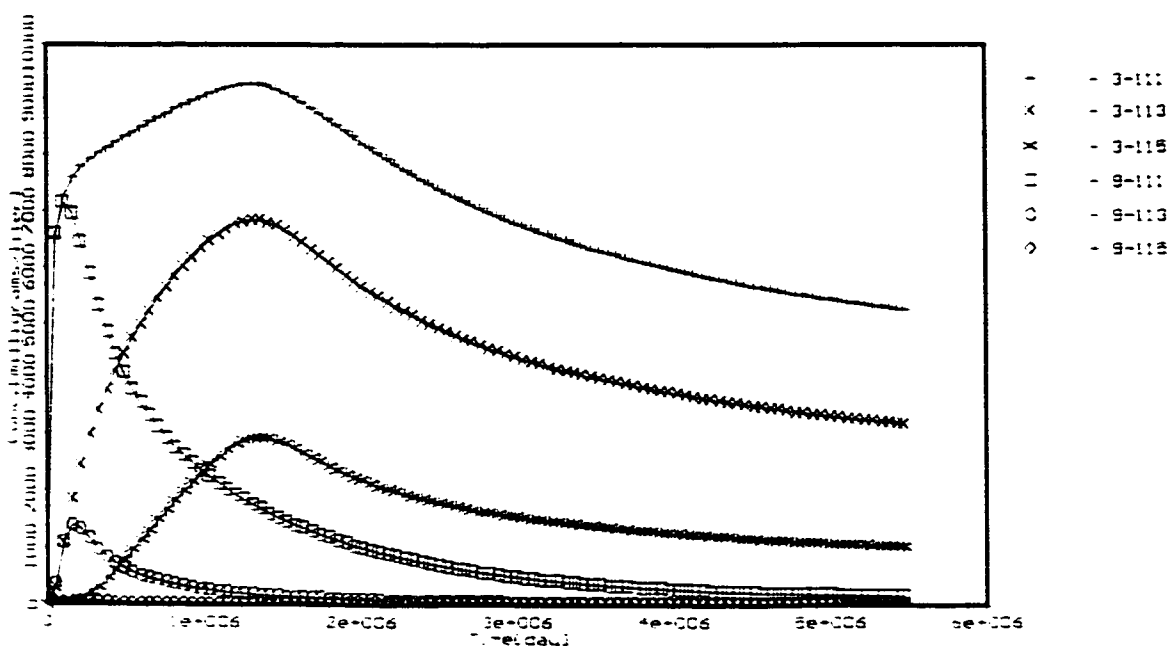


Figure 4.14b Simulated chloride evolution with time for a bedrock initial chloride concentration of 20,000mg/L



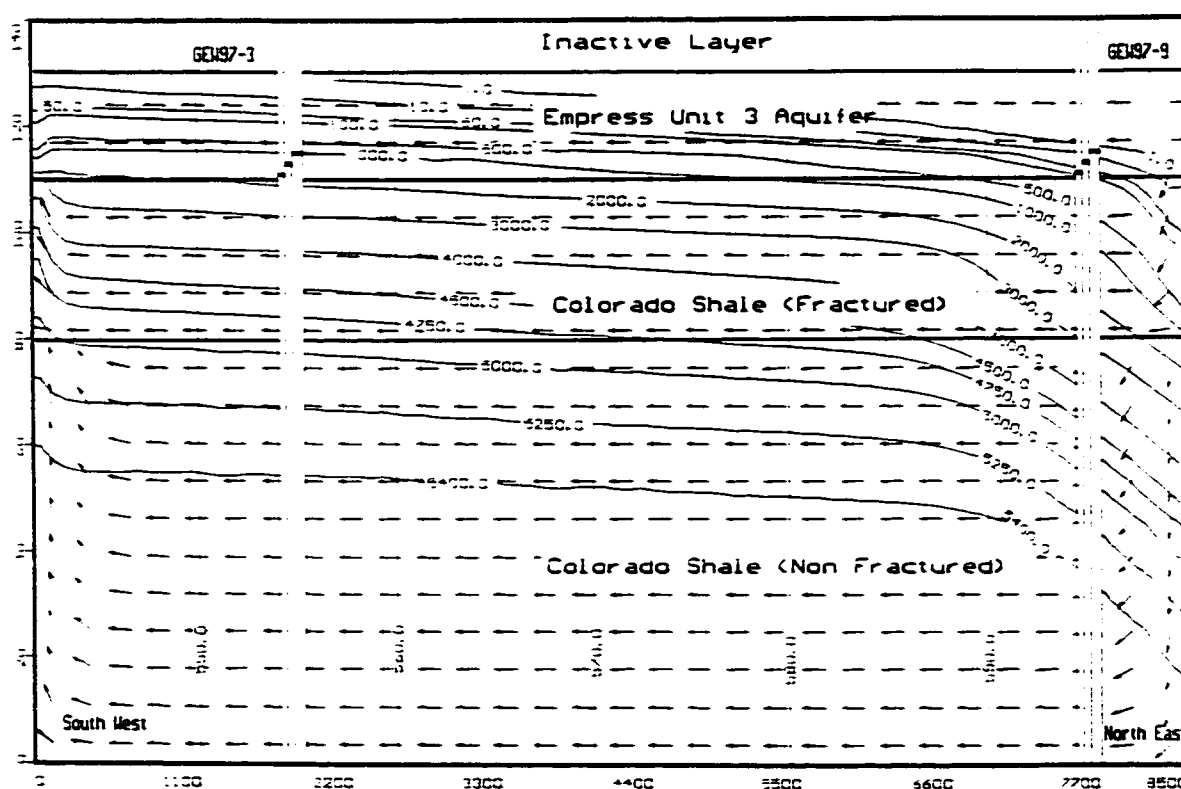
4.14 Effect of the Dispersion on the Solute Flow

It was mentioned earlier that the vertical mechanical dispersivity is a small and negligible fraction, of the longitudinal dispersivity. In such cases like this one where the only vertical dispersivity is involved, it is expected that the solute flow is diffusion-dominated (Freyberg, 1986; Sudicky et al., 1983; Mackay et al., 1986; Yeh and Wang, 1987). In fact, the variation of the longitudinal mechanical dispersivity coefficient between 0 and 75m did not show any change in the results of the model. The simulation using a longitudinal/vertical dispersivity ratio varying from 10^{-6} to 10^{-3} did not indicate any change.

Conversely, the results were significantly affected by variations of the molecular diffusion coefficient calculated with laboratory tests. As shown in Table 4.6 an increase of the molecular diffusion in the Colorado Shale shows a significant increase, from 790mg/L to

1400mg/L in average chloride concentration in the Quaternary aquifer at location GEW97-3 (Figures 4.15a, 4.15b). An increase of the diffusion coefficient in the Empress formation Unit 3 aquifer has no effect on the results.

Figure 4.15a Simulated chloride contours, hydraulic heads and flow directions for diffusion coefficients of $5 \times 10^{-10} \text{ m}^2/\text{s}$ in fractured Colorado Shale and $10^{-10} \text{ m}^2/\text{s}$ in non fractured shale



4.15 Effect of the Porosity on the Solute Flow

The porosity change is expected to have an influence on the velocity. A porosity decrease results in an increase of the velocity as shown in equation (4.6). A variation of the porosity from 0.25 to 0.15 in the Empress Formation Unit 3 does not affect the results of the simulation (Table 4.7). However, the decrease of the porosity from 0.2 to 0.1 in the Colorado Shale results in a dramatic decreasing of the chloride content from 790mg/L to 370mg/L in the discharge area (Figures 4.16a and 4.16b).

Figure 4.15b Simulated chloride evolution with time for diffusion coefficients of $5 \times 10^{-10} \text{ m}^2/\text{s}$ in fractured Colorado Shale and $10^{-10} \text{ m}^2/\text{s}$ in non fractured shale

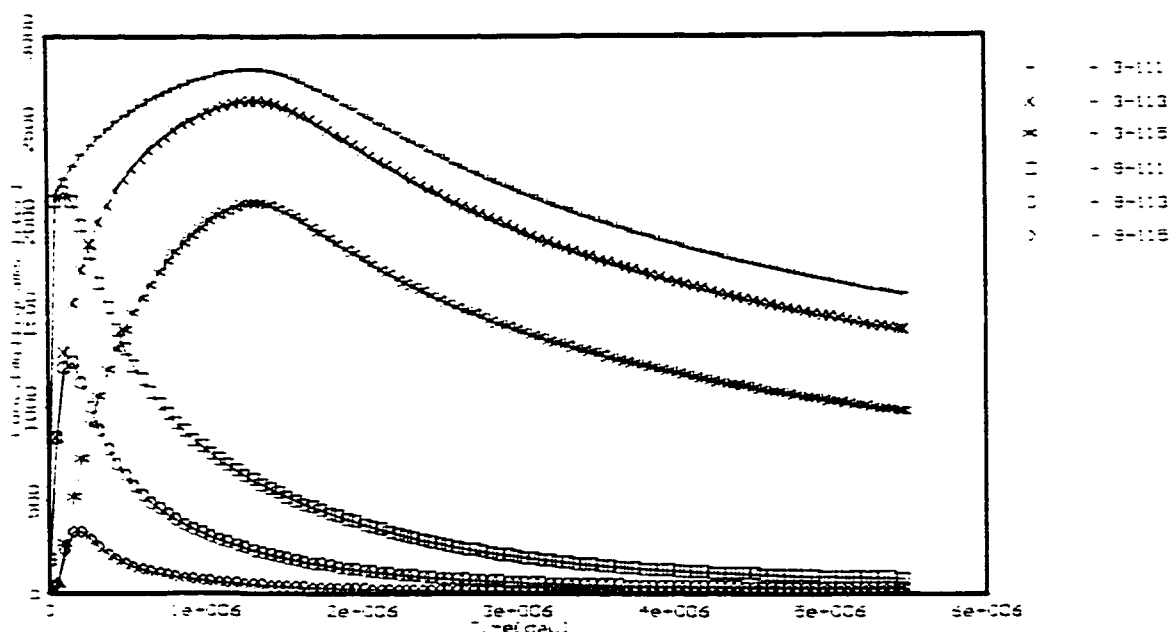
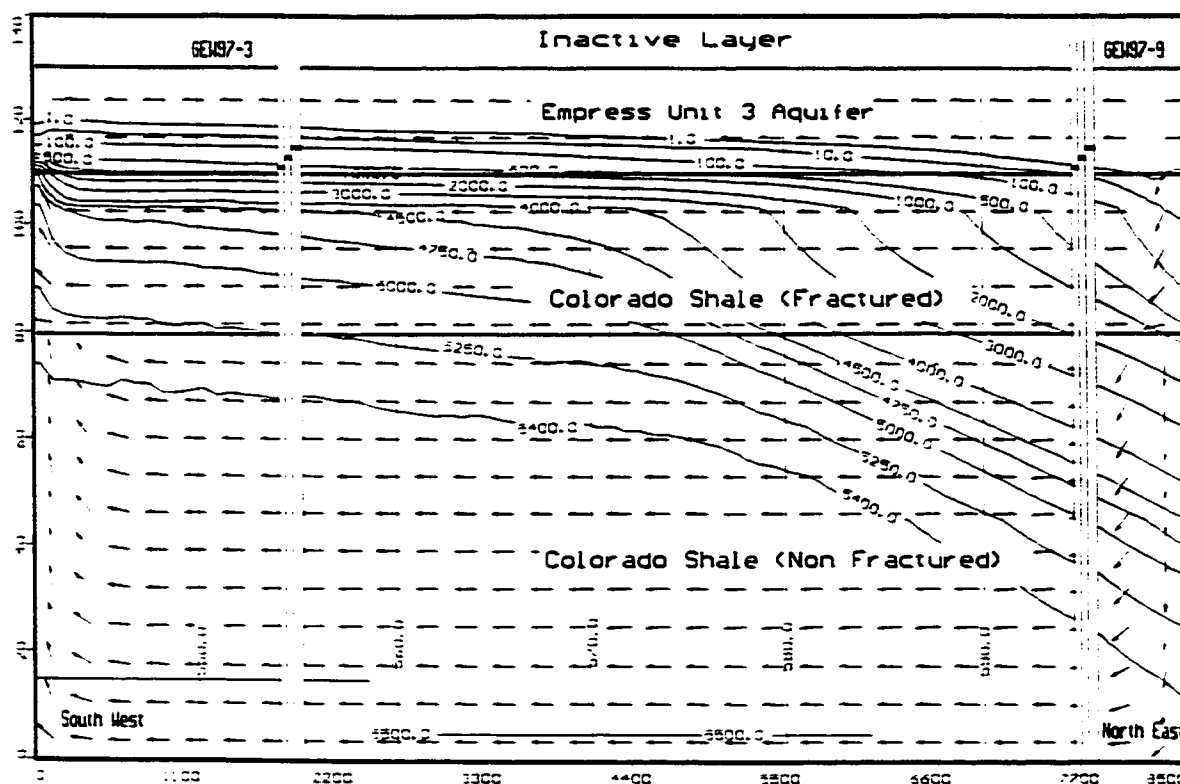


Figure 4.16a Simulated chloride contours, hydraulic heads and flow directions for a porosity of 0.1 in the Colorado Shale



4.16 Effect of Different Numerical Methods on the Simulation Results

In paragraph 4.3.4, different numerical methods used to solve the advection term were explored. In this study, the finite difference method was used for all the results presented above. This method proved to be successful, fast and free of numerical dispersions because the simulation was diffusion-dominated.

An attempt was made to solve the base case with the particle-tracking methods. The chloride concentration evolution with time is given in Figures 4.17 for the Method of Characteristics (MOC), 4.18 for the Modified Method of Characteristics (MMOC) and 4.19 for the Hybrid Modified Method of Characteristics (HMOC). The end-results for all these methods are comparable to the finite element results. However, the MOC and HMOC were very slow due the large number of particles to process for each time step. They are also affected by oscillations as indicated on the corresponding figures. Computing with the MMOC technique using only one particle per cell was fast and free of numerical dispersions.

Figure 4.16b Simulated chloride evolution with time for a porosity of 0.1 in the Colorado Shale

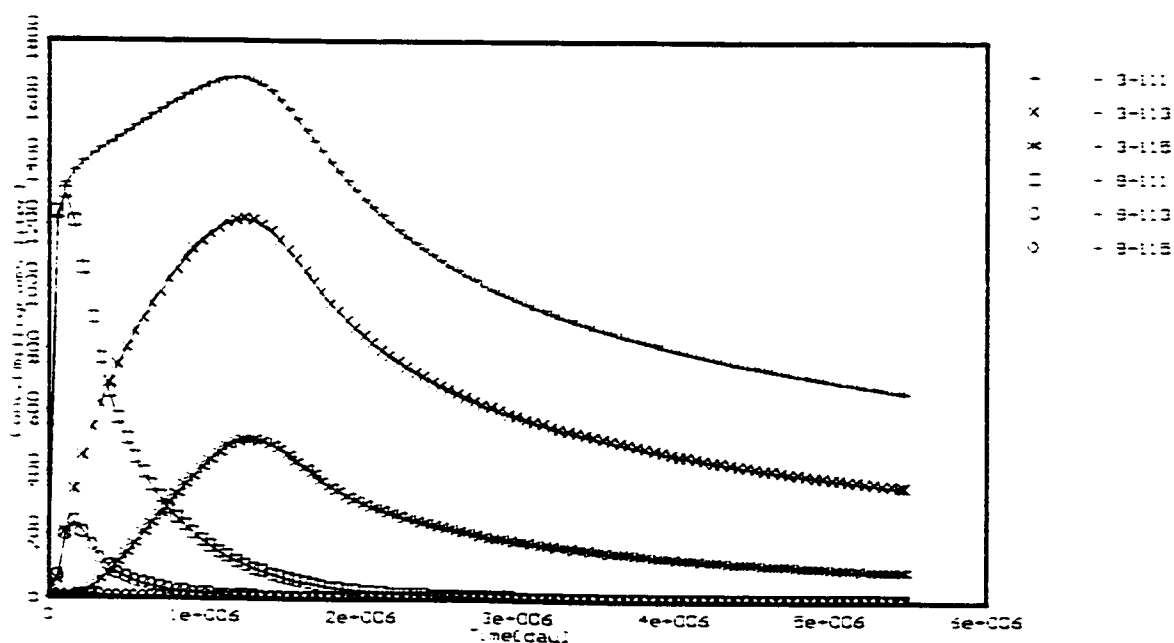


Table 4.6 **Effect of diffusion coefficient variation in the Colorado Shale on the chloride concentration in the Quaternary aquifer**

Molecular diffusion variation	Simulated average chloride concentrations remaining in the Quaternary aquifer at sampled locations after 15000 years		
	GEW97-3 (mg/L)	GEW97-9 (mg/L)	Reference figures
Fractured Colorado Shale: $10^{-10} m^2/s$ Non-fractured Colorado Shale: $1.7 \times 10^{-11} m^2/s$	790	5	4.6a, 4.6b (base case)
Fractured Colorado Shale: $5 \times 10^{-10} m^2/s$ Non-fractured Colorado Shale: $10^{-10} m^2/s$	1400	40	4.15a, 4.15b

Figure 4.17 **Simulated chloride evolution with time for the base case using the method of characteristics**

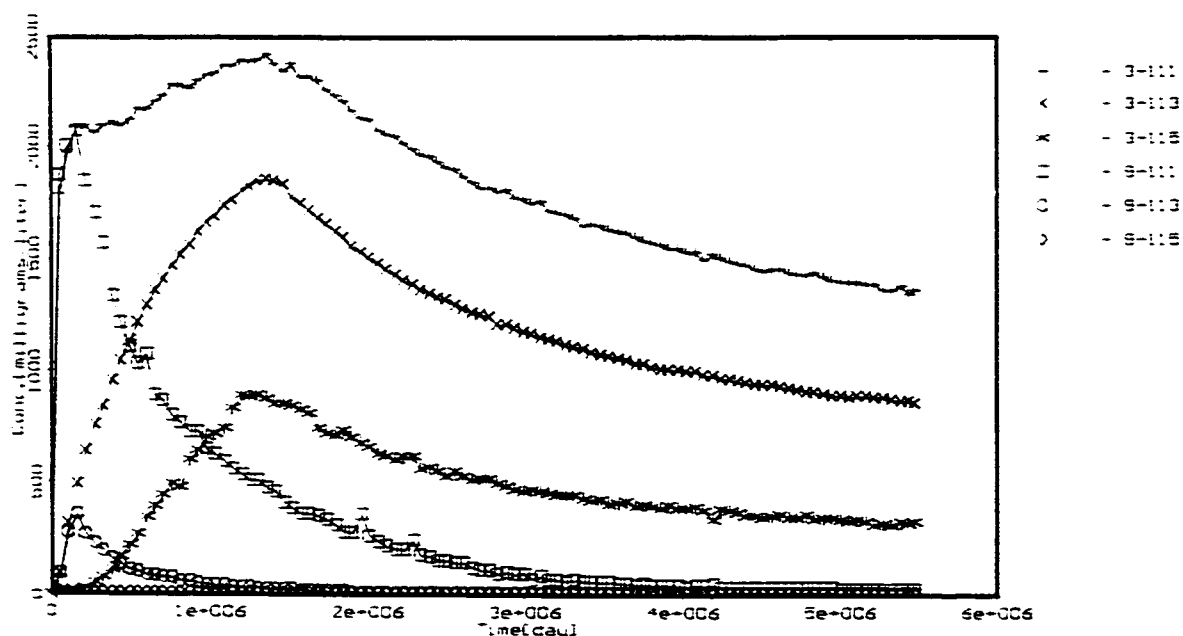


Table 4.7 **Effect of the porosity variation in the Colorado Shale on the chloride concentration in the Quaternary aquifer**

Porosity in the Colorado Shale	Simulated average chloride concentrations remaining in the Quaternary aquifer at sampled locations after 15000 years		
	GEW97-3 (mg/L)	GEW97-9 (mg/L)	Reference figures
$n=0.20$	790	5	4.6a, 4.6b (base case)
$n=0.10$	370	2	4.16a, 4.16b

Figure 4.18 **Simulated chloride evolution with time for the base case using the modified method of characteristics**

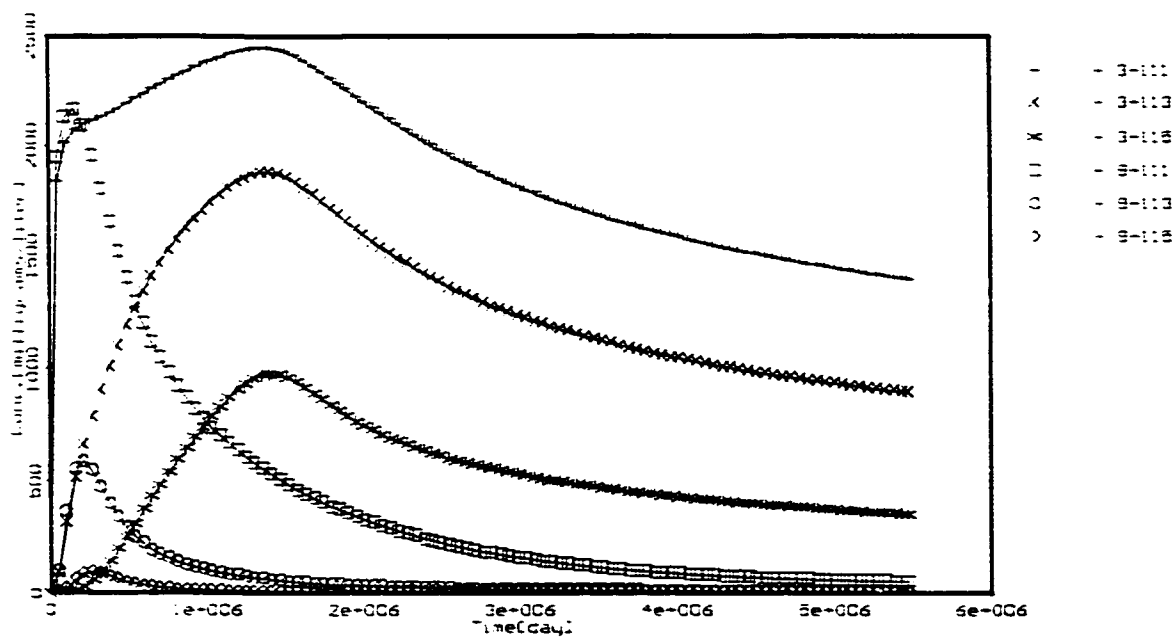
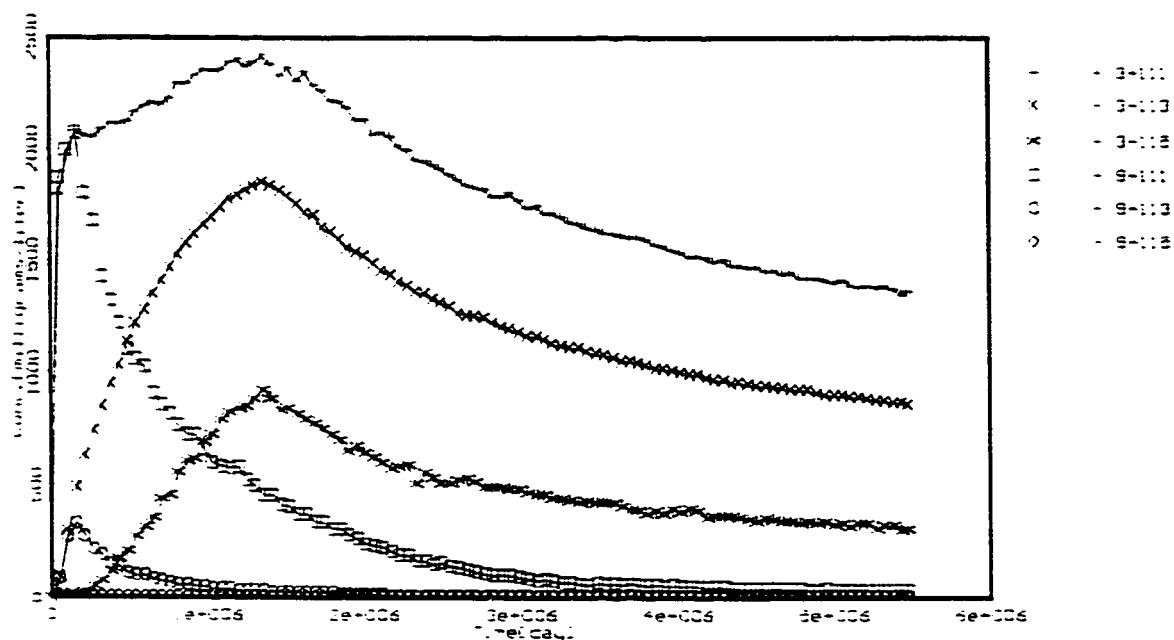


Figure 4.19 Simulated chloride evolution with time for the base case using the hybrid method of characteristics



CHAPTER FIVE

CONCLUSIONS AND RECOMMENDATIONS

The purpose of this thesis was to study the mechanisms of chloride transfer between the Colorado Shale and the Quaternary aquifer around the Cold Lake Production Projects of Imperial Oil. A chemico-osmotic model was set up to history-match the laboratory tests and define the diffusion coefficient of the shale. A transport model, calibrated with field data, was used to study the chloride migration on site. Numerical simulations were applied to case studies on basis of literature data, field information collected by Imperial Oil (1997, 1998) as part of the application for approval for the Cold Lake expansion project, and laboratory experiments performed at the Department of Civil Engineering, University of Calgary.

(i) Conclusions from the Chemico-Osmotic Model and Laboratory Investigations

Laboratory investigations allowed the approximation of the diffusion coefficient of the Colorado Shale, and to determine concentration and pore pressure distributions within tested samples. Two governing flow equations were written, based on (i) the mass balance of the fluid and the solute, (ii) the fluid flow under hydraulic and chemico-osmotic gradients and, (iii) the solute flow by advection and diffusion. The equations

were numerically solved by finite differences for the pore pressure and the chloride concentration.

Diffusion and swelling tests were performed on five Colorado Shale samples. The shale core samples were left in contact with fresh water for a period of 106 to 110 days, and the release of chloride from the shale to the water was monitored with a chloride probe. The results of the diffusion tests were used to calibrate the chemical-hydraulic diffusion model, developed to calculate the diffusion coefficient governing the transfer of chlorides from the shale to the upper Quaternary aquifers.

The diffusion coefficient in the Colorado shale was calculated in the range between $1.7 \times 10^{-11} \text{ m}^2/\text{s}$ and $1.27 \times 10^{-10} \text{ m}^2/\text{s}$. The steady state value for the diffusion coefficient was estimated at $1.7 \times 10^{-11} \text{ m}^2/\text{s}$. The results obtained from the five analyzed samples were consistent with this value. The steady state value should be applied for studies in the non-fractured bedrock. A value in the high end of the range, around $10^{-10} \text{ m}^2/\text{s}$, should be considered as a good approximation for the fractured Colorado shale.

The model and the laboratory investigations showed that only a fraction ranging from 22.52% to 45.68% of the total chloride content in the sample was released from the samples. The higher proportion of chloride was released from the sample where a fracture occurred during the test. The simulation also allowed the chloride concentration distribution within the samples to be determined.

The pore pressure within the sample decreases to a minimum in the early stage of the simulation, starting at the sample - water contact. The pore pressure developing in the sample is due to the combined effect of the sample loading and the osmotic suction. Afterwards, the pore pressure dissipates with a trend to equalization throughout the whole sample.

A sensitivity study indicated that the chloride flow rate depends only on the diffusion coefficient. Variations with respect to other parameters show no impact on the solute flow. The pore pressure was found sensitive to the osmotic efficiency. The variation of the pore pressure does not affect the chloride flow. In return, the pore pressure is insensitive to the variation of the chloride flow rate. This observation suggests that the fluid and solute flow governing equations should be considered as uncoupled in the flow system.

(ii) Conclusions from the Chloride Transport Simulation in Field Conditions

The diffusion coefficient values obtained with laboratory experiments were used to simulate the chloride migration in field conditions. The simulation was completed with MT3D, a three-dimensional contaminant transport algorithm, in conjunction with the flow model MODFLOW. The transport equation involved an advection term describing the transport of miscible contaminants at the same velocity as the groundwater, and a dispersion term describing the transport of contaminants by diffusion and dispersion. The retardation was not considered in this case, as the chloride is a conservative ion. A finite difference method was used for the simulation and the results were compared to particle-tracking methods used in MT3D. Longitudinal and vertical dispersivities were considered. The mechanical vertical dispersivity is a very small fraction, estimated between 10^{-6} and 10^{-3} of the longitudinal dispersivity. For vertical solute flows, the mechanical dispersity is therefore negligible to the molecular diffusion coefficient.

An 8,500m long to 140m thick two-dimensional cross-section in the Cold Lake area was used to simulate the chloride transfer from the Colorado Shale to the Quaternary aquifer. The model was calibrated with observations from two wells located within the section. From bottom to top, the model comprised an 80m-thick layer of non-fractured Colorado Shale, 30m of fractured Colorado Shale, 20m of Empress formation Unit 3 aquifer and a 10m confining layer. A base case was set up to history-match the observation wells. To

do so, the initial chloride concentration for the base case was fixed at 5,500mg/L in the Colorado Shale and the hydraulic head boundaries were set up to match the water heads observed in the wells. A no flow boundary was set up at the top of the Quaternary aquifer, in accord with field observations. The hydraulic permeability, the porosity, the diffusion coefficient and the dispersivity were adopted within the ranges observed in the field or calculated in the laboratory.

It was clearly observed from the base case that the field conditions allow a significant amount of chlorides to migrate from the Colorado Shale to the Quaternary aquifer. The vertical migration of chloride ions is partly swept out of the aquifer by recharging fresh water transiting through the section. Therefore, the amount of chloride remaining at the end of the simulation strongly depends on the velocity of the groundwater. The velocity itself is tributary to the hydraulic conductivity, the hydraulic gradient and the porosity. Increasing the velocity in both the Colorado Shale and the Empress Formation Unit 3 leads to a considerable decrease in the chloride concentration in the Quaternary aquifer. A decrease of the porosity in the Colorado Shale results in a significant decrease of the amount of chloride in the Quaternary aquifer.

Simulations made with higher initial concentrations in the bedrock show that the chloride concentrations found in the Quaternary aquifer increase proportionately to the initial concentration in the shale. The chloride level in the Quaternary aquifer increases also with the molecular diffusion coefficient in the Colorado Shale. Conversely, a change of the molecular diffusion in the Quaternary aquifer has no effect. Overall, it seems like property changes in the Colorado Shale are more effective to impact the amount the amount of chloride in the Quaternary aquifer than changes in the aquifer itself.

In the Quaternary aquifer, the chloride concentration increases progressively from the recharge area to the discharge zone. In the Colorado shale, the concentration isochrones are dramatically depleted in the recharge area. The chloride concentration in the aquifer

decreases rapidly from the bottom contact with the Colorado shale to the top. Most of simulated cases in normal field conditions show small or insignificant amounts of chloride above 10 to 13m from the bottom of the aquifer. However, the level of chloride can increase to 100mg/L or more, slightly above that level in cases of very low velocities. Even in those latter cases, the chloride concentration in the top 3 to 4m of the aquifer does not exceed 10mg/L. Higher initial bedrock concentrations result in a proportionate increase of chloride concentrations in the lower part of the aquifer, but have no significant impact at higher levels.

(iii) Observations and Recommendations for Further Studies

Some observations and recommendations stem from the above conclusions:

1. Laboratory investigations were important to demonstrate physically that chloride migration by diffusion from the Colorado Shale to Quaternary aquifers is possible. Laboratory investigations were used in conjunction with the chemico-osmotic numerical model to quantify the diffusion coefficient. The quantification of this parameter is critical, particularly in porous media with low velocities or in case of vertical solute migration studies. Further studies should be conducted to study the apparent variation of the diffusion coefficient observed with the history-match of laboratory data. The use of fluid and solute flow governing equations as coupled equations should be also reconsidered in further studies.
2. The contaminant transport model was useful to quantify the rate, the amount and the extent of the chloride migration from the shale to the Quaternary aquifer. Calibrated with adequate field and laboratory data, the numerical simulation is a powerful tool to understand the mechanism and to evaluate the extent of contaminant flow in the soil. The simulation showed that the Colorado Shale could be the source of elevated chloride levels found in overlying Quaternary aquifers. In this case, high chloride

concentrations are likely to be found in the bottom layers of Quaternary aquifers. The chloride levels should rapidly decrease from the bottom to the top of the aquifer as suggested by the simulation results. If chloride distributions in the aquifer show a different pattern, careful investigations should be carried out, including the exploration of other chloride sources.

3. Elevated chloride levels above 10m from the Colorado shale-aquifer contact should be also investigated thoroughly. In any case, the model suggests that elevated chloride ions above 15m from the shale-aquifer contact are unlikely to be originated from the bedrock. Elevated chloride levels are likely, but not necessarily, to be found downgradient, particularly in discharging areas. Similarly, low levels of chloride ions should be found preferably towards recharging areas. Chloride concentrations should be low in Quaternary aquifers or portions of aquifers with high flow rates. Elevated chloride levels are expected in cases of low velocity or stagnant flow systems. Elevated chloride levels are also likely to occur in Quaternary aquifers isolated from the regional system and where the groundwater flow is restricted, unless they are related to a recharge zone. If elevated chloride concentrations are otherwise distributed in the field, other sources should be eventually investigated.
4. The results of this study reflect the Cold Lake area field conditions, known to the author. In cases future studies in some sub-area indicate significant discrepancies with respect to field data used in this study, a new simulation using the new field data should be conducted, and the above results should be updated accordingly.

BIBLIOGRAPHY

Anderson M.J. 1979. Modeling of groundwater flow systems as they relate to the movement of contaminants. *CRC Critical Reviews in Environmental Control, Volume 9*, 97-156.

Arya A. 1986. Dispersion and reservoir heterogeneity. *Ph.D. dissertation, University of Texas, Austin, USA*.

Arya A., Hewett T.A., Larson R.G. and Lake L.W. 1988. Dispersion and reservoir heterogeneity. *SPE Reservoir Engineering* 3(1), 139-148.

Bachu S., Perkins E.H., Hitcheon B., Lytviak A.T. and Underschultz J.R. 1989. Evaluation of effects of deep waste injection in the Cold Lake area, Alberta. *Bulletin No.60, Alberta Research Council, Alberta Geological Survey*.

Bear J. 1979. Hydraulics of groundwater. *McGraw-Hill, New York, N.Y.*

Barbour S. L. and Fredlund D.G. 1989. Mechanisms of osmotic flow and volume change in clay soils. *Canadian Geotechnical Journal* 26, 551-562.

Burnett R.D. and Frind E.O. 1987. An alternating direction Galerkin technique for the simulation of groundwater contaminant transport in three dimension; 2. Dimensionality effects. *Water Resources Research, Volume 23, No.4*, 695-705.

Bush P.W. 1988. Simulation of saltwater movement in the Floridan aquifer system, Hilton Head Island, South Carolina. *U.S. Geological Survey Water Supply Paper 2331*, 19p.

Cheng R.T., Casulli V. and Milford S.N. 1984. Eulerian-Lagrangian solution of the convection-dispersion equation in natural coordinates. *Water Resources Research*, Volume 20, No.7, p944-952.

Collins R.E. 1961. Flow of fluids through porous materials. *New York, Reinhold Publishing Corp.*, 270p.

Driscoll G. F. 1989. Groundwater and wells, second edition. *Johnson Filtration Systems Inc., St.Paul, Minnesota 55112*.

Farmer C.L. 1987. Moving point techniques. *In Advances in transport phenomena in porous media. J. Bear and M.Y. Corapcioglu (eds), NATO ASI Series E: Applied Sciences - No.128, Martinus Nijhoff Publishers, Boston, p. 953-1004*.

Fetter C.W. 1994. Applied Hydrogeology, Third Edition. *Prentice Hall Inc. New Jersey*, 691 p.

Freeze R.A. and Cherry J.A. 1979. Groundwater. *Englewood Cliffs, N.J.: Prentice Hall*.

Freyberg D.L. 1986. A natural gradient experiment on solute transport in a sand aquifer. 2. Spatial moments and the advection and dispersion of nonreactive tracers. *Water Resources Research*, Volume 22, No,13, 2031-2046.

Fried J.J. 1975. Groundwater Pollution. *Elsevier, New York*, 330p.

- Garder A.O., Jr., Peaceman D.W. and Pozzi A.L., Jr. 1964. Numerical Calculation of Multidimensional Miscible Displacement by the Method of Characteristics. *Society of Petroleum Engineers Journal*, 4, 26-36.
- Gelhar L.W. 1986. Stochastic subsurface hydrology from theory to application. *Water Resources Research Volume 22 No.9*, 135-145.
- Gens A. and Alonso E. E. 1992. A framework for the behavior of unsaturated expansive clays. *Canadian Geotechnical Journal* 29, 1013-1032.
- Greenberg J.A. 1971. Diffusional flow of salt and water in soils. *Ph.D. Thesis, University of California, Berkeley, USA*.
- Haddad F. 1998. Osmotic-hydraulic swelling in marine shale. *M.Sc. Thesis, Department of Civil Engineering, University of Calgary, Calgary, Alberta, Canada*.
- Hitchon B., Bachu S., Sauveplane C.M, Ing A, Lytviak A.T. and Underschultz J.R. 1989. Hydrogeological and geothermal regimes in the Phanerozoic succession, Cold Lake area, Alberta and Saskatchewan. *Bulletin No.59, Alberta Research Council, Alberta Geological Survey*.
- Hueckel T. A. 1992. Water-mineral interaction in hydromechanics of clays exposed to environmental loads: a mixture-theory approach. *Canadian Geotechnical Journal* 29, 1071-1086.
- Imperial Oil (1997). Cold Lake expansion project – application for approval. *Document submitted to Alberta Energy and Utility Board and to Alberta Environmental Protection*.

Imperial Oil (1998). Cold Lake expansion project, supplemental information – application for approval. *Document submitted to Alberta Energy and Utility Board and to Alberta Environmental Protection*

Istok J. 1989. Groundwater modeling by the finite element method. *Water Resources Monograph 13, American Geophysical Union, Washington, D.C.*

Jackson P.C. 1984. Paleogeography of the Lower Cretaceous Mannville Group of Western Canada. In *Elmworth - Deep basin gas field (J.A. Masters, editor), American Association of Petroleum Geologists, Memoir 38, 49-77.*

Javandel I., Doughty C. and Tsang C. F. 1984. Groundwater transport: handbook of mathematical models. *Water Resources Monograph 10, American Geophysical Union, Washington D.C. 228pp.*

Konikow L.F. and Bredehoeft J.D. 1974. Modeling flow and chemical quality changes in an irrigated stream-aquifer system. *Water Resources Research, Volume 10, No.3. 546-562.*

Lallemand-Barres A. and Peaudecerf P. 1978. Recherche des relations entre la valeur de la dispersivité macroscopique d'un aquifère, ses autres caractéristiques et les conditions de mesure. *Bulletin du Bureau de Recherches Géologiques et Minières, Section 3, 4.*

Mackay D.M., Freyberg D.L., Roberts P.V. and Cherry J.A. 1986. A natural gradient experiment on solute transport in a sand aquifer. 1. Approach and overview of the plume movement. *Water Resources Research, Volume 22, No.13, 2017-2029.*

McDonald J.M. and Harbaugh A.W. 1988. A modular three-dimensional finite-difference flow model. *Techniques of Water Resources Investigations of the U.S. Geological Survey, Book 6, 586pp.*

Metten U. 1966. Desalination by reverse osmosis. *M.I.T. Press, Cambridge, MA.*

Mitchell J. K., Greenberg J. A. and Witherspoon P.A. 1973. Chemico-osmotic effects in fine-grained soils. *Journal of the Soil Mechanic and Foundations Division, Proceedings of the American Society of Civil Engineers, Vol.99, No. SM4, pp 307-322.*

Neuman S.P. 1990. Universal scaling of hydraulic conductivities and dispersivities in geologic media. *Water Resources Research, Volume 26, No. 8: 1749-1758.*

Nzajibwami E. and Wong R.C.K. 1998. Colorado Shale rock-water interaction. *University of Calgary, Department of Civil Engineering, Research Report No. CE98-2.*

Olsen H. 1972. Liquid movement through kaolinite under hydraulic, electric, and osmotic gradients. *American Association of Petroleum Geologists Bulletin, 56: 2022-2028.*

Pickens J.F., and Grisak G.E. 1981. Scale-dependent dispersion in a stratified granular aquifer. *Water Resources Research, Volume 17, No.4: 1191-1211.*

Pinder G.F. 1973. A Galerkin-finite element simulation of groundwater contamination on Long Island, New York. *Water Resources Research, Volume 9, NO.6: 529-544.*

Putnam P.E. 1982. Aspects of the petroleum geology of the Lloydminster heavy oil fields, Alberta and Saskatchewan. *Bulletin of Canadian Petroleum Geology, Volume30, No.2, 81-111.*

Robson S.G. 1978 Application of digital profile modeling techniques to groundwater solute transport at Barstow, California. *U.S. Geological Survey, Water Supply Paper. 2050, 28p.*

Sudicky E.A. 1983. An advection-diffusion theory of contaminant transport for stratified media. *Ph.D. dissertation*, 203p., *University of Waterloo, Ontario*.

Sudicky E.A., Cherry J.A. and Frind E.O. 1983. Migration of contaminants in groundwater at a landfill: A case study, 4, A natural-gradient dispersion test. *Journal of Hydrology* 63, 81-108.

Tang J.S. 1998. Single-well tracer testing to determine fluid drift rates in Cold Lake aquifers. *Imperial Oil, Research and Technology, Report No.IPRCC.OM.98.10*.

Wilson J.L. and Miller P.J. 1978. Two dimensional plume in uniform groundwater flow. *Journal of Hydraulic Division, American Society of Civil Engineers*, 104, 504-514.

Wong R.C.K. and Wang E.Z. 1997. Three-dimensional Anisotropic Swelling Model for Clay Shale - A Fabric Approach. *International Journal of Rock Mechanics and Mining Sciences and Geomechanics*, Volume 34, No. 2, 187-198.

Yeh W.W-G and Wang C. 1987. Identification of aquifer dispersivities: methods of analysis and parameter uncertainty. *Water Resources Bulletin, American Water Resources Association*. Volume 23. No.4, 569-580.

Yu F.X. and Singh V.P. 1995. Improved finite-element method for solute transport. *Journal of Hydraulic Engineering*, Volume 121, No2, 145-158.

Zheng C. 1990. MT3D, a modular three-dimensional transport model for simulation of advection, dispersion and chemical reactions of contaminants in groundwater system. *Prepared for the U.S. Environmental Protection Agency*.

APPENDIX I

CHEMICAL ANALYSES



NORWEST LABS

EDMONTON PH. (403) 438-8822 FAX (403) 438-0386
 CALGARY PH. (403) 281-2022 FAX (403) 281-2021
 LANGLEY PH. (604) 530-4344 FAX (604) 534-8896
 LETHBRIDGE PH. (403) 323-8288 FAX (403) 327-8327
 WINNIPEG PH. (204) 862-8630 FAX (204) 275-6019

UNIVERSITY OF CALGARY
 DEPT. OF CIVIL ENGRNG
 2500 UNIVERSITY DRIVE
 CALGARY, AB
 T2N 1N4

DR. RON WONG

WATER ANALYSIS REPORT

SAMPLE		1
		CL1 WATER
ROUTINE WATER		
pH		7.77
ELECTRICAL COND	uS/cm	2420
CALCIUM	mg/L	134
MAGNESIUM	mg/L	14.8
SODIUM	mg/L	475
POTASSIUM	mg/L	30.1
SULPHATE	mg/L	1050
CHLORIDE	mg/L	61.5
BICARBONATE	mg/L	287
FLUORIDE	mg/L	0.45
T ALKALINITY	mg/L	235
HARDNESS	mg/L	395
T DIS SOLIDS	mg/L	1910
IONIC BALANCE	%	103
WATER NUTRIENTS		
NITRATE-N	mg/L	0.08
NITRITE-N	mg/L	<0.05
PHOSPHORUS(TOT)	mg/L	0.09
NO2&NO3-N	mg/L	0.08
ORGANICS		
DISS ORG CARBON	mg/L	81.5
PHENOLS	mg/L	0.036
ICP METALS, EXTR		
IRON	mg/L	0.28
MANGANESE	mg/L	0.038
ICP METALS, TOTAL		
SILICON	mg/L	9.34
SILICA	mg/L	20.0
TOTAL, COLD VAPO		
MERCURY	mg/L	<0.0001



NORWEST LABS

EDMONTON	PH. (403) 438-5522	FAX (403) 438-0368
CALGARY	PH. (403) 291-2022	FAX (403) 291-2021
LANGLEY	PH. (604) 530-4344	FAX (604) 534-8896
LETHBRIDGE	PH. (403) 328-8266	FAX (403) 327-8527
WINNIPEG	PH. (204) 882-8630	FAX (204) 275-6019

UNIVERSITY OF CALGARY
DEPT. OF CIVIL ENGINEERING
2500 UNIVERSITY DRIVE
CALGARY, AB
T2N 1N4

DR. RON WONG

WATER ANALYSIS REPORT

SAMPLE	1
	CL1 WATER

PHYSIC ANALYSIS

COLOUR TRUE	CO. UNITS	135
TURBIDITY	NTU	60.0

TRACE ICP, TOTAL

LEAD	mg/L	0.006
------	------	-------



NORWEST LABS

EDMONTON PH. (403) 438-5522 FAX (403) 438-0396
 CALGARY PH. (403) 291-2022 FAX (403) 291-2021
 LANGLEY PH. (604) 530-4344 FAX (604) 534-9296
 LETHBRIDGE PH. (403) 329-8298 FAX (403) 327-8327
 WINNIPEG PH. (204) 962-6630 FAX (204) 275-6019

UNIVERSITY OF CALGARY
 DEPT. OF CIVIL ENGRNG
 2500 UNIVERSITY DRIVE
 CALGARY, AB
 T2N 1N4

DR. RON WONG

WATER ANALYSIS REPORT

SAMPLE		1
		CL2 WATER
ROUTINE WATER		
pH		7.17
ELECTRICAL COND	uS/cm	1460
CALCIUM	mg/L	1.6
MAGNESIUM	mg/L	1.0
SODIUM	mg/L	360
POTASSIUM	mg/L	4.25
SULPHATE	mg/L	596
CHLORIDE	mg/L	77.6
BICARBONATE	mg/L	21
FLUORIDE	mg/L	0.36
T ALKALINITY	mg/L	17
HARDNESS	mg/L	8.0
T DIS SOLIDS	mg/L	1050
IONIC BALANCE	%	106
WATER NUTRIENTS		
NITRATE-N	mg/L	0.32
NITRITE-N	mg/L	<0.05
PHOSPHORUS (TOT)	mg/L	0.14
NO2&NO3-N	mg/L	0.32
ORGANICS		
DISS ORG CARBON	mg/L	13.0
PHENOLS	mg/L	<0.001
ICP METALS, EXTR		
IRON	mg/L	0.47
MANGANESE	mg/L	0.019
ICP METALS, TOTAL		
SILICON	mg/L	14.5
SILICA	mg/L	31.0
TOTAL, COLD VAPO		
MERCURY	mg/L	<0.0001



NORWEST LABS

EDMONTON PH. (403) 438-5522 FAX (403) 438-0396
 CALGARY PH. (403) 291-2022 FAX (403) 291-2021
 LANGLEY PH. (604) 530-4344 FAX (604) 534-8898
 LETHBRIDGE PH. (403) 329-8266 FAX (403) 327-5527
 WINNIPEG PH. (204) 982-8830 FAX (204) 275-4019

UNIVERSITY OF CALGARY
 DEPT. OF CIVIL ENGINEERING
 2500 UNIVERSITY DRIVE
 CALGARY, AB
 T2N 1N4

DR. RON WONG

WATER ANALYSIS REPORT

SAMPLE

1

CL2 WATER

PHYSIC ANALYSIS

COLOUR TRUE CO. UNITS
 TURBIDITY NTU

3
 140

TRACE ICP, TOTAL

LEAD

mg/L

0.023



NORWEST LABS

EDMONTON PH. (403) 438-5522 FAX (403) 438-0386
 CALGARY PH. (403) 291-2022 FAX (403) 291-2021
 LANGLEY PH. (604) 530-4344 FAX (604) 534-8898
 LETHBRIDGE PH. (403) 329-8288 FAX (403) 327-8327
 WINNIPEG PH. (204) 952-8630 FAX (204) 275-8019

DATE 28 MAY 98 12:32

P.O. NO.

W.O. NO. 4 155212

PAGE 1

UNIVERSITY OF CALGARY
 DEPT. OF CIVIL ENGINEERING
 2500 UNIVERSITY DRIVE
 CALGARY, AB
 T2N 1N4

RON WONG
 25 05 98

WATER ANALYSIS REPORT

SAMPLE		1 LP1	2 MP2	3 HP3
ROUTINE WATER				
pH		7.20	7.09	7.12
ELECTRICAL COND	uS/cm	312	292	514
CALCIUM	mg/L	0.6	0.8	1.1
MAGNESIUM	mg/L	0.3	0.5	0.4
SODIUM	mg/L	61.6	55.7	104
POTASSIUM	mg/L	4.65	6.95	6.16
SULPHATE	mg/L	16.1	21.1	35.0
CHLORIDE	mg/L	61.6	55.7	113
BICARBONATE	mg/L	42	40	52
FLUORIDE	mg/L	<0.04	<0.04	<0.04
T ALKALINITY	mg/L	34	33	42
HARDNESS	mg/L	2.7	4.1	4.5
T DIS SOLIDS	mg/L	165	160	285
IONIC BALANCE	%	-101	-97.5	-99.1
WATER NUTRIENTS				
NO2&NO3-N	mg/L	0.48	0.88	0.10
ORGANICS				
DISS ORG CARBON	mg/L	8.6	7.7	7.3
PHENOLS	mg/L	0.017	0.013	0.020
ICP METALS, EXTR				
IRON	mg/L	0.04	0.03	0.03
MANGANESE	mg/L	0.014	0.016	0.006
PHYSIC ANALYSIS				
COLOUR TRUE	CO. UNITS	150	250	150
TURBIDITY	NTU	23.5	28.5	8.33

Lab Manager: _____



NORWEST LABS

EDMONTON	PH. (403) 438-6522	FAX (403) 438-0386
CALGARY	PH. (403) 281-3022	FAX (403) 281-3021
LANGLEY	PH. (604) 530-4344	FAX (604) 534-8886
LETHBRIDGE	PH. (403) 323-8288	FAX (403) 327-8827
WINNIPEG	PH. (204) 982-8830	FAX (204) 273-8018

DATE 07 APR 98 10:11

P.O. NO.

W.O. NO. 2 150181

PAGE 3

UNIVERSITY OF CALGARY
DEPT. OF CIV. L. ENGRNG
2500 UNIVERSITY DRIVE
CALGARY, AB
T2N 1N4

DR. RON WONG

WATER ANALYSIS REPORT

note pH pH REPORTED AT ROOM TEMP

note ELECTRICAL COND 'ELECTRICAL COND' (EC) is in microsiemens/cm and is a measure of solids in solution

E.C. CORRECTED TO 25C

note T ALKALINITY 'ALKALINITY' is CARBONATE/BICARBONATE expressed as CALCIUM CARBONATE

note HARDNESS 'HARDNESS' is calcium and magnesium expressed as CALCIUM CARBONATE

note NO₂:NO₃-N is expressed as nitrogen



NORWEST LABS

EDMONTON PH. (403) 438-6522 FAX (403) 438-0386
 CALGARY PH. (403) 281-2022 FAX (403) 281-2021
 LANGLEY PH. (604) 530-4344 FAX (604) 534-8898
 LETHBRIDGE PH. (403) 328-8288 FAX (403) 327-8527
 WINNIPEG PH. (204) 882-8630 FAX (204) 275-8019

DATE 07 APR 98 10:11

P.O. NO.

W.O. NO. 2 150181

PAGE 4

UNIVERSITY OF CALGARY
 DEPT. OF CIVIL ENGINEERING
 2500 UNIVERSITY DRIVE
 CALGARY, AB
 T2N 1N4

DR. RON WONG

WATER ANALYSIS REPORT

PARAMETER	DATE OF ANALYSIS	ANALYZED BY	PARAMETER	DATE OF ANALYSIS	ANALYZED BY
pH	24Mar98	DARREN CRICHTON	ELECTRICAL COND	24Mar98	DARREN CRICHTON
CALCIUM	24Mar98	LANG QUE TRAN	MAGNESIUM	24Mar98	LANG QUE TRAN
SODIUM	24Mar98	LANG QUE TRAN	POTASSIUM	24Mar98	LANG QUE TRAN
SULPHATE	24Mar98	LANG QUE TRAN	CHLORIDE	24Mar98	THERESA LIEU
BICARBONATE	24Mar98	DARREN CRICHTON	FLUORIDE	24Mar98	DARREN CRICHTON
T ALKALINITY	24Mar98	DARREN CRICHTON	HARDNESS	25Mar98	LANG QUE TRAN
T DIS SOLIDS	25Mar98	LANG QUE TRAN	IONIC BALANCE	25Mar98	LANG QUE TRAN
NITRATE-N	24Mar98	THERESA LIEU	NITRITE-N	24Mar98	THERESA LIEU
PHOSPHORUS(TOT)	24Mar98	THERESA LIEU	NO2&NO3-N	24Mar98	THERESA LIEU
DISS ORG CARBON	24Mar98	THERESA LIEU	PHENOLS	23Mar98	THERESA LIEU
IRON	25Mar98	LANG QUE TRAN	MANGANESE	25Mar98	LANG QUE TRAN
SILICA	25Mar98	LANG QUE TRAN	SILICON	25Mar98	LANG QUE TRAN
MERCURY	07Apr98	LANG QUE TRAN	COLOUR TRUE	27Mar98	TO THONG
TURBIDITY	24Mar98	DARREN CRICHTON	LEAD	24Mar98	LANG QUE TRAN



NORWEST LABS

EDMONTON PH. (403) 438-6822 FAX (403) 438-6886
 CALGARY PH. (403) 291-2022 FAX (403) 291-2021
 LANGLEY PH. (604) 850-4344 FAX (604) 854-8886
 LETHBRIDGE PH. (403) 325-8288 FAX (403) 327-8827
 WINNIPEG PH. (204) 952-8838 FAX (204) 278-8818

UNIVERSITY OF CALGARY
 DEPT. OF CIVIL ENGINEERING
 2500 UNIVERSITY DRIVE
 CALGARY, AB
 T2N 1N4

DR. RON WONG

DATE 07 APR 98 10:11

P.O. NO.

W.O. NO. 2 150181

PAGE 5

WATER ANALYSIS REPORT

The following published METHODS OF ANALYSIS were used:

10301L	pH	10602	HARDNESS
	Electrometric (pH meter)		Calculation from $2.5^{\circ}\text{Ca} + 4.1^{\circ}\text{Mg}$
	Ref. APHA 4500-H+		Reported as CaCO_3
02041L	ELECTRICAL COND		Ref. APHA 2140 B
	Conductance meter	00201	T DIS SOLIDS
	Ref. APHA 2510 B		SUM OF IONS CALCULATION
20103	CALCIUM		$\text{Ca} + \text{Mg} + \text{K} + \text{Na} + \text{SO}_4 + \text{Cl} + 0.6^{\circ}\text{T Alk}$
	ICP spectroscopy @ 317.9 nm		Ref. APHA 1030 F
	Ref. APHA 3120 B	NWL4994	IONIC BALANCE
12102L	MAGNESIUM	00100	IONIC BALANCE 2
	ICP spectroscopy @ 285.2 nm		$\text{Diff} = (\text{Sum Cations} - \text{Sum Anions}) /$
	Ref. APHA 3120 B		$(\text{Sum Cations} + \text{Sum Anions}) = 100$
11102L	SODIUM		Ref. APHA 1030 F
19111	POTASSIUM	07301	NITRATE-N
	Disa., ICP Spectroscopy, Ref. APHA 3120 B		Disa., Auto. colorimetry, Cd reduction
16306L	SULPHATE		Ref. APHA 4500 NO3-E
	ICP spectroscopy @ 180.7 nm	07205	NITRITE-N
	Ref. APHA 3120 B		Automated colorimetry
17203L	CHLORIDE		Ref. APHA 4500 NO2-B
	Automated colorimetry, Thiocyanate	15406	PHOSPHORUS(TOT)
	Ref. APHA 4500 Cl-,E		Total, Autoclave with persulphate/H2S04
06201L	BICARBONATE		Auto. colorimetry with ascorbic acid
	Potentiometric titration with standard		Ref. APHA 4500 P,B/E
	acid to pH 8.3 and pH 4.5	07105L	NO2&NO3-N
	Ref. APHA 2320 B		Automated colorimetry Cadmium reduction
09105L	FLUORIDE		Ref. APHA 4500-NO3-,F
	Ion selective electrode	06107L	DISS ORG CARBON
	Ref. APHA 4500 F-,C		Auto persulphate/UV digest. Colorimetric
10101	T ALKALINITY		Ref. APHA MOE(Ontario Environment)
	Potentiometric titration with standard	06537P	PHENOLS
	acid to pH 4.5 & pH 8.3. Report as CaCO_3		Automated, distillation and colorimetry
	Ref. APHA 2320 B		with 4-AAP

Method References:

1. APHA Standard Methods for the Examination of Water and Wastewater, American Public Health Assoc., 17th ed.
2. EPA
 - a. Test Methods for Evaluating Solid Waste, Physical/Chemical Methods SW-846, 1rd ed., US EPA, 1986
 - b. Methods for Chemical Analysis of Water and Wastewater, US EPA, 1983
3. MSS Manual on Soil Sampling and Methods of Analysis, Cdn. Soc. of Soil Science, J. A. McKague, 2nd ed.

* NORWEST SOIL RESEARCH LTD has been accredited by the STANDARDS COUNCIL of CANADA for specific tests registered with the COUNCIL.

Lab Manager: _____



NORWEST LABS

EDMONTON PH. (403) 438-6822 FAX (403) 438-6888
 CALGARY PH. (403) 291-3022 FAX (403) 291-3021
 LAMBLEY PH. (403) 230-4344 FAX (403) 234-8888
 LETHBRIDGE PH. (403) 338-8088 FAX (403) 337-8827
 WYNDHOPE PH. (204) 965-8830 FAX (204) 276-8819

DATE 07 APR 98 10:11

P.O. NO.

W.O. NO. 2 150181

PAGE 6

UNIVERSITY OF CALGARY
 DEPT. OF CIVIL ENGINEERING
 2500 UNIVERSITY DRIVE
 CALGARY, AB
 T2N 1N4

DR. RON WONG

WATER ANALYSIS REPORT

Ref. US EPA 420.2
 26321 IRON
 Acid extr., ICP Spectro. Ref. APHA 3120 B
 25321 MANGANESE
 Acid extr., ICP Spectro. Ref. APHA 3120 B
 14111 SILICA
 Dissolved by ICP spectroscopy @ 251.6 nm
 Ref. APHA 3120 B
 02021L COLOUR TRUE
 Filtration, visual comparison with
 chloroplatinate standards
 Ref. APHA 2120 B
 02071L TURBIDITY
 Nephelometry on turbidimeter
 Ref. APHA 2130 B

Method References:

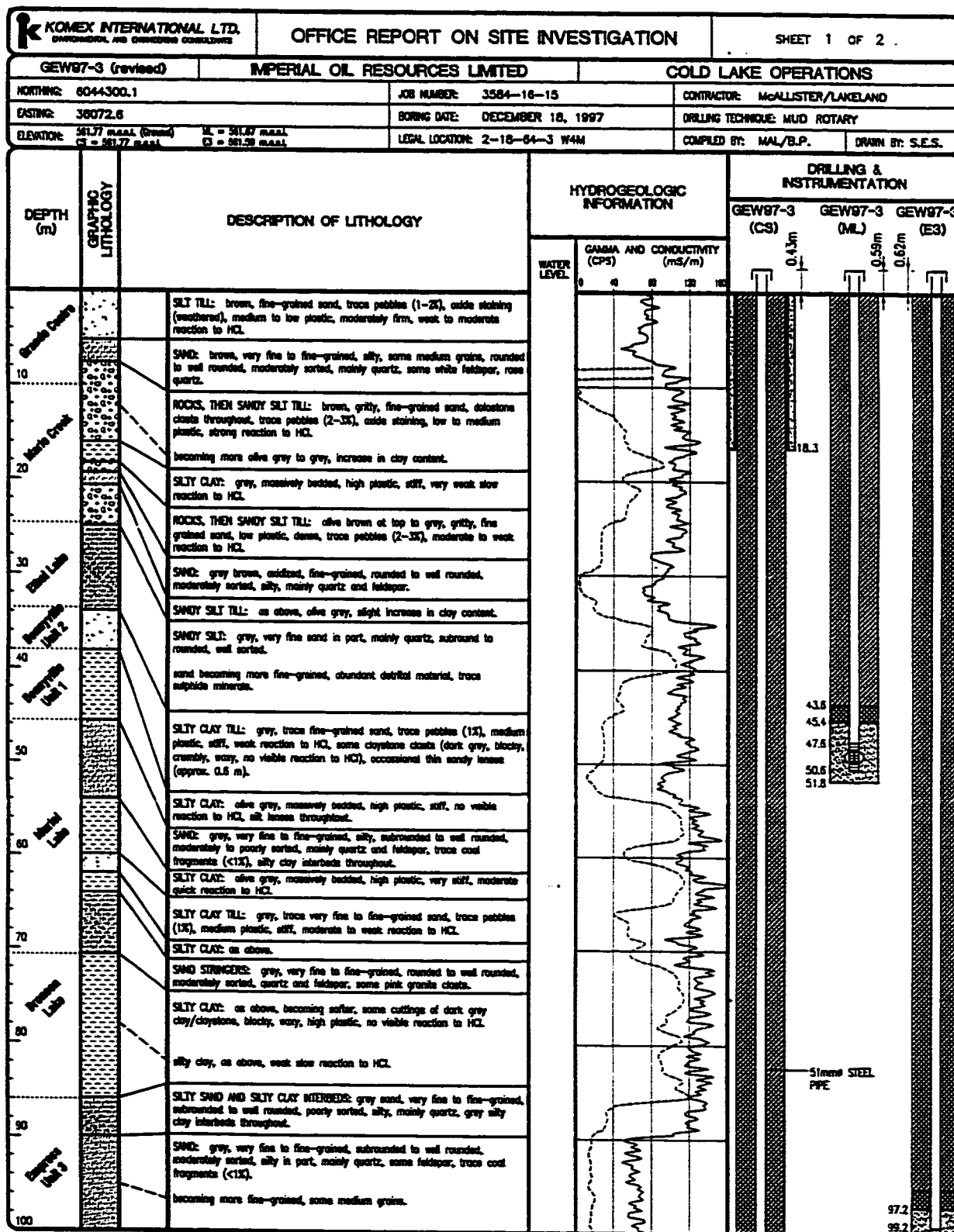
1. APHA Standard Methods for the Examination of Water and Wastewater, American Public Health Assoc., 17th ed.
2. EPA
 - a. Test Methods for Evaluating Solid Waste, Physical/Chemical Methods SW-846, 3rd ed., US EPA, 1986
 - b. Methods for Chemical Analysis of Water and Wastewater, US EPA, 1983
1. MSS Manual on Soil Sampling and Methods of Analysis, Cdn. Soc. of Soil Science, J. A. McKague, 2nd ed.

* NORWEST SOIL RESEARCH LTD has been accredited by the STANDARDS COUNCIL of CANADA for specific tests registered with the COUNCIL.

Lab Manager: _____

APPENDIX II

LOG ANALYSES FOR WELLS LOCATED AT GEW97-3 AND GEW97-9



KOMEX INTERNATIONAL LTD.
ENGINEERING AND CONSTRUCTION CONSULTANTS

OFFICE REPORT ON SITE INVESTIGATION

SHEET 2 OF 2

GEW97-3		IMPERIAL OIL RESOURCES LIMITED		COLD LAKE OPERATIONS	
NORTHING: 8044300.1		JOB NUMBER: 3584-16-15		CONTRACTOR: McALLISTER/LAKELAND	
EASTING: 38072.8		BORING DATE: DECEMBER 15, 1997		DRILLING TECHNIQUE: MUD ROTARY	
ELEVATION: 561.77 MSL (Ground) 561.77 MSL		LEGAL LOCATION: 2-18-64-3 W4M		COMPILED BY: MAL/B.P. DRAWN BY: S.E.S.	

DEPTH (m)	GRAPHIC LITHOLOGY	DESCRIPTION OF LITHOLOGY
105.2		becoming more medium to coarse-grained, some fine gravel (pink granite, dolostone, ultramafic).
109.7		more fine to medium-grained near base, increase in coal fragments.
111.9		SILTY CLAY/CLAYSTONE: olive gray, massively bedded, high plastic, very soft, slow, moderate reaction to HCl, some claystone clasts, dark gray, blocky, crumbly.
120.4		CLAYSTONE: dark gray, blocky, high plastic, hard, indurated, no visible reaction to HCl.
122.5		SILTSTONE: gray, moderately plastic, layered.
123.4		SHALE: medium gray, fine, layered, hard.
132.6		Lost a bit of circulation, harder drilling observed, less hardness, slightly more plastic.
141.7		SILTSTONE: light gray, semi-hard, less plastic.
143.3		SILTSTONE / SHALE LENSE: 4" thick, very hard, siltstone hard, dark gray, moderately plastic.
		TOTAL DEPTH = 143.28 m

HYDROGEOLOGIC INFORMATION	
WATER LEVEL	GAMMA AND CONDUCTIVITY (CPS) (mS/m)
<p>NO GEOPHYSICAL INFORMATION AVAILABLE</p>	

KEY:

Sandy Silt Till	Silt
Silty Clay Till	Mudstak
Sand	Sand & Gravel
Silty Clay/Clay	Claystone/Shale

SY Static Water Level

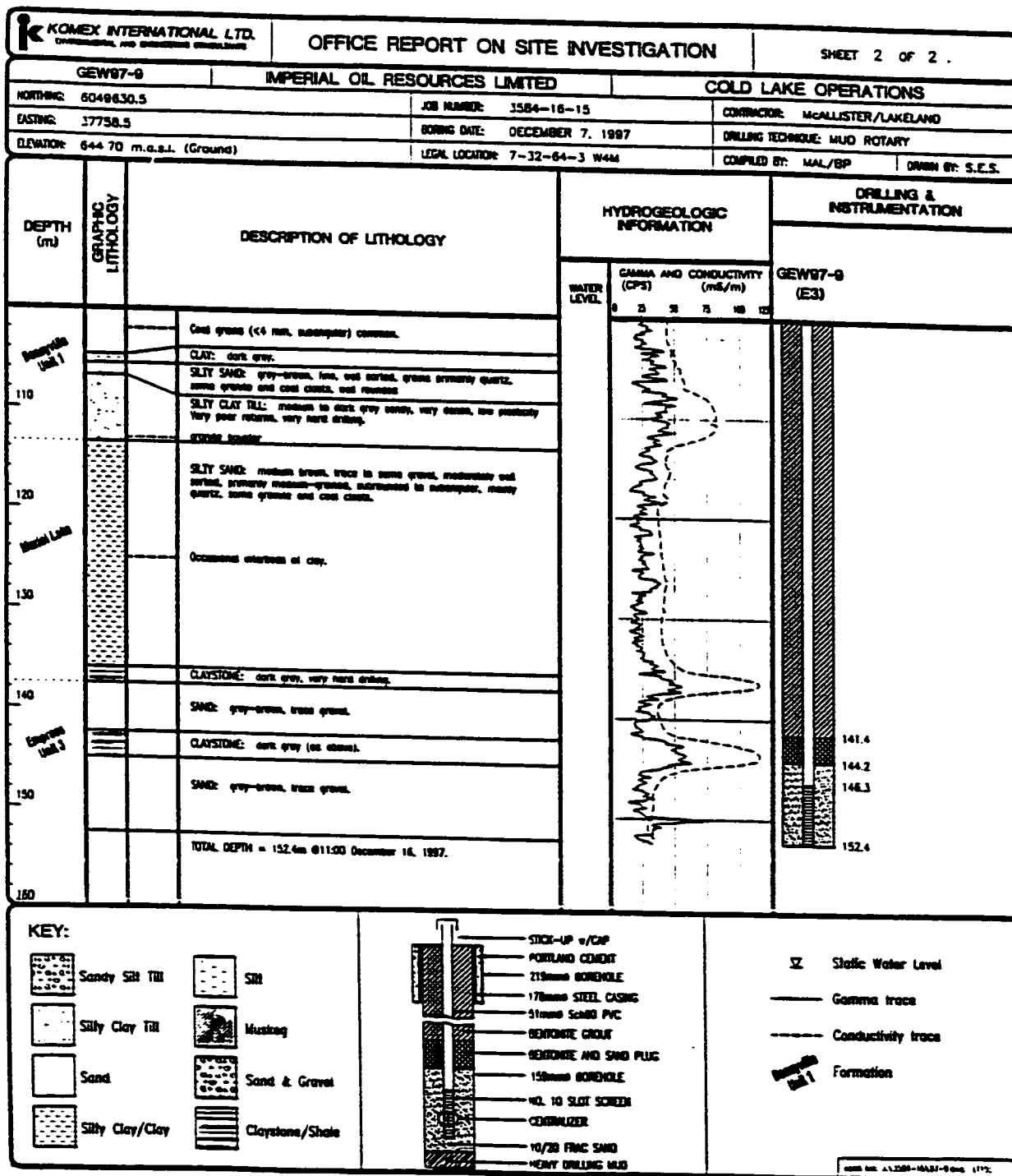
Gamma trace

Conductivity trace

Formation

©2000 Mac & L. 3584-16/97-Long (173)

K KOMEK INTERNATIONAL LTD. CONSTRUCTION AND DRILLING CONSULTANTS		OFFICE REPORT ON SITE INVESTIGATION		SHEET 1 OF 2	
GEW97-9		IMPERIAL OIL RESOURCES LIMITED		COLD LAKE OPERATIONS	
NORTHING: 6049830.5		JOB NUMBER: 3584-16-15		CONTRACTOR: McALLISTER/LAKELAND	
EASTING: 37738.5		BORING DATE: DECEMBER 7, 1997		DRILLING TECHNIQUE: MUD ROTARY	
ELEVATION: 644.70 m.s.l. (GROUND)		LEGAL LOCATION: 7-32-64-3 W4M		COMPILED BY: MAL/BP	
				DRAWN BY: S.E.S.	
DEPTH (m)	GRAPHIC LITHOLOGY	DESCRIPTION OF LITHOLOGY	HYDROGEOLOGIC INFORMATION		DRILLING & INSTRUMENTATION
			WATER LEVEL	GAMMA AND CONDUCTIVITY (CPS) (mS/m)	
0			0	25 50 75 100 125	GEW97-9 (E3)
10		SANDY SILT TILL: medium brown, fine to medium coarse, <1% clasts (primarily granitic), 2-4 mm, subangular to subrounded, low plasticity, thin sand lenses (approximately 0.6m)			0.63
20		SILT CLAY TILL: medium grey, low to medium coarse, <1% clasts (primarily granitic, 2-3 mm, subrounded)			
30		SILT CLAY TILL: medium grey, trace to some sand, very soft, high plasticity, approx. 2% clasts (primarily sand, 2-3 mm, angular), moderate delayed reaction to HCl.			
40		Frequency and size of clasts increasing (approx. 2% granitic, some coarse, 5-20 mm, subrounded).			
50		Many discrete clasts, strong reaction to HCl.			
60		SAND: medium brown, subrounded to subangular, trace gravel and silt, occasional interbeds of clayey silt.			
70		SANDY CLAY, SAND AND GRAVEL: interbedded medium grey sandy clay and grey-brown sand and gravel, clay medium plastic, moderately dense, sand moderately to well sorted (primarily fine to medium-grained) primarily quartz, some granite and coal clasts, strong reaction to HCl from clay.			
80					
90		SANDY CLAY TILL: medium grey, very dense, sand grains subangular, up to 2 mm (primarily quartz, some granitic and shale), moderate reaction to HCl.			
100		SAND: medium grey, medium-grained, well sorted, trace silt, some gravelly layers (approx. 0.2-0.4 m thick, every 2-5 m).			



APPENDIX III

ALGORITHM FOR A ONE-DIMENSIONAL PORE PRESSURE AND CONCENTRATION CALCULATION FOR THE CHEMICO-OSMOTIC MODEL

```

c *****:
c Explicit Formulation for a 1-D Chemico-Osmotic Flow
c*****:
c Symbol dictionary
c*****:
c CMAX: Maximum dimensionless concentration
c CV: Coefficient of consolidation
c D: Diffusion coefficient
c DAYS: Real time in days
c DT: Dimensionless size of the time step
c KH: Hydraulic conductivity
c MC: Osmotic compressibility coefficient
c MV: Compressibility coefficient
c NDIVSX: Number of grid subdivisions
c NSTEPS: Number of time steps
c PHI: Osmotic efficiency
c PORO: Porosity
c R: Gas constant
c SIZE: Real size of the sample
c SIZE1: Dimensionless size of the sample
c T: Temperature (K)
c TIME: Dimensionless time
c TIMH: Real time in hours
c TIMIN: Real time in minutes
c U(I): Old dimensionless pore pressure array
c UMAX: Maximum dimensionless pore pressure
c UV(I): New dimensionless pore pressure array
c X(I): Old dimensionless concentration array
c XV(I): New dimensionless concentration array
c*****:
c Initialization of arrays and input
c*****:
      INTEGER NDIVSX, NSTEPS
      REAL D,SIZE,MV,MC,KH,DD
      REAL X(200),U(200),UV(200),XV(200)
      REAL TI(50)
      OPEN (UNIT=77,FILE='CONSO',STATUS='OLD')
      OPEN (UNIT=78,FILE='CONSO2',STATUS='OLD')
      OPEN (UNIT=79,FILE='CONSO3',STATUS='OLD')
      PRINT*, 'ENTER NUMBER OF X SUBDIVISIONS'
      READ*, NDIVSX
      PRINT*, 'ENTER NUMBER OF TIME STEPS'
      READ*, NSTEPS
      PRINT*, 'ENTER MINIMUM DIFFUSION COEFFICIENT'
      READ*, D
      PRINT*, 'ENTER SIZE OF THE SAMPLE'
      READ*, SIZE

```

```

c*****
c    Basic parameters
c*****
    NDIVSX=10
    SIZE=1
    DD=NDIVSX
    DZ=SIZE/DD
    NDIVSX=NDIVSX+1
    KH=1.2E-11
    MV=1E-5
    MC= 1E-6
    R=8.3145E-3
    T= 300
    PORO=0.20
    PHI= 0.005
    CV=KH/(1000*MV)
    TIME=DT
    DT=0.004
    D1=D
c*****
c    Initial conditions
c*****
    DO 5 I=1,NDIVSX
        U(I)= 0
        X(I)= 1
c*****
c    Boundary conditions
c*****
        U(1)= 0
        X(1)= 0
5        CONTINUE
        CMAX=52
        UMAX=1200
c*****
c    Calculation of pore pressure and concentration distribution
c*****
    DO 10 K=1,NSTEPS
        U(NDIVSX+1)=U(NDIVSX-1)
        X(NDIVSX+1)=X(NDIVSX-1)
    DO 20 I=2,NDIVSX
        R0 = MC*R*T*CMAX/(MV*UMAX)
        R1 = PHI*R*T*CMAX/UMAX
        R2 = PORO+(MC*R*T*CMAX*X(I))
        R3 = MV*UMAX
        R4 = (-PORO*D/CV)+CMAX*PHI*R*T*MV*X(I)
        AA = U(I)-R0*X(I)+ (U(I+1)-2*U(I)+U(I-1))*DT/DZ**2
        AB = R1*(X(I+1)-2*X(I)+X(I-1))*DT/DZ**2
        A1 = AA+AB

```

```

      BA = R2*X(I)-R3*X(I)*U(I)-R4*(X(I+1)-2*X(I)+X(I-1))*DT/DZ**2
      BB = -(R3/4)*(X(I+1)-X(I-1))*(U(I+1)-U(I-1))*DT/DZ**2
      BC = -R3*X(I)*(U(I+1)-2*U(I)+U(I-1))*DT/DZ**2
      A2 = BA+BB+BC
      XV(I) = ((R3*X(I)*A1)+A2)/(R2-(R3*X(I)*R0))
      UV(I) = (R0*XV(I))+A1
20    CONTINUE
      UV(1)= U(1)
      XV(1)= X(1)
c*****
c      Real time calculation
c*****
      TIMH= TIME*(SIZE**2)/(3600*CV)
      TIMIN= 60*TIMH
      DAYS=TIMH/24
c*****
c      Calculation of amount of solute removed from sample
c      and dissipated pore pressure
c*****
      UX=0
      XX=0
      DO 45 I=2,NDIVSX-1
      XX= XX+DZ*(XV(I)+XV(I+1))/2
      UX= UX+DZ*(UV(I)+UV(I+1))/2
45    CONTINUE

c      Fraction of solute removed from the sample
      XX=1-(XX/(SIZE-DZ))

c      Fraction of pore pressure dissipated
      UX=UX/(SIZE-DZ)
c*****
c      Recording results, printing and formatting
c*****
      WRITE (77,*) TIMH
      WRITE (78,*) TIMIN,UX,XX
      WRITE (79,*) TIMIN,D
      PRINT*, 'DAYS,      D      UX      XX      PPRESS      CONC'
      DO 50 I=1,NDIVSX
      WRITE (77,*)UV(I),XV(I)
      PRINT 55, DAYS, D, UX, XX, UV(I), XV(I)
55    FORMAT (1X,F10.3,2X,E10.3,2X,F10.3,2X,F10.3,2X,F10.3,F10.3)
77    FORMAT(F10.3,2X,F10.3,2X,F10.3)
78    FORMAT(F10.3,2X,F10.3,2X,F10.3)
79    FORMAT(F10.3,2X,E10.3)

50    CONTINUE

```

```

c*****
c  Update pore pressure, concentration, initial conditions
c  and time for next calculation
c*****
      DO 75 I=1,NDIVSX
          U(I)= UV(I)
          X(I)= XV(I)
75      CONTINUE
          X(1)=XX*75/850
          TIME = TIME+DT
c*****
c  Empirical adjustment of the Diffusion Coefficient
c*****
          D=D*1.00109
          IF (TIMH.GT.30.AND.D.GT.D1) THEN
              D=D/1.0006
          END IF
10      CONTINUE
      END

```

Example of output for file Conso

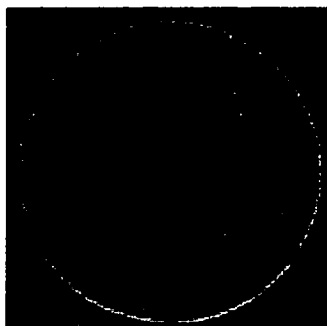
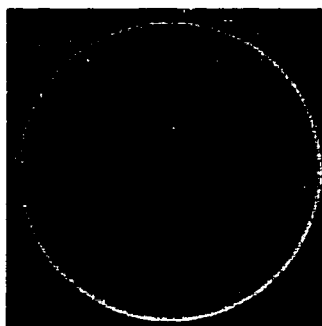
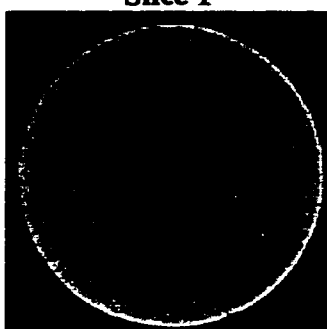
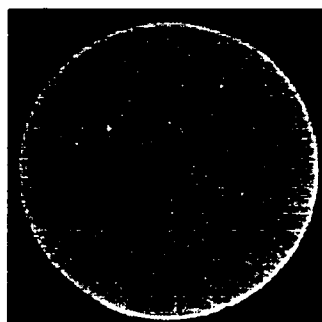
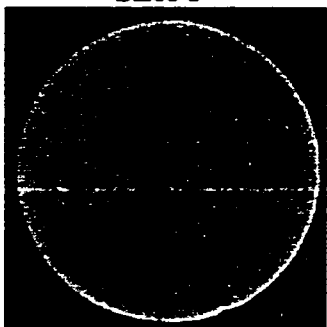
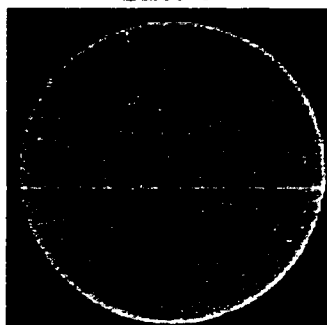
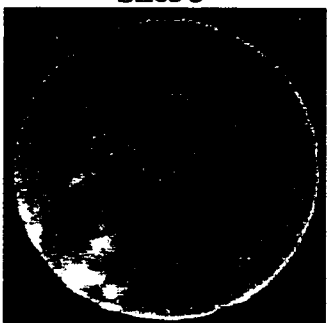
File Conso			
Time (hours)	Dimensionless distance from water contact	Dimensionless pore pressure distribution	Dimensionless concentration distribution
55.5556			
	0	0	0.006139
	0.1	-0.0136584	0.4428712
	0.2	-0.0210942	0.7519526
	0.3	-0.021543	0.9119805
	0.4	-0.0179814	0.9748178
	0.5	-0.0133635	0.9941132
	0.6	-0.0092366	0.9988614
	0.7	-0.0060953	0.9998158
	0.8	-0.0039704	0.9999748
	0.9	-0.0027603	0.9999971
	1	-0.0023691	0.9999994
57.8704			
	0	0	0.0063436
	0.1	-0.013451	0.435948
	0.2	-0.0209689	0.7437676
	0.3	-0.0216796	0.9066248
	0.4	-0.0183388	0.9724162
	0.5	-0.0138205	0.9933109
	0.6	-0.0096988	0.9986523
	0.7	-0.0065161	0.999772
	0.8	-0.0043388	0.9999673
	0.9	-0.0030882	0.999996
	1	-0.0026821	0.9999991

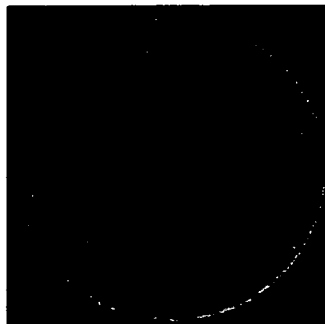
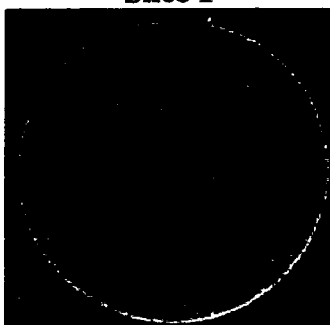
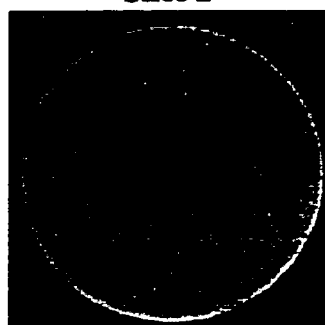
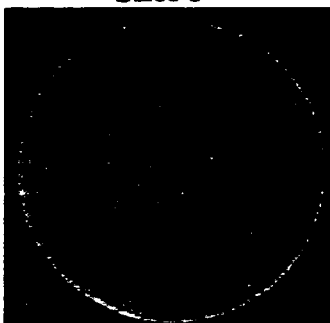
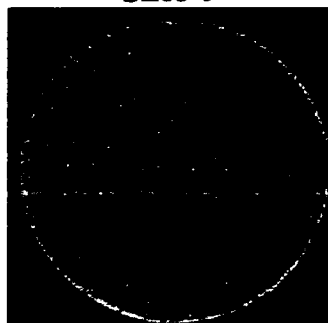
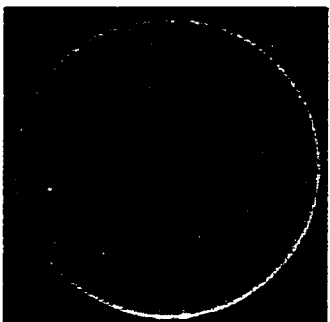
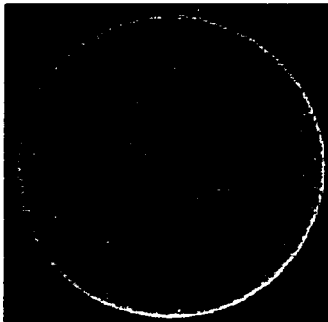
Example of output for files Conso 2 and Conso 3

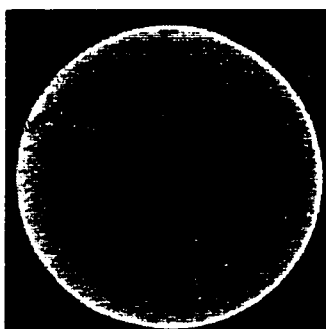
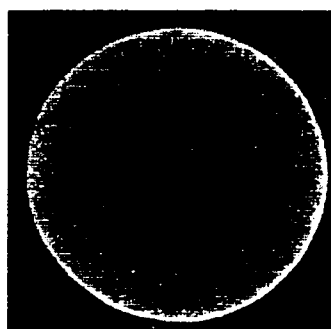
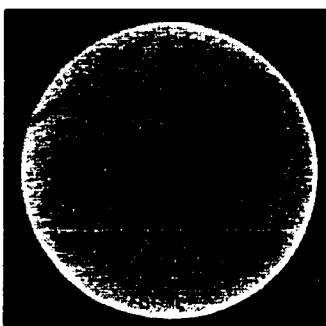
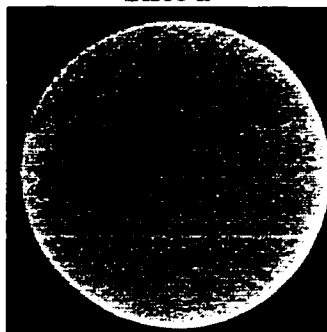
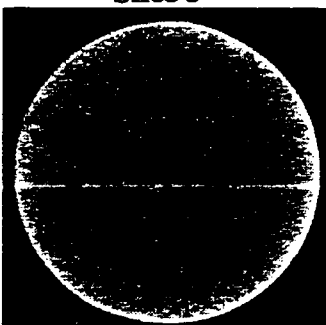
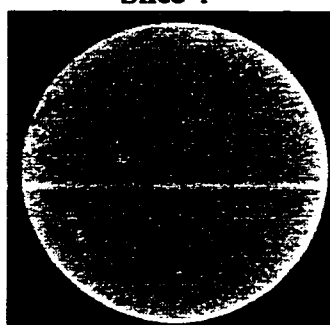
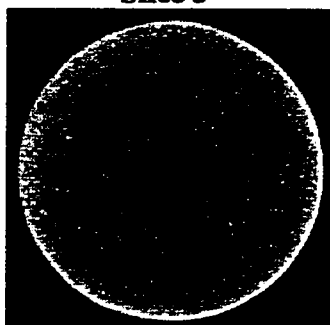
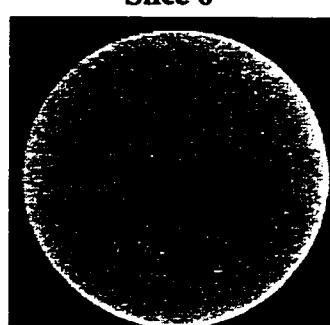
File Conso 2			File Conso 3	
Time (minutes)	Dimensionless pore pressure	Dimensionless concentration	Time (Minutes)	Diffusion coefficient
3333.33	-1.16E-02	7.19E-02	3333.33	1.67E-10
3472.22	-1.18E-02	7.42E-02	3472.22	1.65E-10
6944.44	-1.74E-02	1.20E-01	6944.44	1.35E-10
7083.33	-1.75E-02	1.21E-01	7083.33	1.34E-10
10416.7	-2.14E-02	1.51E-01	10416.7	1.11E-10
10555.6	-2.15E-02	1.52E-01	10555.6	1.10E-10
13750	-2.42E-02	1.74E-01	13750	9.16E-11
13888.9	-2.43E-02	1.74E-01	13888.9	9.09E-11
17222.2	-2.64E-02	1.91E-01	17222.2	7.51E-11
17361.1	-2.65E-02	1.92E-01	17361.1	7.45E-11
20694.5	-2.80E-02	2.05E-01	20694.5	6.15E-11
20833.4	-2.81E-02	2.05E-01	20833.4	6.10E-11
24166.7	-2.92E-02	0.2155699	24166.7	5.04E-11
24305.6	-2.92E-02	0.2159467	24305.6	5.00E-11
27638.9	-3.00E-02	0.2240085	27638.9	4.13E-11
27777.8	-3.00E-02	0.2243069	27777.8	4.10E-11
31111.2	-3.06E-02	0.2307061	31111.2	3.38E-11
31250	-3.06E-02	0.2309435	31250	3.36E-11
69444.1	-3.12E-02	0.2651147	69444.1	1.69E-11
69583	-3.12E-02	0.2652179	69583	1.69E-11
104166	-3.01E-02	0.290096	104166	1.69E-11
104305	-3.01E-02	0.2901928	104305	1.69E-11
138888	-2.90E-02	0.3135982	138888	1.69E-11
139027	-2.90E-02	0.3136896	139027	1.69E-11
173473	-2.80E-02	0.3357514	173473	1.69E-11
173612	-2.80E-02	0.3358381	173612	1.69E-11

APPENDIX IV

COMPUTER AIDED TOMOGRAPHY (CAT) SCAN FOR SAMPLES LP, MP AND HP

Sample LP - CAT Scan results**Slice 1****Slice 2****Slice 3****Slice 4****Slice 5****Slice 6****Slice 7****Slice 8**

Sample MP - CAT Scan results**Slice 1****Slice 2****Slice 3****Slice 4****Slice 5****Slice 6****Slice 7****Slice 8**

Sample HP - CAT Scan results**Slice 1****Slice 2****Slice 3****Slice 4****Slice 5****Slice 6****Slice 7****Slice 8**